HSP90 C-TERMINAL DOMAIN BINDING SITE FOR NOVOBIOCIN AND RELATED COUMARINS

By

KRISTEN LYNN SZABLA

Bachelor of Science

Biochemistry & Molecular Biology

Oklahoma State University

Stillwater, OK

2006

Submitted to the Faculty of the
Graduate College of the
Oklahoma State University
in partial fulfillment of
the requirements for
the Degree of
MASTER OF SCIENCE
May 2010

HSP90 C-TERMINAL DOMAIN BINDING SITE

FOR NOVOBIOCIN AND RELATED COUMARINS

Thesis Approved:

Dr. Robert Matts

Thesis Adviser

Dr. Steve Hartson

Dr. Junpeng Deng

Dr. A. Gordon Emslie

Dean of the Graduate College

ACKNOWLEDGMENTS

I owe my deepest appreciation to my committee members: Dr. Robert Matts, Dr. Steve Hartson, and Dr Junpeng Deng for their support, guidance, and wisdom during the course of this project. I would also like to thank my friends and colleagues in the department. I would particularly like that thank Shawn Daley for his invaluable assistance throughout the past year with kinetic analysis. Finally, I would like to express my appreciation for the love and support of my family without which I would not be here today.

TABLE OF CONTENTS

Chapter Page

Chapter Page

LIST OF TABLES

Table **Page**

LIST OF FIGURES

Figure Page

LITERATURE REVIEW

Heat shock protein 90 (Hsp90) is a highly conserved molecular chaperone which facilitates the stabilization of an assortment of eukaryotic signaling proteins, including steroid hormone receptors, transcription factors, and protein kinases (Pratt & Toft, 2003, Pearl & Prodromou, 2000, Buchner, 1999, Young *et al.*, 2001, Abbas-Terki *et al.*, 2002, Picard, 2002). Hsp90 functions to stabilize its clientele by facilitating their maturation into autonomous components. Hsp90 also directs thermodynamically unstable clients down proteasomal degradation pathways (Pratt & Toft, 2003, Pearl & Prodromou, 2000, Buchner, 1999, Young *et al.*, 2001, Abbas-Terki *et al.*, 2002, Picard, 2002). Consequently, Hsp90 plays essential roles in cell trafficking, signal transduction, and development (Pratt & Toft, 2003, Pearl & Prodromou, 2000, Buchner, 1999, Young *et al.*, 2001, Abbas-Terki *et al.*, 2002, Picard, 2002). Moreover, Hsp90 has been demonstrated to buffer phenotypic variation and to facilitate morphological evolution (Rutherford & Lindquist, 1998).

Hsp90 Structure:

Hsp90 is a homodimer which is composed of three structural domains: a highly conserved 25kD N-terminal domain, a 35kD middle domain, and a 12kD C-terminal dimerization domain (Pearl & Prodromou, 2000, Prodromou & Pearl, 2003, Pearl & Prodromou, 2001). An unstructured charged portion of amino acid residues connects the N-terminal domain to the remainder of the protein (Pearl & Prodromou, 2000, Prodromou

& Pearl, 2003, Pearl & Prodromou, 2001). This flexible linker varies in length and composition depending on species and has been demonstrated to be necessary for the function of yeast hsp90 (Louvion *et al.*, 1996). Although the overall structure of Hsp90 has yet to be elucidated, the crystal structures for isolated domains have been reported. Domainal truncations suggest that Hsp90 shows a high degree of homology to members of the ATPase/kinase Gyrase, Hsp90, Histidine Kinase, MutL (GHKL) superfamily (Prodromou & Pearl, 2003).

Three dimensional structures of the yeast and human Hsp90 N-terminal domains demonstrated that the N-terminus of Hsp90 contains a nucleotide binding site for ATP which additionally functions as a site of binding for the ansamycin antibiotic, geldanamycin (Stebbins *et al.*, 1997, Prodromou *et al.*, 1997b, Prodromou *et al.*, 1997a). An important feature of the N-terminal ATP binding region of Hsp90 is the functionally significant "lid" that is open in apo and ADP Hsp90 states and closed in ATP bound conformations (Pearl & Prodromou, 2006). The architecture Hsp90:p23: nucleotide complexes suggest that Hsp90: ATP complexes have extensive interdomain contacts brought about by in part N domain swapping (Ali *et al.*, 2006). A remodeling of residues 94-125 corresponding to the ATP lid is observed such that these residues fold over the nucleotide pocket and function to stabilize the association of the N-terminal domains (Ali *et al.*, 2006). Middle domain residues interact with segments of the N-terminus of the opposing monomer as well as interfacing with N-terminal regions of the

same monomer to stabilize an overall compact conformation of ATP bound Hsp90 (Ali *et al.*, 2006).

The crystal structure of the yeast middle domain (MD) has also been elucidated (Meyer *et al.*, 2003). The MD consists of an N-terminal and C-terminal α-β-α sandwich connected by an alpha helical coil (Prodromou & Pearl, 2003). Mutagenesis studies implicate the middle domain as a major site for client docking (Pearl & Prodromou, 2006). For example client proteins which have been observed to interact with the Hsp90 MD include PKB/Akt1, eNOS, (Sato *et al.*, 2000, Fontana *et al.*, 2002) and cochaperones Aha1, Hch1 (Pearl & Prodromou, 2006). The Hsp90 MD contains conserved arginine residue which interacts with the γ phosphate of ATP which has been demonstrated by mutagenesis studies to be essential for its ATPase activity *in vitro* and *in vivo* (Pearl & Prodromou, 2006).

Both structural and biochemical studies indicate that the C-terminus is required for Hsp90 dimerization (Harris et al., 2004, Minami *et al.*, 1994). The three dimensional structure of the C-terminal domain of the *Escherichia coli* Hsp90 homologue, HtpG, shows that the C-terminus is a mixed α/β dimer in which alpha helices form the dimer interface and pack at the C-terminal end to form a four helix bundle (Harris *et al.*, 2004). However, C-terminal HtpG is more divergent from the eukaryotic Hsp90 CD in that the HtpG CD lacks an approximate 35 residue region at the extreme C-terminus containing the tetratricopeptide repeat (TPR) motif recognition site (Harris et al., 2004). This conserved MEEVD pentapeptide of eukaryotic Hsp90s has been implicated in its

interaction with co-factors such as immunophilins FKBP51 and FKBP52, Sti1/Hop, cyclophilin-40, PP5, and others (Chen *et al.*, 1998, Young *et al.*, 1998). Despite these dissimilarities, the overall architecture of C-terminal eukaryotic and bacterial Hsp90 is hypothesized to be similar (Harris *et al.*, 2004). And, to date, the bacterial structure continues to be the best working model of the Hsp90 C-terminal domain as eukaryotic crystal structures have yet to be resolved (Pearl & Prodromou, 2006).

Hsp90 is a Conformationally Coupled ATPase:

The Hsp90 ATPase cycle has been hypothesized to be akin to the opening and closing of a molecular clamp (Figure 1A) based on biochemical and mutational analysis which have suggested that the nucleotide free state of Hsp90 corresponds to an open state, whereas the nucleotide bound state corresponds to a closed state in which the N-terminal domains become transiently associated (Chadli *et al.*, 2000, Prodromou *et al.*, 2000). The observation that Hsp90 is a weak ATPase, in which yeast Hsp90 has been observed to hydrolyze 1 molecule of ATP every 1-2 minutes, while human Hsp90 hydrolyzes 1 molecule of ATP every 20 minutes (Wandinger *et al.*, 2008) suggests that conformational transitions of Hsp90 are coupled to the ATPase reaction.

It has been posited that conformational changes that occur within the nucleotide lid region decelerate Hsp90 ATPase activity (Wandinger et al., 2008) The contribution of the lid to the ATPase activity of Hsp90 has been investigated with site-directed mutagenesis and other assays (Wandinger et al., 2008(Pearl & Prodromou, 2006). Lid mutants which

stabilize a closed conformation of Hsp90 have been demonstrated to increase ATP turnover whereas lid mutants which stabilize an open conformation of Hsp90 decreased ATP turnover (Wegele *et al.*, 2004). Hsp90 cochaperones and cohorts have also been observed to modulate Hsp90's ATPase activity (Pearl & Prodromou, 2006, Caplan et al., 2003) (see discussion below).

Hsp90 Cochaperone System and Client Maturation:

Hsp90 does not function alone but utilizes a collection of other cochaperones that influence its interaction with nucleotides and client proteins (Caplan *et al.*, 2003). The best characterized model for Hsp90's interaction with cochaperones comes from studies with steroid hormone receptors (SHRs) in which it was demonstrated that cochaperones appear to enter and exit Hsp90-SHR complexes in a definite order (Figure 1B) (Caplan *et al.*, 2003). The loading of SHRs onto Hsp90 require cochaperones Hsp70, Hsp40, and Hop/Sti1 (Kosano *et al.*, 1998). While Hsp70 with cofactor Hsp40 facilitate early folding intermediates of SHRs, the cochaperone Hop/Sti1 facilitates the loading of Hsp70:SHR complexes onto Hsp90 (Kosano *et al.*, 1998). Hop/Sti interacts with the C-terminal domain of both Hsp90 and Hsp70 via its tetratricopeptide repeat regions, however the mechanism of its recruitment of Hsp70:SHR complexes remains obscure (Wandinger *et al.*, 2008). ATP subsequently binds to this heterocomplex. ATP binding facilitates conformational rearrangements which lead to N-terminal dimerization, the recruitment of final complex cochaperones, p23 and immunophillins, to Hsp90:SHR complexes and

SHR maturation (Kosano *et al.*, 1998). Although the mechanism of final stage cochaperone recruitment remains largely unknown, it has been suggested that immunophilins, such as FKBP52, which contain the peptidylprolyl isomerase activity necessary to mature SHRs, compete with HOP and act to trigger the final folding complex (Kosano *et al.*, 1998). This is consistent with the observation that immunophilins have been only recovered in Hsp90 complexes containing the later stage cochaperone p23 (Wandinger *et al.*, 2008). ATP hydrolysis is proposed to cause the dissociation of bound SHR and cochaperones from Hsp90 (Wandinger *et al.*, 2008).

In contrast, the folding pathways for Hsp90 client kinases are less clearly defined (Wandinger et al., 2008, Terasawa *et al.*, 2005). The loading of immature protein kinases to Hsp90 requires cochaperone p50/Cdc37, which simultaneously interacts with signaling kinases and Hsp90 (Wandinger et al., 2008, Terasawa *et al.*, 2005). The following steps for the Hsp90 facilitated folding of client kinases remain elusive. It may be that for kinases, as well as for SHRs, Hsp70, Hsp40, and Hop are additionally required, however this remains to be determined (Wandinger et al., 2008, Terasawa *et al.*, 2005).

Further, cochaperones have been demonstrated to regulate the ATPase activity of Hsp90 (Pearl & Prodromou, 2006, Caplan et al., 2003). Cochaperones Hop/Sti1, Cdc37, and p23/Sba1 have been observed to have an inhibitory effect on the ATPase cycle of Hsp90 (Siligardi *et al.*, 2002, Panaretou *et al.*, 2002, Prodromou *et al.*, 1999). Both Hop and Cdc37 stabilize an open conformation of Hsp90 which prevent the association of the N-terminal domains, while p23 binds to the ATP binding site and stabilizes the N-

terminally dimerized conformation of Hsp90 at latter stages of the Hsp90 cycle (Chadli *et al.*, 2000, Richter *et al.*, 2006). Hop and Cdc37 are hypothesized to stabilize conformations of Hsp90 which facilitate client loading, whereas p23 is posited to stabilize conformations of Hsp90 which facilitate client maturation (Chadli *et al.*, 2000, Richter *et al.*, 2006). Despite conformational differences, Hop/Sti1, Cdc37, and p23 each function to decrease ATP turnover (Chadli *et al.*, 2000, Richter *et al.*, 2006).

On the contrary, the cochaperone, activator of heat shock 90kDa protein ATPase homolog 1, (Aha1) has been shown to increase the ATPase activity of Hsp90 by up to 10 fold (McLaughlin *et al.*, 2002, Panaretou et al., 2002). Biochemical and structural studies suggest that binding of Aha1 facilitates a restructuring of the middle domain which induces a transition from an open inactive conformation to a closed catalytically active conformation (Pearl & Prodromou, 2006, Wandinger et al., 2008). Similarly, the immunophillin, Cpr6, has been observed to stimulate Hsp90 ATPase activity by two-fold (Panaretou *et al.*, 2002), and reduce the ATPase inhibition by Hop/Sti1 (Prodromou *et al.*, 1999).

INTRODUCTION

Hsp90's Conformational Dynamics:

Recently, much work has focused on Hsp90's varying conformational states. Previous crystal structures for full length E. coli Hsp90 have demonstrated a V-shaped structure which is dimerized by the C-terminal domain (Shiau *et al.*, 2006). Recent cryo-electron micrographs (EM) and small angle x-ray scattering (SAXS) studies have showed that uncomplexed Hsp90 is in equilibrium between two open conformations consisting of a highly extended, open, "seagull" conformation and an intermediate, less extended, "V shaped" conformation (Krukenberg *et al.*, 2009, Bron *et al.*, 2008). These studies suggest that apo Hsp90 is in "dynamic equilibrium" between two open conformations and that binding of nucleotide shifts this equilibrium (Krukenberg *et al.*, 2009, Bron *et al.*, 2008).

Previously, Sullivan and Toft (1997) proposed a model in which binding of nucleotide to the N-terminus of Hsp90 arbitrates between two different conformations of Hsp90. This model was based on the observations that binding of ATP and/or geldanamycin to the N-terminal domain of Hsp90 distinctly altered Hsp90's interactions with p23 and C-terminal protein-protein interactions (Sullivan *et al.*, 2002, Sullivan *et al.*, 1997). More recent ATP binding kinetics indicate that ATP binding induces a conformational switch that may be conferred to the C-terminus by the docking of the N and middle domains

(McLaughlin *et al.*, 2004). Additionally, H/D exchange studies suggest that binding of N-terminal inhibitors to the nucleotide binding pocket stabilizes a differential conformational state of Hsp90 in which the interface between the C-terminal, middle, and N-terminal domains has been tightened (Phillips *et al.*, 2007). Further, geldanamycin and molybdate have also been demonstrated to stabilize distinct Hsp90 conformations (Nemoto *et al.*, 1997, Hartson et al., 1999). This conclusion was based on the following observations: (1) GA stabilized the recovery of Hsp90: Hop: Hsp70 complexes from RRL, whereas molybdate stabilized the recovery of Hsp90:p23: immunophilin complexes (Hartson *et al.*, 1999), and (2) molybdate protected Hsp90FL from proteolysis through the restructuring of the C-terminal domain of Hsp90, while GA did not induce a protease protected conformation of Hsp90FL (Nemoto *et al.*, 1997, Hartson et al., 1999).

Hydrogen deuterium exchange mass spectrometry (HX-MS) in combination with fluorescence resonance energy transfer (FRET) assays has provided recent insights into the conformational changes which occur upon binding of ATP to *E. coli* Hsp90 (Hessling *et al.*, 2009, Graf *et al.*, 2009). ATP binding induces a series of sequential conformational changes which begin at the N-terminal nucleotide binding pocket and progress in a stepwise manner through the catalytic loop of the middle domain. Based on this data at least four different conformations for the ATP induced Hsp90 cycle have been suggested. (1). apo Hsp90 resides in an open conformation whose NTD is in the lid open position. (2). Binding of ATP leads to the stabilization of an "I_1" conformer in which the N-terminal ATP lid is closed but not interacting with the middle domain. (3).

The NTD then rotates so that the lid interfaces with the MD stabilizing an I_2 conformation. (4) Finally, interaction of N and M domains completes the dimerization leads to a fully closed state. In contrast to Buchner and co workers' findings, "autoinhibitory" conformations of apo Hsp90 structures have been observed in *E. coli* and yeast Hsp90 in which helix 5 of the nucleotide capping lid has been demonstrated to occlude the nucleotide binding pocket (Shiau et al., 2006, Richter *et al.*, 2006).

Inhibition of Hsp90 Function:

N-terminal inhibition: ATP has been demonstrated to bind to the N-terminal nucleotide binding pocket in an atypical bent manner, which is mimicked by the structurally unrelated natural products geldanamycin (GA) and radicicol (Wandinger *et al.*, 2008). GA and radicicol bind Hsp90 with higher affinity than ADP or ATP and inhibit Hsp90's ATPase activity as well as block the maturation of substrate proteins, including ErbB-1 and ErbB-2 kinases, glucocorticoid receptors, Src kinases, and tumor necrosis factor receptors (Whitesell & Lindquist, 2005). Geldanamycin and radicicol have also been observed to deplete cells of the prosurvival kinases, AKT and Raf-1(Chiosis *et al.*, 2003, Basso *et al.*, 2002, Taiyab *et al.*, 2009). These compounds have additionally been shown to inhibit the prosurvival nuclear factor (NF –κβ) pathway (Chiosis et al., 2003, Basso et al., 2002). Moreover, inhibition of Hsp90 by GA and radicicol has been shown to potentiate the activity of radiation and chemotherapy in the treatment of a variety of cancer types by depleting tumor cells of Raf-1 ErbB2, and Akt

and enhancing tumor cell sensitivity to proteasomal inhibition (Whitesell & Lindquist, 2005).

C-terminal inhibition: Biochemical studies have recently suggested that the C-terminal region of Hsp90 possesses a secondary cryptic ATP binding site which upon occupancy of N-terminal nucleotide binding pocket becomes available (Marcu *et al.*, 2000a, Soti *et al.*, 2002). Although the contribution of the C-terminus and of this site to the regulation of Hsp90 chaperone machinery remains unclear, novobiocin (Figure 2) has been reported to bind to this site (Marcu et al., 2000a) and to alter the chaperone cochaperone interactions (Marcu et al., 2000a, Yun *et al.*, 2004). Further, novobiocin and related coumarins (Figure 2) have been demonstrated to inhibit Hsp90 chaperone machinery altering basal cochaperone interactions and inducing the depletion of an assortment of Hsp90 dependent oncogenic signaling proteins, including mutant p53, Raf-1, $p185^{erbB2}$, AKT kinase, and Her2 (Yun et al., 2004, Marcu et al., 2000a, Marcu *et al.*, 2000b, Burlison & Blagg, 2006, Allan *et al.*, 2006, Itoh *et al.*, 1999).

The existence of an Hsp90 binding site for novobiocin and related coumarins has been suggested through studies with purified constructs (Marcu et al., 2000b, Allan et al., 2006, Marcu et al., 2000a, Yun et al., 2004, Langer *et al.*, 2002). Langer and coworkers showed that increasing concentrations of novobiocin inhibited the autophosphorylation of purified Hsp90 (Langer *et al.*, 2002). Pre-addition of novobiocin to both recombinant Hsp90FLβ and Hsp90CTβ increased the rate of aggregation in chaperone activity assays for both Hsp90FL and Hsp90CT (Allan et al., 2006). Moreover, pretreatment of

purified, His- tagged full length Hsp90β and purified, his-tagged, C-terminal Hsp90β with increasing concentrations of novobiocin led to the inability to detect subsequently added GST-tagged immunophilins by ELISA (Allan et al., 2006).

Novobiocin was additionally shown to bind purified, recombinant Hsp90FL in complex with geldanamycin Sepharose resins (Marcu et al., 2000b). Novobiocin and the related coumarin, coumermycin, also bound Hsp90α coated magnetic beads (Marszall *et al.*, 2008b). Further, purified recombinant Hsp90CT bound to novobiocin sepharose resins, and novobiocin was shown to compete recombinant Hsp90CT from ATP-linked Sepharose resins (Marcu *et al.*, 2000b, Marcu *et al.*, 2000a). Yun et al similarly demonstrated that the recombinant Hsp90 C-terminus became resistant to trypsinolysis in protease nicking assays in the presence of increasing concentrations of novobiocin (Yun et al., 2004). Further, increasing concentrations of coumermycin inhibited the chemical crosslinking of Hsp90CTβ (Allan *et al.*, 2006).

Currently, novobiocin and related coumarins are being developed into higher affinity analogs for the treatment of various cancers based on their inhibition of Hsp90 chaperone function (Burlison *et al.*, 2008, Burlison & Blagg, 2006). However, nothing to date has been published which confirms structure activity relationships for coumarin derivatives in the context of purified Hsp90 components. Further, no work to date has established affinity constants for novobiocin related compounds for purified Hsp90 and compared those binding constants to those estimated on the basis of the inhibition of chaperone function assays *in vivo* and *in vitro*. Moreover, with the current lack of a co-crystal

structure of the Hsp90 C-terminal domain with bound inhibitor, it is difficult to definitively establish the site of binding for novobiocin and related compounds on Hsp90.

In order to address this gap in our knowledge, we used the technique of surface plasmon resonance (SPR) to assay the affinities of novobiocin derivatives for Hsp90 FL and a C-terminal Hsp90 truncation. We also examined the effect of bound N-terminal ligands, ATP, ADP, and GA, on the affinities for our compounds of interest. Results demonstrate that novobiocin and related coumarins bind to apo Hsp90FL and apo Hsp90CT with comparable affinities ranging from micromolar to millimolar range, which is consistent with previously reported affinities for the novobiocin induced depletion of Hsp90 substrates (Yun et al., 2004, Marcu et al., 2000a, Marcu *et al.*, 2000b, Burlison & Blagg, 2006, Allan *et al.*, 2006, Itoh *et al.*, 1999). Additionally, coumarin derivatives bound to Hsp90: ADP complexes with enhanced affinity, and docking of N-terminal ligand abrogated nonspecific binding observed for novobiocin: apo Hsp90 complexes. We further demonstrate an inability to resolve nucleotide binding prior to treatment of Hsp90 with 0.01% Igepal. These results not only support the hypothesis that the conformation of the N-terminus influences the conformation of the C-terminus but demonstrate that a binding site for novobiocin compounds resides in the C-terminus of Hsp90. Further, the inability to resolve nucleotide binding prior to treatment with Igepal suggests that Igepal loosens an autoinhibitory conformation of Hsp90 which facilitates the binding of nucleotide. Our results provide new insights into the mode of action by which novobiocin related compounds interact with Hsp90 *in vitro* and may suggest novel

approaches to the development of higher affinity novobiocin derivatives in the treatment of cancer and related diseases.

EXPERIMENTAL PROCEDURES:

***Reagents**:* Geldanamycin, coumermycin A1(C9270), novobiocin (N6160), adenosine 5' triphosphate (A26209), and adenosine 5' diphosphate (A2754) were purchased from Sigma Aldrich. Chlorobiocin was a gift from the National Institutes of Health Drug Synthesis Division.

Protein Purification:

Hsp90β Purification: Sf9 cells containing overexpressed human Hsp90β were purchased from the Baculovirus/Monoclonal Antibody Core Facility Baylor College of Medicine (Alnemri & Litwack, 1993). Sf9 cells were lysed as detailed previously, replacing sonication with homogenization (Sullivan *et al.*, 1997). The Sf9 lysate was put through successive chromatographic steps as described previously, omitting the DEAE cellulose column (Johnson *et al.*, 1998, Kosano *et al.*, 1998). Full length Hsp90 (Hsp90FL) was purified to apparent homogeneity as assessed by loading 2 μg of protein on an SDS-PAGE gel and staining with Coomassie blue. The purified Hsp90 was flash frozen and stored at -80 ˚C in 20 mM Tris-HCl, 350 mM NaCl, 1 mM DTT, and 10% glycerol, pH7.4.

Hsp90CT Purification: The C-terminal domain of human Hsp90 (Hsp90CT) was designed as previously described (Yun et al., 2004), with the exception that the PCR product was ligated into a pProEx-HTa vector (Gibco-BRL), containing a *trc* promoter, an N-terminal His_6 tag, and a TEV consensus cleavage site. In consequence, the final,

uncleaved, gene product contained human Hsp90alpha residues Q531-D732 including an extended N-terminal tag derived from vector sequences. The Hsp90CT gene product was extracted from *Escherichia coli* lysates as described previously (Yun et al., 2004). Peak fractions were pooled and desalted into buffer containing 20 mM imidazole. The extended N-terminal tag was cleaved overnight at 4 ˚C using recombinant TEV protease (Invitrogen) to yield a purified product which retained vector residues GAM as an N-terminal tag fused to Hsp90CT residues Q531-D732. This product was then applied to a Superdex 200 HR gel filtration column (GE Healthcare). Peak Hsp90CT fractions were pooled and concentrated. Hsp90CT was purified to apparent homogeneity as assessed by loading 2 μg of protein on an SDS-PAGE gel and staining with Coomassie blue. Purified Hsp90CT was flash frozen and stored at-80 ˚C in 20 mM Tris, 500 mM NaCl, 1 mM DTT, and 10% glycerol, pH7.4.

Cdc37 Purification: Cdc37 was constructed by amplifying a PCR product encoding amino acids M1-V378 of human Cdc37 and by ligating the resultant PCR product into a pProEx-HTa vector (Gibco-BRL). Ion-metal affinity chromatography was employed to isolate the Cdc37 gene product from *E. coli* lysates. Recombinant Cdc37 was eluted from nickel affinity resin (Sigma) with 250 mM imidazole. Peak fractions were pooled and desalted into buffer containing 20mM imidazole to facilitate overnight cleavage of the His_6 tag by recombinant TEV protease (Invitrogen), thereby yielding a purified product comprised of Cdc37 residues M1-V378 fused to the N-terminal tag, GAM, derived from vector sequences. This product was then subjected to gel filtration on a

Hiprep Superdex200 16/60 HR column (GE Healthcare). Fractions corresponding to Cdc37 were pooled and concentrated. Cdc37 was purified to apparent homogeneity as assessed by loading 3 μg of protein on an SDS-PAGE gel and staining with Coomassie blue. Purified Cdc37 was flash frozen and stored at -80 ˚C in 20 mM Tris, 250 mM NaCl, 1 mM DTT, and 10% glycerol, pH 7.4.

Surface Plasmon Resonance:

Protein Immobilization: SPR analysis was performed with a Sensi-Q dual channel biomolecular analysis system (ICX Nomadics, USA*).* All proteins were immobilized to a research grade SSOO carboxylic acid chip (ICX Nomadics, USA) using traditional N-(3-dimethylaminopropyl)-N'-ethylcarbodiimide hydrochloride/ N-hydroxysuccinimide (EDC/NHS; Sigma) coupling protocol. Proteins were extensively desalted into running buffer consisting of 20 mM sodium bicarbonate and 150 mM NaCl, pH 8.0. Proteins were injected at flow rates of 10 μL/min at concentrations ranging from 6 mg/mL-8 mg/mL to yield an approximate 3000 resonance units of protein coupled to the surface of flow cell 1. Unreacted esters were quenched with 1.0 M ethanolamine, pH 8.2. The surface of flow cell 2 was activated and blocked so that a comparable surface could serve as a reference.

Binding of Small Molecules: Analytes were dissolved in running buffers, which are indicated in the figure legends. To eliminate any contribution to changes in bulk refractive index, double referencing was employed, in which all relative response units represent the difference between the raw response curves obtained for the sample cell and

the reference cell in addition to buffer curve subtraction (Myszka, 1999). Assays were conducted at 25 ˚C at a flow rate of 25 μL/min.

Data analysis: Analysis of data was performed using Nomadics Quantitative Data Analysis Tool (QDAT) software. Binding constants were fitted using the equations: $R_{eq} = K_A (A) R_{max} / (K_A(A) +1)$ for one-sited binding and $R_{eq} = (K_{A1} (A) R_{max} / (K_{A1}(A) +1)) +(K_{A2} (A) R_{max} / (K_{A2}(A) +1))$ for two-sited binding. Regraphs and statistical analysis of SPR data were performed with GraphPad Prism software.

RESULTS

Binding of Novobiocin-Derivatives to Hsp90FL

Binding of Coumermycin (Cm) toHsp90FL: In order to test the hypothesis that a drug binding pocket for coumermycin exists on Hsp90FL, successive concentrations of coumermycin were co-injected over an Hsp90FL surface, as described in Figure 3. Coumermycin revealed a concentration dependent binding response (Figure 3A). Affinity analysis fitted one site of binding for the Cm: Hsp90FL interaction and estimated the K_D of Cm for Hsp90FLto be 50 ± 20 μM. In order to determine if Cm exhibited a saturable binding response for Hsp90FL, a replot of the Cm steady state binding signals was performed. The binding isotherm for Cm showed a hyperbolic curve in which Cm saturated the surface of Hsp90FL at a maximum concentration of 600 μM (Figure 3B). Nonlinear regression of the Cm: Hsp90FL binding isotherm calculated the affinity of Cm for Hsp90FL to be equal to 60 ± 20 μM, R^2 =0.99. In order to elucidate the mechanism of Cm binding, a Hill plot of Cm SPR signals was performed. The Hill plot for Cm: Hsp90FL response curves delineated a straight line with a calculated Hill coefficient of 1.0 (Figure 3C). Coumermycin's robust response in combination with its saturable hyperbolic replot, calculated Hill coefficient of 1.0, and low micromolar range affinity constant, which could be fitted for only one site of binding, indicates that Cm specifically binds to Hsp90FL at a discrete site.

Binding of Chlorobiocin (Cb) to Hsp90FL: In order to expand our investigation, a compound of similar structure was assayed for its affinity to Hsp90FL. Successive concentrations of chlorobiocin were co-injected over an Hsp90FL surface, as described in Figure 3. Chlorobiocin demonstrated a significant binding response when injected over the surface of Hsp90FL (Figure 5A). Affinity analysis calculated a high affinity K_{D1} = 45 ± 5 μM and a low affinity K_{D2} = 155 ± 10 μM. A replot of the binding isotherm for chlorobiocin (Figure 5B) showed a deviation from the rectangular hyperbola and demonstrated saturation at a maximal concentration of 500 μM chlorobiocin. This departure from hyperbolic behavior is diagnostic of a cooperative binding event (Acerenza & Mizraji, 1997). To determine the type of cooperative mechanism by which chlorobiocin binds to Hsp90, a Hill plot was constructed from Cb response signals (Figure 5C). The Hill plot for the Cb: Hsp90FL interaction was sigmoidal in shape with a calculated Hill coefficient of 1.7, R^2=0.99. The sigmoidal binding isotherm together with the curved Hill plot substantiates a positive cooperative binding event and confirms our hypothesis that Cb binds to Hsp90.

Binding of Novobiocin (Nb) to Hsp90FL: Because coumermycin and chlorobiocin, demonstrated significant binding responses to Hsp90FL (Figures 3 and 5), we expanded our analysis to include the related compound, novobiocin, which has been shown to inhibit Hsp90 function in prior work (Yun et al., 2004, Marcu et al., 2000a, Marcu *et al.*, 2000b, Burlison & Blagg, 2006, Allan *et al.*, 2006, Itoh *et al.*, 1999). Consecutive concentrations of novobiocin were co-injected over an Hsp90FL surface, as described in Figure 5. Novobiocin demonstrated an exaggerated binding response, with a rapid off rate (Figure 7A). A replot of the steady state binding signals (Figure 7B) showed that

saturation was not achieved, suggesting that novobiocin binds to Hsp90FL nonspecifically. In order to determine if nonspecific binding could be subtracted from specific binding, novobiocin's binding isotherm was globally fit for total and nonspecific binding as described in Figure 7C. The subtraction of nonspecific binding from total binding revealed that saturable binding was achieved at concentrations approximating 6 mM (Figure 7C-D). Nonlinear regression of the baseline corrected data points (Figure 7D) calculated the half maximal occupancy of Nb for Hsp90FL to be 3.3 ± 0.9 mM, R^2 =0.99. A Hill plot of the Nb : Hsp90FL response curves (Figure 7E) was sigmoidal in shape (n=1.3; R^2=0.98), thereby indicating a positive cooperative binding event. These results indicate that novobiocin binding is comprised of a significant nonspecific response that when subtracted from the total response facilitates the conclusion that that more than one novobiocin binding site resides on Hsp90FL. Further, these sites demonstrate specificity as indicated by the saturable subtracted binding isotherm and the sigmoidal Hill plot.

Binding of Novobiocin-Derivatives to Hsp90CT:

Binding of Cm to Hsp90CT: Because coumermycin demonstrated affinity for Hsp90FL (Figure 3), we extended our study to the C-terminal domain of Hsp90. A series of Cm concentrations were co-injected over an Hsp90CT surface, as described in Figure 4. Cm demonstrated robust signals when injected over the surface of Hsp90CT (Figure 4A). Affinity analysis fitted one site of binding for the Cm: Hsp90CT interaction and calculated the K_D of Cm for Hsp90CT to be 40 ± 10 μM. To determine whether binding was saturable, a replot of the Cm binding response was constructed. The Cm binding

isotherm traced a hyperbola and saturated at concentrations spanning 300 μM and 600 μM (Figure 4B). Nonlinear regression of the data points calculated the affinity of Cm for Hsp90CT to be equal to 45 ± 10 μM, R^2 =0.99. A Hill plot of Cm: Hsp90CT response curves (Figure 4C) depicted a straight line with a Hill coefficient of 1.0. The saturable, hyperbolic, binding isotherm combined with the straight Hill plot and binding constants which can be fitted for only one site of binding suggests that coumermycin binds independently to a single site on Hsp90. This data further indicates that coumermycin binds to a site which is located on the C-terminus of Hsp90.

Binding of Chlorobiocin (Cb) to Hsp90CT: Similarly, our study of chlorobiocin was broadened to the C-terminus of Hsp90 due to chlorobiocin's demonstrated affinity for Hsp90FL (Figure 5) and coumermycin's exhibited affinity for Hsp90CT (Figure 4). A series of chlorobiocin concentrations were co-injected over an Hsp90CT surface (Figure 6). Upon binding and subsequent release of chlorobiocin, we observed a reproducible concentration dependent net drop in refractive index (Figure 6A). Affinity analysis calculated a high affinity K_{D1} = 35 ± 5 μM and a low affinity K_{D2} = 110 ± 10 μM. A replot of the binding isotherm for chlorobiocin (Figure 6B) showed a sigmoidal curve which saturated at a maximal concentration of 600 μM. A Hill plot of Cb response signals (Figure 6C) revealed a curved line with an estimated Hill coefficient of 1.78, R^2=0.99. The sigmoidal binding isotherm together with the S-shaped Hill plot substantiates a positive cooperative binding event and confirms our hypothesis that Cb allosterically interacts with Hsp90CT. These results further indicate that chlorobiocin binds to the C-terminus of Hsp90.

Binding of Novobiocin (Nb) to Hsp90CT: Our analysis of novobiocin was extended to the C-terminal domain of Hsp90 due to novobiocin's multifaceted binding behavior for Hsp90FL (Figure 7) and due to previous work suggesting that novobiocin interacts with the C-terminal domain of Hsp90 (Marcu *et al.*, 2000a, Marcu *et al.*, 2000b, Yun et al., 2004). Successive concentrations of novobiocin were co-injected over Hsp90CT, as described in Figure 8. Novobiocin demonstrated exaggerated, atypical, binding responses, with concentration dependent positive and negative deflections which were respectively apparent at the beginning and end of each injection (Figure 8A). Such refractive index deflections are indicative of ligand-protein dependent conformational transitions (Winzor, 2003). A replot of the steady state binding signals (Figure 8B) demonstrated that saturation was not achieved and indicated that there is a nonspecific component to the binding of novobiocin to Hsp90CT. Subtraction of nonspecific binding from total binding revealed that saturable binding was achieved at concentrations approaching 6 mM (Figure 8C-D). The concentration of half maximal occupancy of Nb for Hsp90CT was equivalent to 1.9 ± 0.6 mM, R^2 =0.98 (Figure 8D) . The Hill plot of novobiocin:Hsp90CT responses (Figure 8E) depicted a straight line (n=1.0). Thus, novobiocin binding is comprised of a large nonspecific component which can be subtracted from the total component to reveal a saturable hyperbolic binding component, which, collectively, exhibit complex Hsp90CT binding interfaces.

Effect of Geldanamycin (GA) on the Affinities of Novobiocin Derivatives:

GA has been shown to bind to the adenine nucleotide binding pocket in Hsp90's N-terminal domain, inhibiting the binding of ATP and inducing an altered conformation of

Hsp90 (Prodromou *et al.*, 1997b). In order to assess the affect of GA on the binding of our compounds, we initially confirmed that GA demonstrated binding to our Hsp90FL surface. Initial results yielded negligible binding for GA concentrations as high as 50 μM (data not shown). Treating Hsp90 with 0.01% Nonidet-P40 has previously been shown to activate Hsp90s ATP binding activity (Sullivan et al., 1997). Therefore, we pretreated the protein surface with 0.01% Igepal (the equivalent of Nonidet-p40), as described in Figure 9. Subsequently injection of 2 μM GA yielded a significant binding response approximating 160 RU with a post injection baseline leveling off at 120 RU (Figure7A), consistent with higher affinity interactions (Winzor, 2003). To confirm that the GA response was specific for the N-terminus of Hsp90, GA was assayed over an Hsp90CT surface under similar conditions. A GA binding response could not be demonstrated to the Hsp90CT surface (Figure 9B).

Binding of Cm to Hsp90:GA Complexes: In order to assess the effect of GA on the binding of coumermycin to Hsp90FL, a series of Cm concentrations were co-injected over an Hsp90FL:GA surface, as described in Figure 9A. Cm demonstrated robust, concentration dependent binding responses, which differed from Cm binding responses to apo Hsp90FL, in that lower concentrations of Cm demonstrated a binding response, and, apparent saturation was achieved at 150 μM (Figure 10B). Affinity analysis calculated a high affinity $K_{D1} = 1.5 \pm 0.5$ μM and a lower affinity $K_{D2} = 20 \pm 15$ μM. In contrast to these results, only one binding constant could be fitted for the Cm:Hsp90FL interaction (Figure 3). The hyperbolic binding isotherm for the Cm: Hsp90FL:GA interaction revealed saturation at a maximal concentration of 150 μM, and nonlinear regression of these data points estimated the concentration of half maximal occupancy to be 10.75 ± 2

μM, R^2=0.99. A Hill plot of the Cm: Hsp90FL: GA interaction (Figure 0C) revealed a straight line with an estimated Hill coefficient of 1.0, R^2=0.99. The hyperbolic binding isotherm together with the calculated Hill value of 1.0 substantiates a noncooperative binding event and demonstrates that coumermycin and GA bind at discrete sites. These results also suggest that GA acts to allosterically enhance the affinity of coumermycin for Hsp90FL through the induction of conformation transitions in the N-terminus of Hsp90FL which are transmitted to the C-terminus. Further, this data argues in favor of the hypothesis that the GA conformation of Hsp90 is distinct from the apo conformation of Hsp90.

In order to test the hypothesis that N-terminal GA binding alters C-terminal conformation to affect coumermycin binding, coumermycin was assayed on an Hsp90CT surface in the presence of GA (Figure 11A). Affinity analysis fitted one site of binding for the Cm:Hsp90CT in the presence of GA and calculated the K_D to be 40 ± 10 μM, consistent with the data for Cm:Hsp90CT (Figures 4). Analogous to Cm:Hsp90CT interactions in the absence of GA (Figure 4B), a replot of Cm: Hsp90CT:GA response curves demonstrated saturation at concentrations spanning 320 and 640 μM (Figure 11B). A Hill plot of Cm response signals (Figure 31C) revealed a straight line with an estimated Hill coefficient of 1.0, R^2=0.99. The consistency of these results as to previous Cm Hsp90Ct results suggests that GA does not influence the binding of coumermycin to Hsp90CT. Moreover, the absence of a GA effect on the C-terminus is consistent with the hypothesis that binding of GA to the N-terminus induces global structural rearrangements which are conferred to the C-terminus and enhance coumermycin binding (Figure 10).

Binding of Cb to Hsp90:GA Complexes: In order to assess the effect of GA on the binding of chlorobiocin to Hsp90FL, a series of Cb concentrations were co-injected over an Hsp90FL:GA surface, as described in Figure 10A. Affinity analysis calculated a high affinity K_{D1} = 45 ± 5 μM and a low affinity K_{D2} = 170 ± 20 μM, consistent with the affinities calculated for Cb: Hsp90FL. A replot of the Cb:Hsp90FL: GA binding isotherm (Figure 12B) showed a deviation from the rectangular hyperbola and demonstrated saturation at a concentration range of 400 -1250 μM, while nonlinear regression of the data points estimated the $K_{0.5}$ to be 120 ± 20 μM, R^2=0.99. A Hill plot of the Cb: Hsp90FL: GA interaction was sigmoidal in shape with calculated a Hill coefficient of 1.5, R^2 =0.99. The sigmoidal binding isotherm together with the S-shaped Hill plot substantiates a positive cooperative binding event and demonstrates that chlorobiocin and GA bind to discrete sites on Hsp90FL. Further, these results demonstrate that GA does not alter the binding of chlorobiocin as it does for coumermycin and suggests a differential mechanism of binding for these two novobiocin derivatives.

The examination of chlorobiocin binding in the presence of GA was extended to an Hsp90CT surface (Figure 13A). Affinity analysis calculated a high affinity K_{D1} = 35 ± 5 μM and a lower affinity K_{D2} = 88 ± 10 μM for Cb: Hsp90CT: GA, consistent with previous results (Figure 6). Analogous to the previous Cb: Hsp90CT interaction (Figures 4), a replot of Cb: Hsp90CT: GA response curves demonstrated saturation at concentrations spanning 320 and 640 μM in a nonhyperbolic fashion (Figure 13B). A Hill plot of Cb response signals (Figure 13C) revealed a sigmoidal curve with an estimated Hill coefficient of 1.7, R^2=0.99. The consistency of these results as to the

previous Cb Hsp90CT results suggests that GA does not influence the binding of chlorobiocin to Hsp90CT. Moreover, the absence of a GA effect on the C-terminus for chlorobiocin as well as for coumermycin further supports the hypothesis that binding of GA to the N-terminus induces a conformation in the C-terminus which augments the binding of the of dicoumarin, coumermycin, to the C-terminus.

Binding of Nb to Hsp90: GA Complexes: In order to assess the effect of GA on the binding of novobiocin to Hsp90FL, a series of Nb concentrations were co-injected over an Hsp90FL: GA surface, as described in Figure 12A. Novobiocin revealed concentration dependent response curves when applied to the Hsp90FL: GA surface (Figure14A), which were 3 times less robust than the novobiocin binding responses to apo Hsp90 (Figure 7A). Affinity analysis calculated a high affinity K_{D1} = 800 ± 80 μM and a low affinity K_{D2} = 2.0 ± 0.2 mM. A replot of steady state signals revealed a nonhyperbolic, binding isotherm which saturated at concentrations ranging between 5 and 7 mM. (Figure 14B). The calculated concentration of half maximal occupancy of Nb for the Hsp90FL:GA conjugate was 1.3 ± 0.20 mM, R^2 =0.975. A Hill plot of the Nb: Hsp90FL: GA interaction traced a curved lined with an estimated Hill coefficient of 1.3, R^2 =0.99. The sigmoidal binding isotherm together with the curved Hill plot confirms a positive cooperative binding event and demonstrates that novobiocin and GA bind at discrete site on Hsp90. Our data further indicates that GA alters the structure of Hsp90FL such that the nonspecific component to novobiocin binding is no longer observed.

The examination of novobiocin binding in the presence of GA was then extended to an Hsp90CT surface. Novobiocin demonstrated exaggerated, atypical, binding responses

(Figure 15A) analogous to novobiocin responses for Hsp90CT in the absence of GA (Figure 8A). The binding isotherm did not demonstrate saturation (Figure 15B) in a manner similar to novobiocin responses for Hsp90CT in the absence of GA (Figure 8B). These results show that GA does not abrogate novobiocin's nonspecific binding component on Hsp90CT surfaces as it does on Hsp90FL surfaces (Figure 14). Subtraction of nonspecific binding from total binding revealed that saturable binding was achieved at concentrations approaching 6 mM (Figure 15C-D). The concentration of half maximal occupancy of Nb for Hsp90CT in the presence GA was equivalent to 1.86 ± 0.58 mM,, R^2 =0.99 (Figure 15D). The Hill plot of the Nb: Hsp90CT: GA responses (Figure 35E) depicted a straight line (*n*=1.0). Novobiocin binding to the C-terminal domain of Hsp90 in the presence of GA is therefore comprised of a large nonspecific component which can be subtracted from the total component to reveal a saturable hyperbolic binding component which is comparable to Nb: Hsp90CT responses in the absence of GA (Figure 8). Thus, novobiocin and GA do not compete for a discrete site of binding on recombinant Hsp90CT. The absence of a GA effect on the C-terminus for novobiocin, adds further support for the argument that binding of GA to the N-terminus induces a conformation in the C-terminus.

Effect of ATP on the Affinities of Novobiocin Derivatives:

Previous work has demonstrated that binding of nucleotide to Hsp90FL confers conformational changes which are distinct from GA (Sullivan et al., 1997, Sullivan *et al.*, 2002). In order to confirm the availability of the N-terminal nucleotide binding pocket for the Hsp90 immobilized on our chip, we injected varying concentrations of ATP over

the Hsp90 surface. Similar to our observations with GA binding to Hsp90, initial results yielded a poor binding response of less than 10 RU for 5 mM ATP, suggesting that the nucleotide binding pocket was not available, possibly due to steric conditions created by protein immobilization. However, after pretreatment of the protein surface with 0.01% Igepal (as described in Figure 9), 0.2 mM ATP yielded a significant binding response approximating 60 RU with a post injection baseline leveling off at 25 RU (Figure 16A). In a similar manner, we injected varying concentrations of ATP over an Hsp90CT surface, in order to test the hypothesis that a secondary C-terminal nucleotide binding pocket exists in the C-terminus of Hsp90, as prior literature has indicated (Soti *et al.*, 2002, Marcu et al., 2000a). However, 5.0 mM ATP did not produce a detectable binding response (Figure 16B). In contrast to Hsp90FL, pretreatment of the C-terminal surface with Igepal did not induce nucleotide binding.

Binding of Cm to Hsp90: ATP Complexes: In order to determine to effect of ATP on coumermycin binding, a series of Cm concentrations were co-injected over an Hsp90FL: ATP surface, as described in Figure 16. Cm demonstrated robust, concentration dependent binding responses (Figure 17A). Affinity analysis fitted one site of binding for the Cm: Hsp90FL: ATP interaction and calculated the K_D of Cm for Hsp90FL: ATP to be 49 ± 7 μM. A replot of the binding isotherm for coumermycin (Figure 17B) traced a hyperbola which saturated at a maximal concentration of 300 μM, while nonlinear regression of the data points estimated the K_D of Cm for the Hsp90FL:ATP conjugate to be 55 ± 20 μM, R^2 =0.99. A Hill plot of Cm response signals (Figure 17C) revealed a straight line with an estimated Hill coefficient of 1.0, R^2=0.99. From these results, we

conclude that coumermycin and ATP bind to distinct sites on Hsp90, we further conclude that ATP does not alter the affinity of coumermycin for Hsp90FL.

Although we were unable to directly demonstrate ATP binding to our Hsp90CT surface, we tested the hypothesis that a cryptic C-terminal nucleotide binding site may compete with coumermycin, in order to exclude the possibility that low levels of specific ATP binding to Hsp90CT were being masked through real time reference curve subtraction of high levels of nonspecific ATP binding to the control surface. Cm demonstrated robust, concentration dependent binding responses to the Hsp90CT surface in the presence of ATP (Figure 18A). Affinity analysis fitted one site of binding and calculated the K_D for the interaction to be 18.6 ± 10 μM. A replot of the binding isotherm for coumermycin (Figure 18B) traced a hyperbola which saturated at a concentrations spanning 320 and 640 μM, while nonlinear regression of the data points estimated the K_D of Cm for Hsp90CT in the presence of ATP additive to be 20 ± 10 μM, R^2 =0.99. A Hill plot of Cm response signals (Figure 18C) revealed a straight line with an estimated Hill coefficient of 1.0, R^2=0.99. This data indicates that coumermycin binds with similar affinity to Hsp90CT in presence of ATP as in absence of ATP. The inability to resolve ATP-binding to Hsp90CT, together with the lack of any effect of ATP on coumermycin binding to the C-terminal domain of Hsp90, suggests a number of possibilities: 1) coumermycin does not bind to the ATP-binding site in Hsp90CT; 2) Hsp90CT does not bind nucleotide; and/or 3) immobilized Hsp90CT may not adopt an ATP-binding competent conformation.

Binding of Cb to Hsp90: ATP Complexes: We expanded our investigation of the effect of ATP binding to the related compound, chlorobiocin. A series of chlorobiocin

concentrations were co-injected over an Hsp90FL: ATP surface (Figure 19). Chlorobiocin demonstrated robust, concentration dependent binding responses (Figure 19A). Affinity analysis calculated a high affinity K_{D1} = 40 ± 10 μM and a low affinity K_{D2} = 170 ± 20 μM. A replot of the binding isotherm for chlorobiocin (Figure 19B) showed a saturable sigmoidal curve, while nonlinear regression of the data points estimated the $K_{0.5}$ of Cm for the Hsp90FL:ATP conjugate to be 110 ± 20 μM, R^2 =0.99. A Hill plot of Cb response signals (Figure 19C) revealed a curved line with an estimated Hill coefficient of 2.0, R^2=0.99. The sigmoidal binding isotherm together with the S-shaped Hill plot substantiates a positive cooperative binding event and demonstrates that chlorobiocin and ATP bind to discrete sites on Hsp90FL. These results further show that ATP does not alter the affinity of chlorobiocin for Hsp90.

We similarly assayed chlorobiocin binding to the Hsp90CT in the presence of ATP (Figure 20A). A reproducible concentration dependent net drop in refractive index was observed upon chlorobiocin release (Figure 20A), in an analogous manner to Cb:Hsp90CT responses assayed in the absence of ATP (Figure 4A). Affinity analysis calculated a high affinity K_{D1} = 30 ± 5 μM and a low affinity K_{D2} = 110 ± 10 μM. Chlorobiocin displayed a sigmoidal binding isotherm (Figure 20B), which saturated at concentrations spanning 320 to 640 μM. The calculated concentration of half maximal occupancy was 68 ± 15 μM, R^2 =0.98. The Hill plot of Cb response signals (Figure 20C) revealed a curved line with an estimated Hill coefficient of 1.70, R^2=0.99. The sigmoidal binding isotherm together with the S-shaped Hill plot again confirms a positive cooperative binding event and demonstrates that chlorobiocin is not competed by ATP.

Binding of Nb to Hsp90: ATP Complexes: In order to determine if ATP affected binding of novobiocin to Hsp90FL, novobiocin was assayed as described in Figure 21. Novobiocin revealed concentration dependent response curves when applied to the Hsp90FL: ATP surface (Figure 21A), which were 3 times less robust than the novobiocin binding responses to apo-Hsp90FL (Figure 7A), yet similar to the binding responses observed for the Hsp90:GA curves (Figure 12A). Affinity analysis calculated a high affinity K_{D1} = 980 ± 80 μM and a low affinity K_{D2} = 2.1 ± 0.20 mM. A replot of steady state signals revealed a sigmoidal binding isotherm which saturated at concentrations ranging between 5 and 7 mM. (Figure 21B). The calculated concentration of half maximal occupancy of Nb for the Hsp90FL ATP conjugate was 1.5 ± 0.50 mM, R^2 =0.975. A Hill plot of the Nb: Hsp90FL: ATP interaction traced a curved lined with an estimated Hill coefficient of 2.0, R^2 =0.99. The sigmoidal binding isotherm together with the curved Hill plot confirms a positive cooperative binding event and demonstrates that novobiocin and ATP bind at discrete site on Hsp90. Our data further indicates that ATP alters the structure of Hsp90FL such that the nonspecific component to novobiocin binding is no longer observed.

In order to test the hypothesis that ATP competes for novobiocin binding on recombinant Hsp90CT, novobiocin binding was assayed in the presence of ATP as previously described (Figure 22). Novobiocin demonstrated exaggerated, atypical, binding responses (Figure 22A) analogous to novobiocin responses for Hsp90CT in the absence of ATP (Figure 8A). The binding isotherm did not demonstrate saturation (Figure 22B) in a similar manner to novobiocin responses for Hsp90CT in the absence of ATP (Figure 8B). These results show that ATP does not abrogate novobiocin's

nonspecific binding component on Hsp90CT surfaces as it does on Hsp90FL surfaces (Figure 21). Subtraction of nonspecific binding from total binding revealed that saturable binding was achieved at concentrations approaching 6 mM (Figure 22C-D). The concentration of half maximal occupancy of Nb for Hsp90CT was equivalent to 1.6 ± 0.7 mM, R^2 =0.97 (Figure 22D). The Hill plot of novobiocin-Hsp90CT responses in the presence of ATP (Figure 22E) depicted a straight line (*n*=1.0). Novobiocin binding to the C-terminal domain of Hsp90 in the presence of ATP is therefore comprised of a large nonspecific component which can be subtracted from the total component to reveal a saturable hyperbolic binding component which is comparable to novobiocin binding in the absence of ATP (Figure 8). Thus, novobiocin and ATP do not compete for a discrete site of binding on recombinant Hsp90CT.

Effect of ADP on the Affinities of Novobiocin Derivatives:

Earlier studies report that ADP confers structural transitions upon Hsp90 which are distinct from the structural rearrangements which are induced upon ATP and GA binding (Southworth & Agard, 2008, Zhang *et al.*, 2004). In order to assess the effect of ADP on the binding of our compounds, we first confirmed that ADP was able to bind to our Hsp90FL surface. ADP binding was unable to be determined until the nucleotide-binding competent conformation of Hsp90 was activated by 0.01% Igepal, as described for ATP and GA binding. ADP (0.5 mM) demonstrated a rapid binding response which did not achieve steady state during injection, and a slow, consistent release (Figure 23A), which differed the binding response of ATP (Figure 16A).

Former work indicates that hydrolysis of ATP does not occur in the C-terminus of Hsp90 and suggests that an ADP binding site does not reside in Hsp90CT (Soti et al., 2002). In order to test this hypothesis, ADP was injected onto Hsp90CT surfaces with and without 0.01% Igepal pretreatment. Consistent with previous reports (Soti et al., 2002), ADP binding could not be resolved on Hsp90CT surfaces (Figure 23B).

Binding of Cm to Hsp90: ADP Complexes: In order to assess the effect of ADP on the binding of coumermycin to Hsp90FL, a series of Cm concentrations were co-injected over an Hsp90FL: ADP surface, as described in Figure 24. Cm demonstrated robust, concentration dependent binding responses, which differed from Cm binding responses to Hsp90FL:ATP complexes and apo, in that, lower concentrations of Cm demonstrated a binding response, and, apparent saturation was achieved at 150 μM (Figure 24A). Analogous to the Cm:Hsp90FL:GA interaction, two binding constants could be fitted for the Hsp90FL: ADP surface. Affinity analysis calculated a high affinity K_{D1} = 1.5 ± 0.5 μM and a lower affinity K_{D2} = 7.5 ± 2 μM. In contrast to these results, only one binding constant could be fitted for the Cm: Hsp90:ATP and Cm: apo interactions (Figures 3 and 17). The hyperbolic binding isotherm for the Cm: Hsp90FL: ADP interaction revealed saturation at a maximal concentration of 150 μM, and nonlinear regression of these data points estimated the concentration of half maximal occupancy to be 3.6 ± 1.5 μM, R^2=0.98. A Hill plot of the Cm: Hsp90FL: ADP interaction (Figure 24C) revealed a straight line with an estimated Hill coefficient of 1.0, R^2=0.99. The hyperbolic binding isotherm together with the calculated Hill value of 1.0 substantiates a noncooperative binding event and demonstrates that coumermycin and ADP bind at discrete sites. These results also suggest that ADP acts to allosterically enhance the affinity of coumermycin

for Hsp90FL. Thus, ADP appears to induce conformation transitions in Hsp90FL which are distinct from both the apo conformation of Hsp90 and the ATP conformation of Hsp90, yet similar to the GA conformation of Hsp90.

As a negative control, coumermycin was assayed on an Hsp90CT surface in the presence of ADP (Figure 25A). Affinity analysis fitted one site of binding for the Cm: Hsp90CT in the presence of ADP and calculated the K_D to be 49 ± 7 μM, consistent with previous assays (Figures 4 and 18). Analogous to previous Cm: Hsp90CT interactions (Figures 4 and 18), a replot of Cm: Hsp90CT: ADP response curves demonstrated saturation at concentrations spanning 320 and 640 μM (Figure 25B). A Hill plot of Cm response signals (Figure 25C) revealed a straight line with an estimated Hill coefficient of 1.0, R^2=0.99. The consistency of these results as to previous Cm Hsp90CT results suggests that ADP does not influence the binding of coumermycin to Hsp90CT. Moreover, the absence of an ADP effect on the C-terminus is consistent with the hypothesis that binding of ADP to the N-terminus induces global structural rearrangements which are conferred to the C-terminus which promote coumermycin binding.

Binding of Cb to Hsp90: ADP Complexes: In order to assess the effect of ADP on the binding of chlorobiocin to Hsp90FL, a series of Cb concentrations were co-injected over an Hsp90FL:ADP surface, as described in Figure 26A. Affinity analysis calculated a high affinity K_{D1} = 15 ± 5 μM and a lower affinity K_{D2} = 30 ± 20 μM for Cb: Hsp90FL: ADP. The affinity of Cb for Hsp90FL: ADP was more avid than the affinity of Cb for Hsp90FL:ATP, Hsp90FL:GA, and apo-Hsp90. A replot of the binding response deviated from a rectangular hyperbola and saturated at concentrations spanning 400 and 800 μM

(Figure 26B). Nonlinear regression estimated the $K_{0.5}$ of Cb for the Hsp90FL:ADP complex to be 30 ± 20 μM. The Hill plot for this interaction shows a curved line with an estimated Hill value of 2.6 (Figure 26C). The non-hyperbolic binding isotherm together with the calculated Hill value of 2.6 substantiates a positive, cooperative binding event and demonstrates that chlorobiocin and ADP bind at discrete sites. These results further suggest that ADP allosterically enhances the affinity of chlorobiocin for Hsp90FL in a manner that differs from its allosteric effects on coumermycin (Figure 25) and lend credence to the hypothesis that the conformational changes induced by ADP alter binding affinities for novobiocin derivatives in the C-terminus of Hsp90.

Chlorobiocin was assayed on an Hsp90CT surface in the presence of ADP to assess the validity of the previous results (Figure 27A). Affinity analysis calculated a high affinity K_{D1} = 35 ± 5 μM and a lower affinity K_{D2} = 88 ± 10 μM for Cb: Hsp90FL: ADP, consistent with previous assays (Figures 6 and 20). Analogous to previous Cb: Hsp90CT interactions (Figures 6 and 20), a replot of Cb: Hsp90CT: ADP response curves demonstrated saturation at concentrations spanning 320 and 640 μM in a nonhyperbolic fashion (Figure 27B). A Hill plot of Cb response signals (Figure 27C) revealed a sigmoidal curve with an estimated Hill coefficient of 1.8, R^2=0.98. The consistency of these results as to previous Cb Hsp90Ct results suggests that ADP does not influence the binding of chlorobiocin to Hsp90CT. Moreover, the absence of an ADP effect on the C-terminus for chlorobiocin as well as for coumermycin provides further support in favor of the hypothesis that binding of ADP to the N-terminus induces a conformation in the C-terminus which augments the binding of novobiocin derivatives.

Binding of Nb to Hsp90: ADP Complexes: In order to assess the effect of ADP on the binding of novobiocin to Hsp90FL, a series of Nb concentrations were co-injected over an Hsp90FL: ADP surface, as described in Figure 28A. Similar to the Nb: Hsp90FL: ATP responses (Figure 21A), novobiocin Hsp90FL: ADP responses were approximately 3 times less robust than the novobiocin binding responses to apo-Hsp90 (Figure 7A). Unlike Nb: Hsp90FL: ATP responses, affinity analysis calculated a high affinity K_{D1} = 130 ± 30 μM and a lower affinity K_{D2} = 600 ± 200 μM for Nb: Hsp90FL: ADP. Analogous to the results obtained for coumermycin and chlorobiocin for Hsp90FL: ADP, the affinity of Nb for Hsp90FL: ADP was more avid than the affinity of Nb for Hsp90FL: ATP and apo Hsp90. The sigmoid binding isotherm for Nb:Hsp90FL:ADP demonstrated saturation at concentrations ranging between 4 and 8 mM (Figure 28B). Nonlinear regression estimated the $K_{0.5}$ of Nb for the Hsp90FL ADP complex to be 250 ± 50 μM. The Hill plot for Nb responses depict a curved line with an estimated Hill value of 3.0 (Figure 28C). The non-hyperbolic binding isotherm together with the calculated Hill value of 3.0 substantiates a positive, cooperative binding event and demonstrates that novobiocin and ADP bind at discrete sites on Hsp90. This data also indicates that ADP alters the structure of Hsp90 such that the nonspecific binding component to is not longer observed. However, the enhanced affinity of novobiocin for the ADP: Hsp90 complex further argues that ADP alters Hsp90 structure in a way that differs from both ATP and GA, as enhanced novobiocin affinity is not observed for Nb: Hsp90FL: ATP and GA interactions (Figures 21 and 14). These results additionally suggest that ADP allosterically enhances the affinity of chlorobiocin for Hsp90FL in a manner that differs from its allosteric effects on coumermycin (Figure 24) and lend credence to the

hypothesis that the conformational changes induced by ADP alter binding affinities for novobiocin derivatives in the C-terminus of Hsp90.

Novobiocin was assayed on an Hsp90CT surface in the presence of ADP to substantiate the Nb: Hsp90FL: ADP interaction. Novobiocin demonstrated exaggerated, atypical, binding responses (Figure 29A) analogous to previous novobiocin: Hsp 90CT responses (Figures 8A and Figures 22A). The binding isotherm did not demonstrate saturation (Figure 29B), consistent with previous Nb: Hsp90CT interactions (Figures 8B and 22B). Nonspecific subtraction revealed that saturable binding was achieved at concentrations approaching 6.4 mM (Figures 29C-D) comparable to prior Nb:Hsp90CT data (Figures 8 and 22). The concentration of half maximal occupancy was estimated to be 1.7 ± 0.69 mM, R^2 =0.97 (Figure 29D). The Hill plot of novobiocin:Hsp90CT responses in the presence of ADP (Figure 29E) depicted a straight line (*n*=1.0). The consistency of these results with previous Nb Hsp90Ct results suggests that ADP does not influence the binding of novobiocin to Hsp90CT. Furthermore, the absence of an ADP effect on the C-terminus for novobiocin as well as for both coumermycin and chlorobiocin advances the hypothesis that binding of ADP to the N-terminus induces a conformation in the C-terminus which induces the binding of novobiocin to the C-terminus.

Effect of ADP/ phosphate and ADP/ molybdate on Novobiocin Derivative Affinities for Hsp90:

Sullivan et al (2002) proposed that phosphate and molybdate may function structurally as the γ-phosphate of ATP when used in conjunction with ADP. In order to test this

hypothesis, we injected ADP in the presence of phosphate (Figure 30A) and/or molybdate (Figure37A). Binding responses were again unable to be detected until the protein surface had been pretreated with Igepal, as described above. ADP/ phosphate demonstrated a comparable binding response to ATP in that 0.25 mM ADP with phosphate additive yielded a significant binding response approximating 60 RU with a post injection baseline leveling off at 25 RU (Figures 30 A and 16A). Likewise, ADP/ molybdate demonstrated a maximal binding response approaching 120 RU with a post injection baseline leveling off at 80 response units analogous to the Hsp90FL: ATP response (Figures 37A and 16A). Both the ADP/ phosphate and the ADP/ molybdate response differed from the ADP response in that ADP demonstrated a slow, steady off to a zero baseline (Figure 23A). ADP/ phosphate and ADP/ molybdate were then assayed over an Hsp90CT surface under similar conditions. Binding responses could not be demonstrated on the Hsp90CT surface (Figures 30B and 37B).

Binding of Cm to Hsp90: ADP/ phosphate and Hsp90: ADP/ molybdate complexes: In order to assess the effect of ADP/ phosphate and ADP/ molybdate on the binding of coumermycin to Hsp90FL, a series of Cm concentrations were co-injected over an Hsp90FL: ADP/ phosphate or an Hsp90FL: ADP/ molybdate surface (Figures 31A and Figure 38A, respectively). Cm demonstrated robust, concentration dependent binding to both Hsp90FL: ADP/ phosphate (Figure 31B) and Hsp90FL: ADP/ molybdate (Figure 38B), which saturated at concentrations spanning 320 and 640 μM consistent with Cm: Hsp90FL and CM: Hsp90FL: ATP interactions. Calculated binding constants of Cm for Hsp90FL: ADP/ phosphate and Hsp90FL: ADP/ molybdate were 25 ± 10 μM and 33 ±

15 μM, respectively. Hill plots for both interactions depicted straight lines with calculated Hill values of 1.0 (Figures 31C and 38C). The similarity of these results to the Cm: Hsp90: ATP and the Cm :apo results combined with the dissimilarity of these results from Cm: Hsp90:ADP results suggests that ADP/ phosphate and ADP/ molybdate stabilize an Hsp90 conformation which is different from the ADP conformation.

Binding of Cb to Hsp90: ADP/ phosphate and Hsp90: ADP/ molybdate complexes: Our analysis on the effect of ADP/ phosphate and ADP/ molybdate on the binding of coumarin compounds was then extended to chlorobiocin. Cb demonstrated robust, concentration dependent binding to both Hsp90FL: ADP/ phosphate (Figure 33 A &B) and Hsp90FL: ADP/ molybdate (Figure 39A &B), which saturated in a nonhyperbolic fashion at concentrations spanning 320 and 640 μM consistent with Cb: Hsp90FL, Cb: Hsp90FL: ATP and Cb: Hsp90: GA interactions. Calculated binding constants of Cm for Hsp90FL: ADP/ phosphate and Hsp90FL: ADP/ molybdate were: K_{D1} = 35 ± 8 μM and K_{D2} = 145 ± 20 μM, and K_{D1} = 30 ± 8 μM and K_{D2} = 125 ± 20 μM, respectively. Hill plots for both interactions were sigmoidal with average Hill values of 1.45 (Figures 33C and 39C). The similarity of these results to the Cm: Hsp90:ATP and the Cm :apo-Hsp90 results combined with the dissimilarity of these results from Cm: Hsp90:ADP results suggests that ADP/ phosphate and ADP/ molybdate stabilize an Hsp90 conformation which is distinct from the ADP conformation of Hsp90.

Binding of Nb to Hsp90: ADP/ phosphate complexes and Hsp90: ADP/ molybdate complexes: The effect of ADP/ phosphate and ADP/ molybdate was further determined on the binding of novobiocin to Hsp90FL. Nb demonstrated robust, concentration dependent binding to both Hsp90FL: ADP/ phosphate (Figure 35 A &B) and Hsp90FL:

ADP/ molybdate (Figure 40A &B), which saturated in a nonhyperbolic fashion at concentrations spanning 4 and 8 mM consistent with Nb: Hsp90FL: ATP and Nb: Hsp90FL: GA interactions. Calculated binding constants of Nb for Hsp90FL: ADP/ phosphate and Hsp90FL: ADP/ molybdate were: K_{D1} = 900 ± 100 μM and K_{D2} = 2.2 mM ± 0.25 mM, and K_{D1} = 750 ± 100 μuM and K_{D2} = 2.3 ± 0.2 mM, respectively. Hill plots for both interactions were sigmoidal with average Hill values of 1.5 (Figures 35C and 40C). The similarity of these results to the Cm: Hsp90: ATP and the Cm: apo results combined with the dissimilarity of these results from Cm: Hsp90: ADP results suggest that ADP/ phosphate and ADP/ molybdate stabilize an Hsp90 conformation which is different from the ADP conformation. These results further support that hypothesis that phosphate and molybdate act as a γ-phosphate analog.

Competition Assays: In order to determine if the compounds, coumermycin, chlorobiocin, and novobiocin compete for a single site of binding, the protein surface was equilibrated in running buffer containing excess competitor, while the compound of interest was assayed over the surface (Figure 41). Coumermycin (320 μM) was unable to bind to Hsp90 surfaces pre-equilibrated with the indicated concentrations of chlorobiocin and novobiocin (Figures 41A and B). Likewise, chlorobiocin (640 μM) demonstrated no net response on surfaces equilibrated with the indicated concentrations of coumermycin and novobiocin (Figures 41C and D). Further, 4 mM novobiocin was unable to bind to Hsp90 pre-bound to the indicated concentrations of coumermycin and chlorobiocin (Figures 41E and F). The ability of these compounds to compete each other in this assay suggests that these novobiocin derivatives bind to a common discrete site on Hsp90.

Negative Controls:

Dicoumarol Binding: To rule out the possibility that Hsp90 promiscuously binds all small molecules with a conjugated ring structure, we assayed the binding of the chemically related compound, dicoumarol, to both Hsp90FL and Hsp90CT. Dicoumarol did not demonstrate binding to Hsp90FL or Hsp90CT surfaces (Figures 42 A1 and A2). Thus, the binding of coumermycin, chlorobiocin, and novobiocin appears to represent a specific binding response to the C-terminal domain of Hsp90.

Coumarin Compounds Do No Bind Cochaperone Cdc37: To further demonstrate specificity of coumarin antibiotics for Hsp90 and to rule out the possibility that their previously reported depletion of signaling kinases (Burlison & Blagg, 2006) was not due to the combinatorial effects of cochaperone inhibition, we assayed Cm, Cb, and Nb over a Cdc37 surface, as described in Figure 42B. The indicated concentrations of Cm, Cb, and Nb did not produce a binding response to Cdc37 (Figures 42B1, B2, &B3), further substantiating the specificity of these compounds for Hsp90.

DISCUSSION

Coumarin Derivatives Bind to the C-terminus of Hsp90:

Data presented in this thesis suggests that one or more binding sites for novobiocin and related coumarins reside on Hsp90CT. This conclusion is based on the observation that coumermycin demonstrated comparable affinity for both Hsp90FL and Hsp90CT (Tables 1 & 2). Similarly, chlorobiocin showed equivalent affinities for both Hsp90FL and Hsp90CT (Tables 1 & 2). Two sites of binding could also be fitted for chlorobiocin for both the full length protein and the C-terminal construct. Chlorobiocin additionally exhibited the same degree of positive cooperative binding for both Hsp90FL and Hsp90CT (n=1.7). Further, novobiocin exhibited similar affinities for both Hsp90FL and Hsp90CT (Tables 1 & 2). Moreover, novobiocin and related compounds did not bind to the Hsp90 N-terminal nucleotide binding pocket (Figures 17, 19 & 21).

Our conclusion is consistent with previous work, which suggests the existence of an Hsp90 binding site for novobiocin and related coumarin antibiotics based on a number of indirect assays (Yun *et al.*, 2004, Marcu *et al.*, 2000a, Marcu *et al.*, 2000b, Burlison & Blagg, 2006, Allan *et al.*, 2006). Incubation of rabbit reticulocyte lysate and or cell culture lysate with novobiocin quantitatively decreased the amount of p23 and Hsp70 which coimmunoadsorbed with Hsp90 (Marcu et al., 2000a, Yun et al., 2004). Novobiocin also reduced the levels of Hsp90 dependent signaling proteins, p53, Raf-1, and to a lesser extent $p185^{erbB2}$ in SKBR3 cells, while, the related coumarin compounds, chlorobiocin and coumermycin, induced the degradation of Hsp90 dependent clients, Raf-1 and $p185^{erbB2}$/Her2 (Marcu et al., 2000a, Marcu

et al., 2000b, Burlison & Blagg, 2006, Allan *et al.*, 2006). Pretreatment of cell lysates with increasing amounts of novobiocin also lead to an inability to recover Hsp90 in complex with immunophillins (Yun et al., 2004). Both novobiocin and coumermycin depleted glucocorticoid receptors in HeLA cells (Allan et al., 2006), while novobiocin inhibited the co adsorption of Hsp90 and Cdc37 from heme-regulated eIF2α kinase (HRI) in rabbit reticulocyte lysate (Yun et al., 2004). Thus, the inhibition of chaperone function in presence of these compounds suggests a direct biophysical interaction between coumarin molecules and the Hsp90 chaperone machinery.

Our conclusions regarding the existence of an Hsp90 binding site for coumarin molecules are also consistent with studies with purified Hsp90 constructs (Marcu et al., 2000b, Allan et al., 2006, Marcu et al., 2000a, Yun et al., 2004, Langer *et al.*, 2002). Langer and coworkers showed that increasing concentrations of novobiocin inhibited the autophosphorylation of purified Hsp90 (Langer *et al.*, 2002). Pre-addition of novobiocin to both recombinant Hsp90FLβ and Hsp90CTβ increased the rate of aggregation of rhodanese in chaperone activity assays for both Hsp90FL and Hsp90CT (Allan et al., 2006). Moreover, pretreatment of purified recombinant His- tagged full length Hsp90β or His-tagged C-terminal Hsp90β with increasing concentrations of novobiocin led to the inability to detect subsequently added GST-tagged immunophilins by ELISA (Allan et al., 2006).

Novobiocin was additionally shown to bind purified, recombinant Hsp90FL in complex with geldanamycin Sepharose resins (Marcu et al., 2000b). Novobiocin and the related coumarin, coumermycin, also bound Hsp90α coated magnetic beads (Marszall *et al.*, 2008b). Further, purified recombinant Hsp90CT bound to novobiocin sepharose resins, and novobiocin was shown to compete recombinant Hsp90CT from ATP-linked Sepharose resins (Marcu *et al.*,

2000b, Marcu *et al.*, 2000a). Yun et al similarly demonstrated that the recombinant Hsp90 C-terminus became resistant to trypsinolysis in protease nicking assays in the presence of increasing concentrations of novobiocin (Yun et al., 2004). Further, increasing concentrations of coumermycin inhibited the chemical crosslinking of Hsp90CTβ (Allan *et al.*, 2006). The above results not only support our conclusion that Hsp90 possesses a binding site for coumarin compounds; they argue in favor of our conclusion that the binding site for coumarin antibiotics resides on the C-terminus of Hsp90.

The affinities obtained for the compounds in this study are consistent with previously published data suggesting the chlorobiocin and coumermycin are 5 to 10 times more effective than novobiocin, respectively, in inhibiting Hsp90 chaperone function (Burlison & Blagg, 2006, Marcu et al., 2000b, Galam *et al.*, 2007, Yun et al., 2004, Marcu et al., 2000a). Chlorobiocin and coumermycin have been reported to induce maximal depletion of the Hsp90 dependent oncogenic proteins Raf-1 and $p185^{erbB}$ at concentrations of 500 µM and 100 µM, respectively, whereas maximal depletion of Raf-1 and $p185^{erbB}$ was not observed until novobiocin concentrations approached 1 mM (Marcu et al., 2000b), Analogously, coumermycin caused Hsp90 dependent depletion of the oncogenic client, Her2, at half maximal concentrations of 1 µM, while novobiocin depleted Her2 at half maximal concentrations of 300 µM (Burlison & Blagg, 2006). Millimolar concentrations of novobiocin have been demonstrated to inhibit the coimmunoadsorption of p23 and Hsp70 with Hsp90 from rabbit reticulocyte lysate (Marcu et al., 2000a, Yun et al., 2004, Allan et al., 2006). Similarly, 2 -5 mM novobiocin was shown to inhibit co-precipitation of FKBP52 and PP5 with Hsp90 (Yun et al., 2004). Further, Yun et al demonstrated that 1-5 mM novobiocin abrogates the maturation of Hsp90, client, heme regulated eIF2α kinase (HRI), as evidenced by the absence

of HRI's autophosphorylation activity (Yun *et al.*, 2004). Moreover, the IC_{50}'s for coumarin compounds' inhibition of the Hsp90-dependent renaturation of denatured luciferase in rabbit reticulocyte lysate have been reported to be 400 μM, 60 μM, and 40 μM for novobiocin, chlorobiocin, and coumermycin, respectively (Galam *et al.*, 2007). The above results are consistent with the average binding constants for novobiocin (1.4 mM), chlorobiocin (75 μM), and coumermycin (40 μM) calculated for Hsp90FL in this study.

The work of Marszall et al (2008), however, contradicts our findings. Affinities for novobiocin and coumermycin were determined using a frontal chromatography system, in which serial concentrations of the compounds were injected in mobile phase and the various retention volumes were used to calculate binding affinities for Hsp90, which was covalently immobilized to an APS resin (Marszall *et al.*, 2008a). In contrast to our estimated average affinities of novobiocin and coumermycin for Hsp90FL of 1.4 mM and 40 μM, respectively, Marszall et al reported IC_{50}s of approximating 100 nM for novobiocin and 200 nM for coumermycin (Marszall et al., 2008a),. Further, these authors report no nonspecific binding component of novobiocin to Hsp90 while our data shows extensive nonspecific binding of novobiocin to Hsp90 in the absence of N-terminal ligand (Figure 7). While these discrepancies might be rationalized by the different Hsp90 isoforms assayed, Marszall and coworkers assayed binding to Hsp90α, whereas we assayed binding to Hsp90β (Marszall et al., 2008a), this is unlikely as we also assayed binding of the drugs to the Hsp90CT construct of the α-isoform of Hsp90. Differential results could also be resolved on the basis of differences in experimental techniques. We coupled Hsp90 to a planar surface at pH 8.0, whereas Marszall and colleagues report coupling their Hsp90 construct to a three dimensional resin at pH 6.0 (Marszall et al., 2008a). The exposure of Hsp90 to a lower pH may have altered the

conformation of Hsp90, hiding exposed regions of the protein susceptible to nonspecific interaction with novobiocin and increasing the affinity of Hsp90 for both novobiocin and coumermycin. Alternatively, immobilization of Hsp90 onto a planar surface may have loosened Hsp90 structure thereby promoting nonspecific Hsp90: Nb interactions and lowering Hsp90's affinity for both compounds.

However, it is difficult to understand how the authors could make an accurate estimate of the binding affinities for novobiocin and coumermycin when the highest concentration of drug utilized in their assays failed to approach previously report affinities and in no manner approached saturation. Further, the authors failed to demonstrate specificity. Their results are likely an artifact. These discrepancies, however, remain unresolved and require further investigation by other techniques.

Coumarin Derivatives Demonstrate Specificity for Hsp90

Our results indicate that coumarin derivatives bind Hsp90 with specificity. This conclusion is based on the observations that novobiocin and related coumarins compete with each other for binding (Figure 41) and that the structurally related compound, dicoumarol, did not demonstrate binding to Hsp90FL or Hsp90CT (Figure 42, A1 & A2). Since Hsp90 has been reported to be in equilibrium between conformational states and that binding of ligand has been shown to shift this conformational equilibrium (Shiau *et al.*, 2006, Krukenberg *et al.*, 2008), we cannot exclude the possibility that pre-binding of coumarin derivative A to Hsp90 does not alter Hsp90 conformation and thereby mask a secondary binding site for coumarin derivative B. However, the simplest conclusion is that novobiocin derivatives share a common site of binding located in the C-terminal domain of Hsp90.

Our binding results for dicoumarol disagree with previously published results, in which dicoumarol was observed to inhibit the renaturation of denatured luciferase in HCT116 cells, deplete cells of the Hsp82 clients Erb2/Her2, Akt, and securin, and induce apoptosis (Hernandez *et al.*, 2008). Perhaps this discrepancy resides from possibility that dicoumarol is chemically modified in biological systems and this chemical modification facilitated the *in vivo* inhibition of Hsp90 machinery which cannot be reproduced *in vitro*. Alternatively, the dicoumarol induced depletion of Hsp90 clients demonstrated in the previous assay could be explained by the observation that dicoumarol has been shown to induce the production of the mitochondrial reactive oxygen species, superoxide and hydrogen peroxide, through its inhibition of the two electron reductase NADPH quinone oxidoreductase and mitochondrial quinone mediated electron transfer (Du *et al.*, 2006). Likely, these differential results reflect the differences in techniques utilized. These inconsistencies remain to be explored further.

However, it should be noted that dicoumarol-induced decrease in securin expression reported by Hernandez and colleagues correlated with a decrease in the level of expression of its mRNA. Hsp90 inhibitor-induced decrease in client protein levels is a consequence of their ability to inhibit the folding of nascent protein and in some cases inhibit Hsp90's stabilization of the mature active protein, leading to their degradation via the proteasome (Whitesell & Lindquist, 2005). Suppression of the transcription of the mRNA encoding an Hsp90 dependent client is not a hallmark of Hsp90 inhibition.

Binding of Nucleotide Hsp90FL:

Our nucleotide binding data is consistent with current models (Mickler *et al.*, 2009, McLaughlin et al., 2004, Hessling et al., 2009). Binding of ATP, ADP/ phosphate, and ADP/

molybdate to Hsp90 demonstrate comparable responses (Figures 16A, 30A, &37A). We rationalize that both phosphate and molybdate mimic the gamma phosphate of ATP and facilitate the stabilization of a range of ATP conformations (Sullivan *et al.*, 2002). We demonstrate a rather fast initial on rate in which we conclude ATP, ADP/ phosphate, and ADP/ molybdate bind to an open conformation of Hsp90. We hypothesize that during and after injection the conformation of "I_2" is being stabilized (Hessling et al., 2009, McLaughlin *et al.*, 2004). The initial rapid drop within the first 10 seconds after the injection ceases suggests that the "I_2" conformation of ATP bound Hsp90 represents a relaxed transition state in which a large population of Hsp90 conformers are in an open lid conformation. Consequently, ATP is readily able to diffuse. Seconds 250-260 represent the transition from I_2 to a closed Hsp90conformation for the ATP and ADP/ phosphate curves, while seconds 520-530 correspond to this transition for the ADP/ molybdate curve. The steady 25 response units (RUs) that are observed for ATP and ADP/ phosphate after 260 seconds have transpired corresponds to the stable N-terminally dimerized closed conformation, while the positive 85 response units following 600 seconds represents the closed conformation of Hsp90:ADP/ molybdate. Moreover, 25 RU is consistent with the percentage of ATP which are committed to slow hydrolysis (Mickler *et al.*, 2009, Hessling et al., 2009, McLaughlin et al., 2004), while the 25 RU (Figure 30A) and the 85 RU(Figure 37A) correspond to the percentage of ADP/ phosphate and ADP/ molybdate which are trapped by Hsp90. Conversely, the ADP binding response revealed a rapid on rate which did not approach steady state during injection and a slow steady off which did not demonstrate a positive baseline plateau (Figure 13A).

Novobiocin and Related Coumarins Do Not Bind to the N-terminal Nucleotide Binding

Pocket:

Our results support the conclusion that apo-Hsp90 and Hsp90: ATP complexes are distinct Hsp90 conformations which bind coumarin derivatives with equivalent affinities. This conclusion is based on the following observations: (1) Coumermycin exhibits similar affinities for the Hsp90: ATP complex as it does for uncomplexed Hsp90 (Table 1). (2) Chlorobiocin and novobiocin demonstrate comparable affinities for Hsp90 in complex with ATP as they do for apo (Table 1). (3) Both chlorobiocin and novobiocin exhibited cooperative binding for both interactions with estimated Hill coefficients of 1.85 and 1.65, respectively. (4) Binding data for the Nb: Hsp90FL: ATP interaction indicated that ATP eliminates the nonspecific binding that was observed in the Nb: apo Hsp90 interactions.

These results suggest the conclusion that novobiocin nonspecifically binds to charged residues within the N-terminal domain, as novobiocin has been shown to bind to highly basic amino acid residues in a nonspecific manner (Cotten *et al.*, 1986). Because the linker which connects the N-terminus with the middle domain consists of a highly unstructured region of charged amino acid residues which are extended in the absence of N-terminal ligand (Krukenberg *et al.*, 2009, Pearl & Prodromou, 2006, Krukenberg *et al.*, 2008), we hypothesize that ATP restricts the conformation freedom of the charged linker region and leads to a compaction of the linker such that it is no longer available to nonspecifically interact with novobiocin. Our results are consistent with current models which suggest that ATP stabilizes a tense conformation of Hsp90 (Chadli *et al.*, 2000, Graf *et al.*, 2009, McLaughlin *et al.*, 2004, Hessling *et al.*, 2009, Mickler *et al.*, 2009, Prodromou *et al.*, 2000, Maruya

et al., 1999), while apo Hsp90 exists in at least two extended conformations which are in dynamic equilibrium (Bron *et al.*, 2008, Krukenberg et al., 2008).

Our data is also consistent with the conclusion that phosphate and molybdate function structurally as a γ-phosphate analog (Sullivan et al., 2002), which together with ADP induce the formation of a range of ATP conformations. Coumermycin, chlorobiocin, and novobiocin bind to ADP/ phosphate and ADP/ molybdate liganded Hsp90 complexes (Figures 31-35 & 38-40) with comparable affinities to Hsp90 ATP complexes and apo. ADP/ phosphate and ADP/ molybdate abrogated the nonspecific binding component of novobiocin in a manner suggestive of ATP (Figures 35, 39 & 21). The similarities of the affinities of coumarin derivatives for Hsp90FL:ADP/ phosphate, Hsp90FL:ADP/ molybdate, and Hsp90FL:ATP complexes coupled with the dissimilarly of their affinities for Hsp90FL:ADP complexes (see discussion below) together with the comparable responses of ATP, ADP/ phosphate, and ADP/ molybdate (Figures 14A, 28A, & 35A) for Hsp90FL suggests that ADP/ phosphate and ADP/ molybdate facilitate an assortment of Hsp90 conformations which is distinct from Hsp90:ADP conformations yet comparable to Hsp90: ATP conformations.

Our results additionally indicate that geldanamycin stabilizes a population of Hsp90 conformers which are distinct from apo and Hsp90: ATP conformers. This conclusion is based on observation that GA increased the affinity of the dicoumarin, coumermycin, for Hsp90FL by opening a higher affinity binding site as indicated by the high affinity binding constant 3.3 ± 5 μM and low affinity binding constant 20 ± 15 μM (Figure 10). These results contrast with the previously described lower

affinities of Cm for apo and Hsp90FL: ATP, Hsp90FL: ADP/ phosphate, and Hsp90FL: ADP/ molybdate complexes. GA eliminated the nonspecific binding component of novobiocin in a manner reminiscent to ATP, ADP/ phosphate and ADP/ molybdate. Affinities of novobiocin and of the novobiocin derivative, chlorobiocin, for the Hsp90: GA complex approximated the affinities for apo Hsp90 and Hsp90: ATP complexes, ($K_{0.5}$ =1.3 mM ± 200 μM and $K_{0.5}$ =120 μM ± 20 μM, respectively). We therefore conclude that geldanamycin binds to the nucleotide binding site and allosterically induces a conformational change such that the affinity of coumermycin is enhanced and the conformational freedom of the charged linker region is restricted resulting in an overall compaction of the protein as evidenced by the absence of novobiocin nonspecific interactions.

Our results are consistent with previous biochemical and structural characterizations (Zhang *et al.*, 2004, Phillips *et al.*, 2007). H/D exchange suggests that binding of N-terminal inhibitors to the nucleotide binding pocket stabilized a differential conformational state of Hsp90 in which the interface between the C-terminal, middle, and N-terminal domains has been tightened (Phillips *et al.*, 2007). Similarly, small angle x-ray scattering (SAXS) indicates a reduction in Hsp90 hydrodynamic radius upon complexation with geldanamycin (Zhang *et al.*, 2004).

ADP Allosterically Enhances Affinity of Coumarin Derivatives for Hsp90FL:

Our results further indicate that ADP stabilizes a conformation of Hsp90 which is distinct from the GA, ATP, ADP/ phosphate, ADP/ molybdate, and apo Hsp90 conformations. This rationalization is based on our results which demonstrate that ADP

enhances the affinity of coumarin derivatives for Hsp90FL (Figures 24, 26, 28). ADP increased the affinities of coumermycin and novobiocin for Hsp90 by a factor of 15 (3.6 ± 1.5 μM versus 50 ± 10 μM, and, 250 ± 50 μM versus 3.3 mM ± 0.9 mM), respectively. Likewise, ADP enhanced the affinity of chlorobiocin for Hsp90 by a factor of 4 (30 ± 20 μM versus 100 ± 20 μM). Analogous to GA, ADP induced the opening of a higher affinity binding site for the larger dicoumarin compound, coumermycin, with the two sites binding in a noncompetitive fashion as suggested by the Hill coefficient of 1.0 (Figure 24C). In contrast to GA, ADP appears to have increased the cooperativity of the smaller structured molecules, chlorobiocin and novobiocin, as evidenced by the increase in Hill coefficients from 1.7 to 2.6 and 1.3 to 3.0, respectively. Moreover, ADP appears to eliminate the nonspecific binding effects of novobiocin observed in the absence of ADP analogous to both GA and ATP. Thus, we conclude that ADP alters the conformation of Hsp90 leading to changes in the conformation of the N-terminus such that nonspecific binding sites are no longer exposed. N-terminal conformational changes are then conferred to the C-terminus resulting in the allosteric enhancement of the affinity of coumarin derivatives. Our results are consistent with a host of experimental data (e.g., X-ray crystallography, EM, and HD-exchange studies) that indicate that the ADP-bound conformation of Hsp90 is distinct from Hsp90's apo and ATP-bound conformations (Southworth & Agard, 2008, Shiau et al., 2006, Graf et al., 2009, Hessling et al., 2009, Krukenberg et al., 2008).

Our results further support the conclusion that it is the docking of N-terminal ligand that induces the conformational change in the C-terminus which alters the affinity of coumarin derivatives. This conclusion is based on the observations that GA and ADP

did not bind to the Hsp90 C-terminal truncation (Figures 9B and 23B). Moreover, assays of coumarin derivatives on the C-terminus in the presence of GA and/or ADP produced equivalent results to binding assays of the C-terminus in the absence of these additives. Furthermore, addition of ADP or GA did not abrogate the nonspecific component of novobiocin binding to Hsp90CT (Figures 15 and 29). Our results are consistent with earlier work which suggests the absence of binding sites for ADP and/or GA on the C-terminal domain of Hsp90 (Prodromou *et al.*, 1997a, Soti et al., 2002, Stebbins *et al.*, 1997, Marcu et al., 2000a, Marcu et al., 2000b).

Novobiocin and Chlorobiocin Induce Conformational Transitions on Recombinant Hsp90CT:

As previously described, novobiocin exhibited significant nonspecific binding to both Hsp90FL and Hsp90CT (Figures 7& 8). Whereas we concluded that the nonspecific binding component of novobiocin on Hsp90FL was due to the extended charged linker connecting the N and middle domains, we rationalize that the nonspecific binding component of the Nb: Hsp90CT interaction originates from the composition of our C-terminal truncation which consists of a string of approximately 20 amino acid residues from the middle domain, which we hypothesize to be unstructured and susceptible to nonspecific interaction. Moreover, this unstructured region may not facilitate cooperative binding of Nb to Hsp90CT. While Nb binds to Hsp90FL in a cooperative manner and confirms the existence of more than one site of binding for the full length interaction, the calculated Hill value of 1.0 together with the extensive nonspecific binding observed for Hsp90 CT does not facilitate the discernment between one and two- site binding for

Hsp90CT. However, photoactive novobiocin analogs were observed to crosslink to the Hsp90 C-terminus at 2 positions (Robert Matts personal communication), and novobiocin was shown to inhibit this crosslinking (Steve Hartson personal communication), suggesting that novobiocin binds to more than one site on both Hsp90CT and Hsp90FL.

Our results suggest that novobiocin responses for Hsp90 CT were not governed by the laws of simple mass action. This conclusion is based on the concentration dependent spikes, plateaus, and valleys apparent upon each novobiocin injection (Figure 8), which we propose represents four states and at least two apparent conformations of Hsp90CT. During the first 10 seconds of injection (Figure 8), the initial binding response depicts a rapid spike in response to novobiocin binding to apo-Hsp90CT (Winzor, 2003). While seconds 15 - 20 depict the transition from the more extended Hsp90CT:novobiocin complex to a less extended Hsp90CT:novobiocin complex. As novobiocin binding continues, Hsp90CT is observed to occupy a smaller fractional volume (a plateau), which is stabilized during the remainder of the injection (seconds 20-60). After novobiocin release, Hsp90CT remains in the more compact conformation, as evidenced by the negative response spanning 65 and 75 seconds (the valley), and returns to its original pre novobiocin conformation as represented by the zero response following 80 seconds (Figure 8). These results are consistent with ligand-induced global conformational transitions (Flatmark *et al.*, 2001, Gestwicki et al., 2001, Winzor, 2003)

Similarly, our results suggest that chlorobiocin responses for Hsp90CT were not ruled by simple mass action, as suggested by net negative signal that is stabilized after chlorobiocin release from Hsp90 CT. We propose that this net negative signal represents a distinct chlorobiocin induced conformation of Hsp90CT, which reflect a decrease in

Hsp90CT hydrodynamic radius upon chlorobiocin binding and release (Figure 6). These atypical binding responses are consistent ligand-induced conformational shifts (Flatmark *et al.*, 2001, Gestwicki et al., 2001, Winzor, 2003).

ATP Does Not Bind to Recombinant Hsp90CT:

Our results suggest that a secondary nucleotide binding pocket does not reside on the C-terminus of Hsp90. This conclusion was based on a complement of four observations: (1) binding of ATP, ADP/ phosphate and ADP/ molybdate to Hsp90CT was not observed (Figures 16B , 30B and 37B), (2) secondary nucleotide binding to Hsp90FL: GA complexes was unable to be demonstrated (data not shown), (3) assays of coumarin derivatives on the C-terminus with additives, ATP, ADP/ phosphate, and/or ADP/ molybdate, produced equivalent results as binding assays to apo Hsp90CT (Table 1), and (4) ATP, ADP/ phosphate, and/or ADP/ molybdate addition did not mitigate the nonspecific binding component of novobiocin (Figures 22, 29, and 36).

Our conclusions, however, are inconsistent with previous work that suggests the existence of a secondary ATP binding site on the C-terminal domain of Hsp90 (Soti et al., 2002, Marcu et al., 2000a, Marcu et al., 2000b, Garnier *et al.*, 2002, Callebaut *et al.*, 1994). Scanning differential calorimetry, fluorescence spectroscopy, and isothermal titration calorimetry on the *in vivo* function of Hsp90 and a recombinant C-terminal truncation indicate that a second ATP binding site resides in the carboxyl terminus (Callebaut *et al.*, 1994, Garnier *et al.*, 2002). Previous oxidative nucleotide-affinity cleavage assays showed that the occupation of the N-terminal nucleotide binding pocket with GA or radicicol exposed a C-terminal ATP binding site (Soti et al., 2002). The C-

terminus of Hsp90 has also been observed to interact with both purines and pyrimidines (Soti et al., 2002). Further, novobiocin has been observed to block the binding of ATP to both the N-terminal and the C-terminal sites (Soti et al., 2002) and compete recombinant Hsp90 CT from ATP-linked Sepharose resins (Marcu et al., 2000a, Marcu et al., 2000b).

The disparities between our results and previously reported results likely reflect the different techniques utilized. Although we were unable to demonstrate a positive nucleotide binding response to the C-terminus of Hsp90, it cannot be ruled out that alternative conformations of Hsp90CT may induce the binding of ATP to recombinant Hsp90CT. Additionally, steric conditions created by protein immobilization may have restricted the conformational freedom necessary to bind C-terminal nucleotide, thereby explaining the discrepancy in our results from previous findings. These important questions remain unanswered and require further investigation by other means.

CONCLUSIONS

It has been proposed that the Hsp90 chaperone cycle can be utilized to identify small molecule inhibitors which selectively affect different states of the Hsp90 cycle (Mayer *et al.*, 2009, Whitesell & Lindquist, 2005). This study demonstrates that novobiocin and related coumarins bind preferentially to the ADP conformation of Hsp90 *in vitro*. Our study also suggests that Igepal loosens an "autoinhibitory" conformation of Hsp90 to facilitate the binding of N-terminal ligands. We propose that Igepal may function as an *in vitro* pseudo-substrate which lowers the energy barrier necessary to bind N-terminal ligand in a manner consistent with current models of cochaperone regulation of the ATPase cycle (Abbas-Terki *et al.*, 2002, Pearl & Prodromou, 2000, Pearl & Prodromou, 2006, Terasawa *et al.*, 2005, Buchner, 1999). We further propose a model in which binding of N-terminal ligands to the Igepal-facilitated conformation of Hsp90 causes a structuring of the charged linker connecting the N-terminal and middle domains thereby leading to a reduction in the hydrodynamic radius of Hsp90 (Figure 43). This model, while consistent with previous work (Zhang et al., 2004, Sullivan *et al.*, 1997, Shiau et al., 2006, Mickler et al., 2009, Krukenberg et al., 2008, Hessling et al., 2009, Graf et al., 2009), is based on the observation that the presence of bound N-terminal ligand abolished the nonspecific binding component to novobiocin**.**

FUTURE DIRECTIONS

With the current lack of a crystal structure for the eukaryotic Hsp90 C-terminal domain, it is difficult to definitively ascertain the site of binding for novobiocin and related compounds. Recent computational modeling suggests a probable binding site for novobiocin and related coumarins to be localized between H18 and H20-H21 on the Hsp90 C-terminal domain (Sgobba *et al.*, 2008). However crystallization and mutational analyses have yet to confirm this conclusion. Therefore, important future and current work includes obtaining the structural and biochemical data necessary to elucidate of the site of binding for novobiocin related compounds. Important future work additionally includes the elucidation of the mechanisms by which C-terminal ligand binding induces conformational changes and contributes to the inhibition of chaperone function. The determination of the mechanisms by which novobiocin compounds bind to the C-terminus and compete for binding site(s), together with structural data regarding the architecture of the binding pocket will lead to the development of higher affinity pharmacological derivatives for the treatment of cancer and related illnesses and will assist in the deconvolution of the biochemical mechanism by which Hsp90 facilitates the maturation of protein substrates.

FIGURES

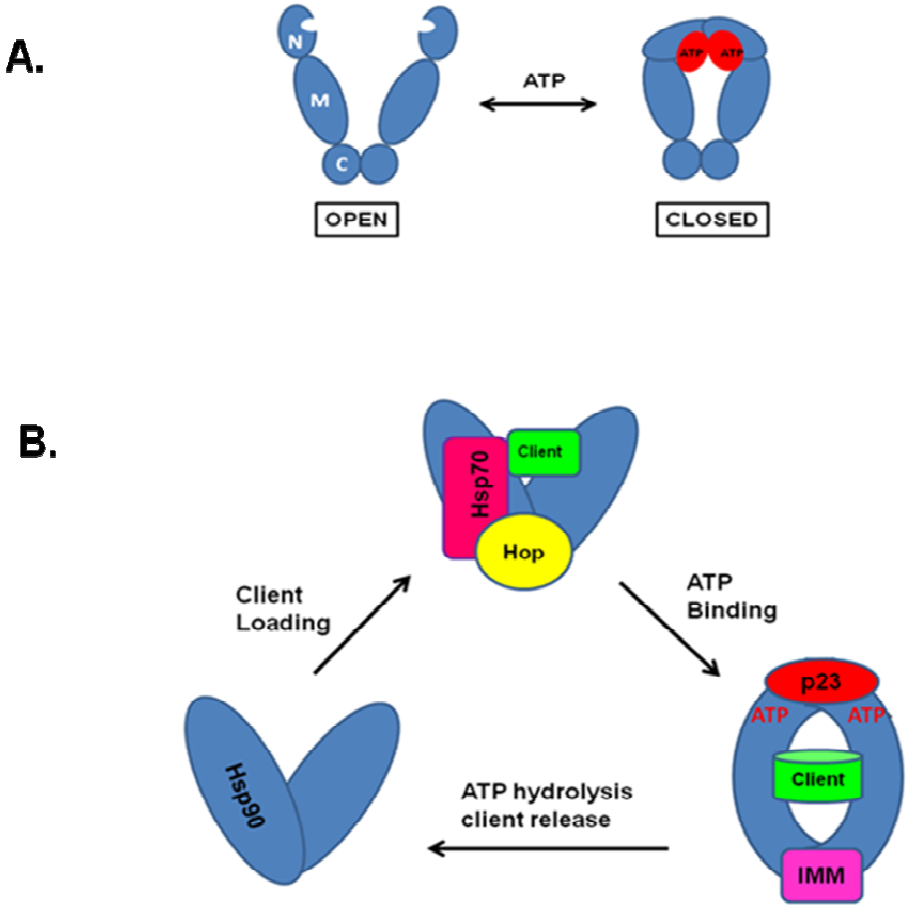

Figure 1: Hsp90 Stucture and Function:
(A). The Hsp90 ATPase cycle. The nucleotide free state corresponds to an open state. Binding of nucleotide induces conformational changes resulting in a closed or tense conformation. (B). The Hsp90 chaperone cyle.

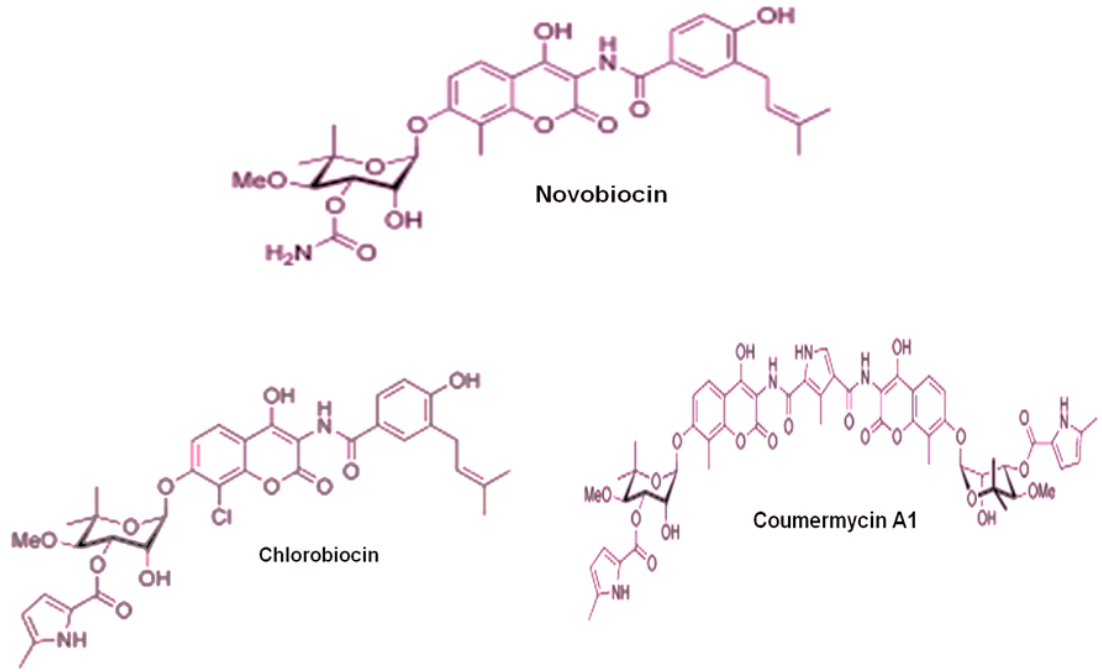

Figure 2:
Structures of Novobiocin and Related Coumarins

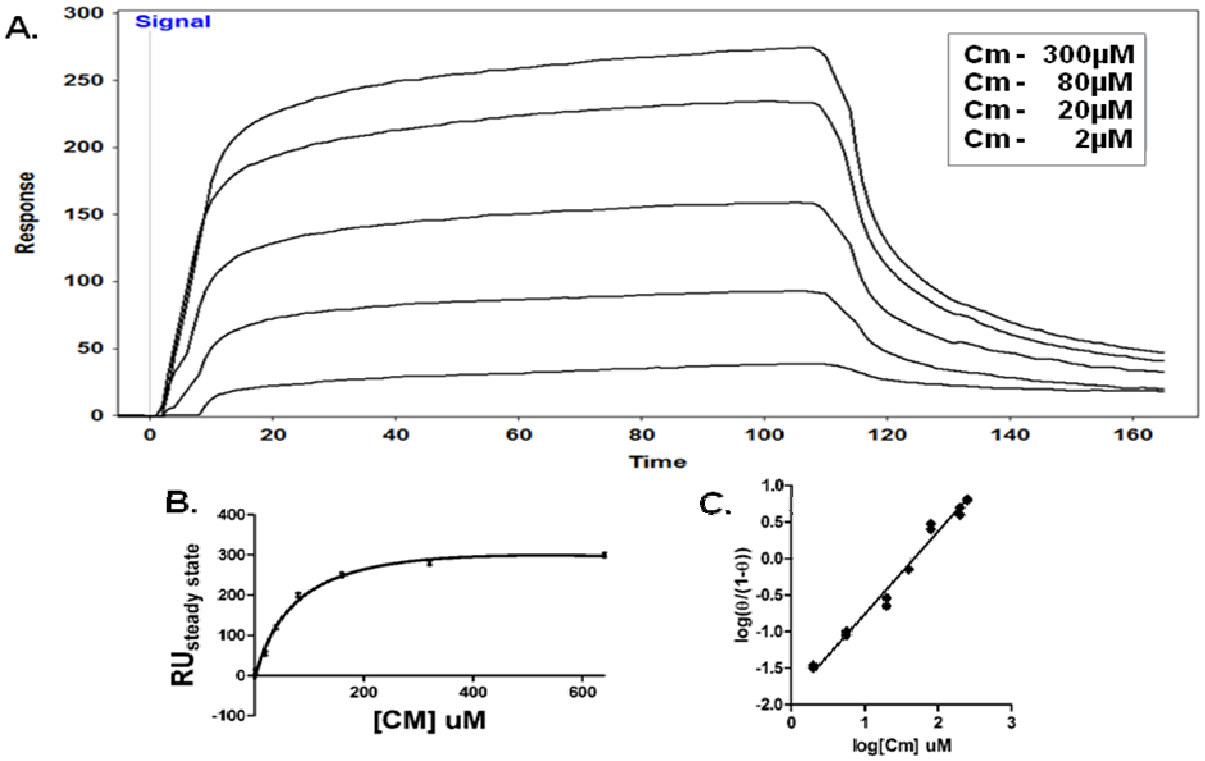

Figure 3: Binding of Coumermycin A1 to Hsp90FL:
(A). Coumermycin A1 was dissolved in standard running buffer (10 mM PIPES, 300 mM NaCL, 2% DMSO, pH 7.4) and the concentrations indicated in the figure legend were co-injected randomly over a surface bearing 33 nmol/mm^2 (3000 RU) Hsp90 FL and a blank reference surface. All concentrations were repeated 3 times at a flow rate of 25 µL/min in order to allow for a 1.5min contact time. Double referencing was employed to obtain relative response units, as described in material and methods. Affinity analysis by SPR QDAT analysis software calculated the K_D to be equal to 50 ± 10µM. (B). A hyperbolic replot of the steady state Cm sensorgram. Nonlinear regression estimated the K_D of Cm for Hsp90FL to be 60 ± 20 µM, R^2 =0.99. (C). A Hill plot of steady state Cm SPR signals; n = 1, R^2 =0.99.

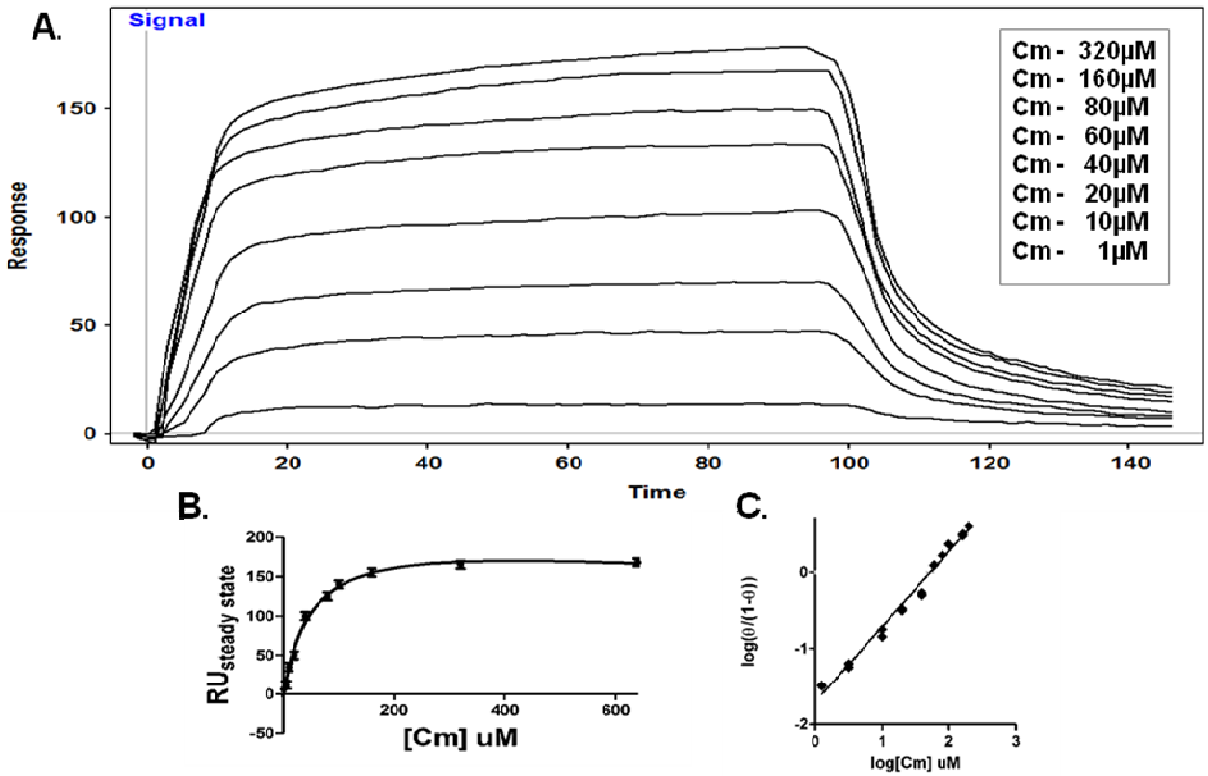

Figure 4: Binding of Cm to Hsp90CT:

(A). Coumermycin A1 was dissolved in standard running buffer and the concentrations indicated in the figure legend were co-injected randomly over a surface bearing 24 nmol/mm^2 (600 RU) Hsp90CT and a blank reference surface. All concentrations were repeated 3 times at a flow rate of 2 5 µL/min in order to allow for a 1.6 min contact time. Double referencing was employed in order to obtain relative response units. Affinity analysis by SPR software calculated the K_D of Cm for Hsp90CT to be 40 ± 10 µM. (B). A hyperbolic replot of the steady state Cm sensorgram. Nonlinear regression estimated the K_D of Cm for Hsp90FL to be 45 ± 10 µM, R^2 =0.99. (C). A Hill plot of steady state Cm SPR signals; n = 1, R^2 =0.99.

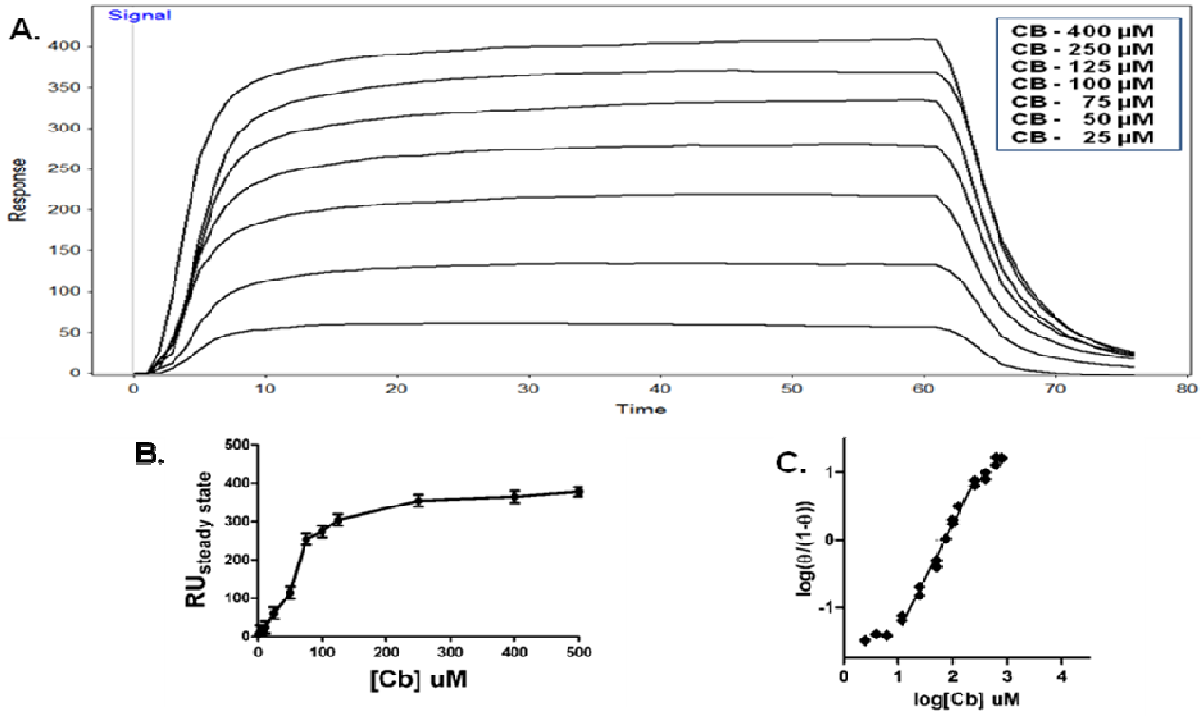

Figure 5: Binding of Chlorobiocin to Hsp90FL:

(A). Chlorobiocin was dissolved in standard running buffer and the concentrations indicated in the figure legend were co-injected randomly over a surface containing 33nmol/mm^2 (3000 RU) Hsp90 FL and blank control surface. All concentrations were repeated 3 times at a flow rate of 25uL/min in order to allow for a 1.0 min contact time. As described in material and methods, double referencing was employed to obtain relative response units. Affinity analysis by SPR analysis software calculated a high affinity K_{D1} = 45 ± 5 µM and a low affinity K_{D2} = 155 ± 10 µM. (B). A hyperbolic replot of the steady state Cb SPR response curves. The concentration of half maximal occupancy of Cb for Hsp90FL calculated by nonlinear regression of the data points was 100 ± 20 µM, R^2 =0.98. (C). A Hill plot of steady state SPR signals; n = 1.7, R^2 =0.99.

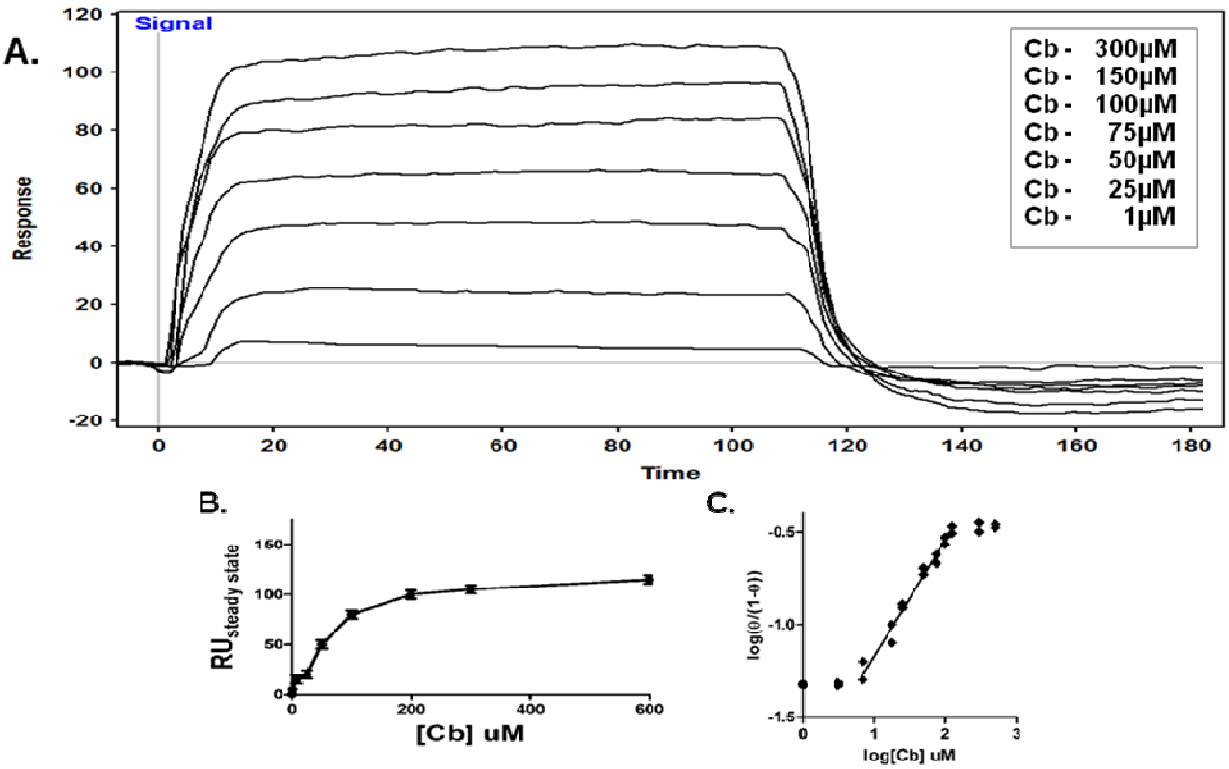

Figure 6: Binding of Cb to Hsp90CT:

(A). Chlorobiocin was dissolved in standard running buffer and the concentrations indicated in the figure legend were co-injected randomly over a surface containing 24 nmol/mm^2 (600 RU) Hsp90CT and blank control surface. All concentrations were repeated 3 times at a flow rate of 25 µL/min in order to allow for a 1.8 min contact time. Double referencing was employed to obtain relative response units. Affinity analysis by SPR analysis software calculated a high affinity K_{D1} = 35 ± 5 µM and a low affinity K_{D2} = 110 ± 10 µM. (B). A hyperbolic replot of the steady state Cb SPR response curves. 70 ± 15 µM is the concentration of half maximal occupancy of Cb for Hsp90CT as calculated by nonlinear regression of the data points, R^2 =0.98. (C). A Hill plot of steady state SPR signals; *n* = 1.78, R^2 =0.99.

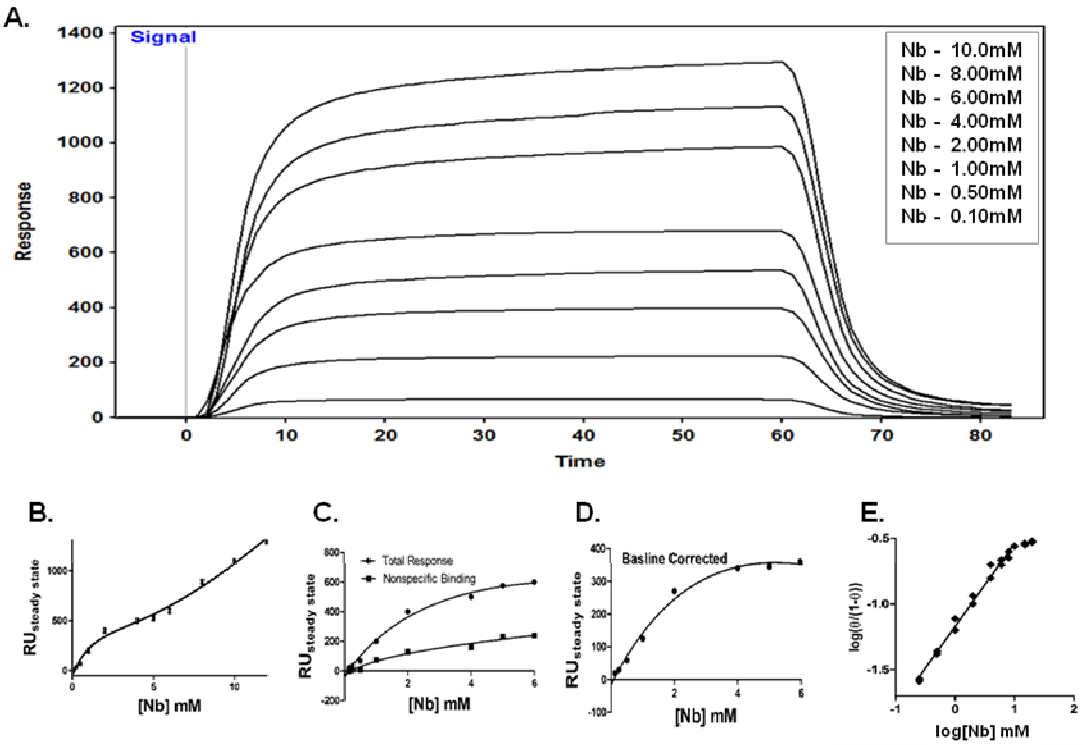

Figure 7: Binding of Novobiocin to Hsp90FL

(A). Novobiocin was dissolved in standard running buffer and the concentrations indicated in the figure legend were co-injected randomly over a surface containing 33nmol/mm^2 (3000 RU) Hsp90 FL and a blank control surface. All concentrations were repeated 3 times at a flow rate of 25uL/min in order to allow for a 1.0 min contact time. Double referencing was employed to obtain all relative response units. (B) A hyperbolic replot of steady state Nb response curves. (C) Nb binding isotherm globally fit for total and nonspecific binding using the equation $Y= (B_{max}(X))/(K_D +X)) +NS(X)$ to fit total binding and the equation $Y=NX(X)$ to fit nonspecific binding. (D). A baseline corrected hyperbolic replot of Nb steady state response curves, representing the subtraction of nonspecific binding from total binding. Nonlinear regression of the baseline corrected data points estimated the $K_{0.5}$ of Nb for Hsp90FL to be 3.3mM ± 0.9mM, R^2 =0.99. (E). A Hill plot of Nb SPR signals, n = 1.3, R^2 =0.98.

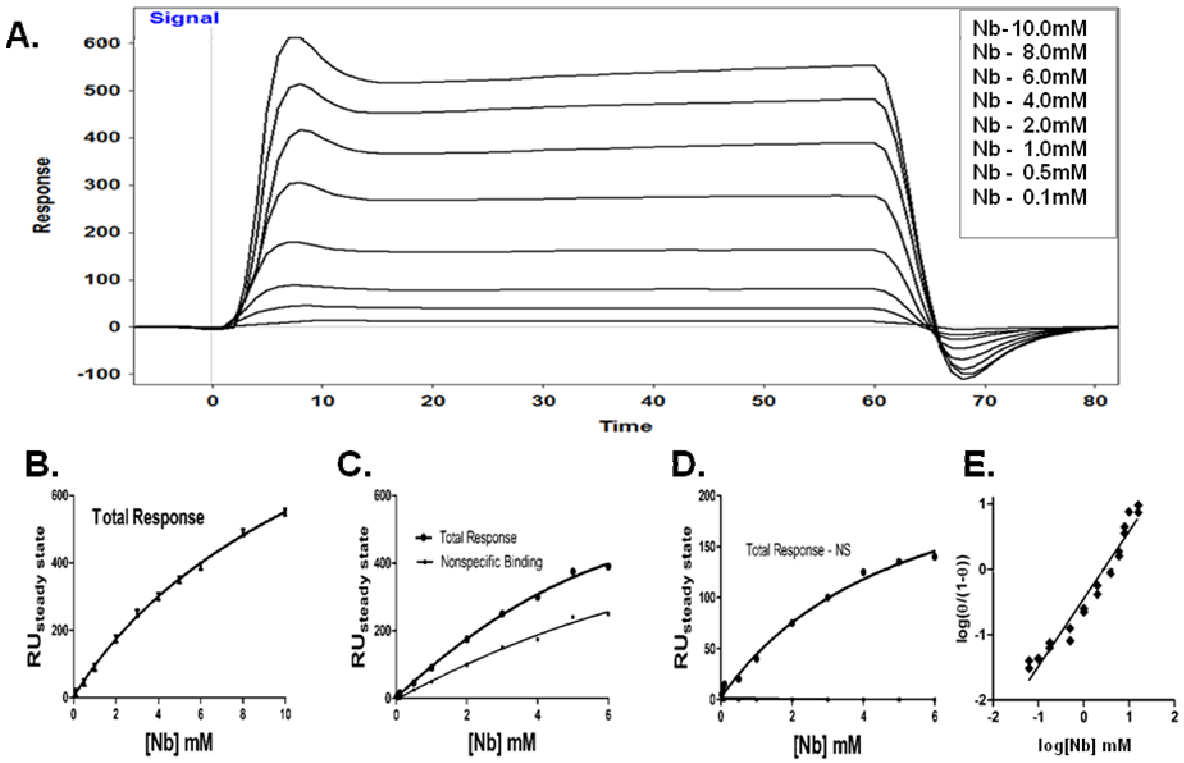

Figure 8: Binding of Nb to Hsp90CT:

(A). Novobiocin was dissolved in standard running buffer and the concentrations indicated in the figure legend were co-injected randomly over a surface containing 24nmol/mm^2 (600 RU) Hsp90CT and a blank control surface. All concentrations were repeated 3 times at a flow rate of 25uL/min in order to allow for a 1.0 min contact time. Double referencing was employed to obtain all relative response units. (B) A hyperbolic replot of steady state Nb response curves. (C) Nb binding isotherm globally fit for total and nonspecific binding using the equation $Y= (B_{max}X/(K_D +X)) +NS(X)$ to fit total binding and the equation $Y=NX(X)$ to fit nonspecific binding. (D). A baseline corrected hyperbolic replot of Nb steady state response curves, representing the subtraction of nonspecific binding from total binding. Nonlinear regression of the baseline corrected hyperbolic replot estimated the K_D of Nb for Hsp90CT to be 1.9mM ± 0.6mM, R^2=0.98. (E). A Hill plot of Nb SPR signals, n = 1.0, R^2=0.98.

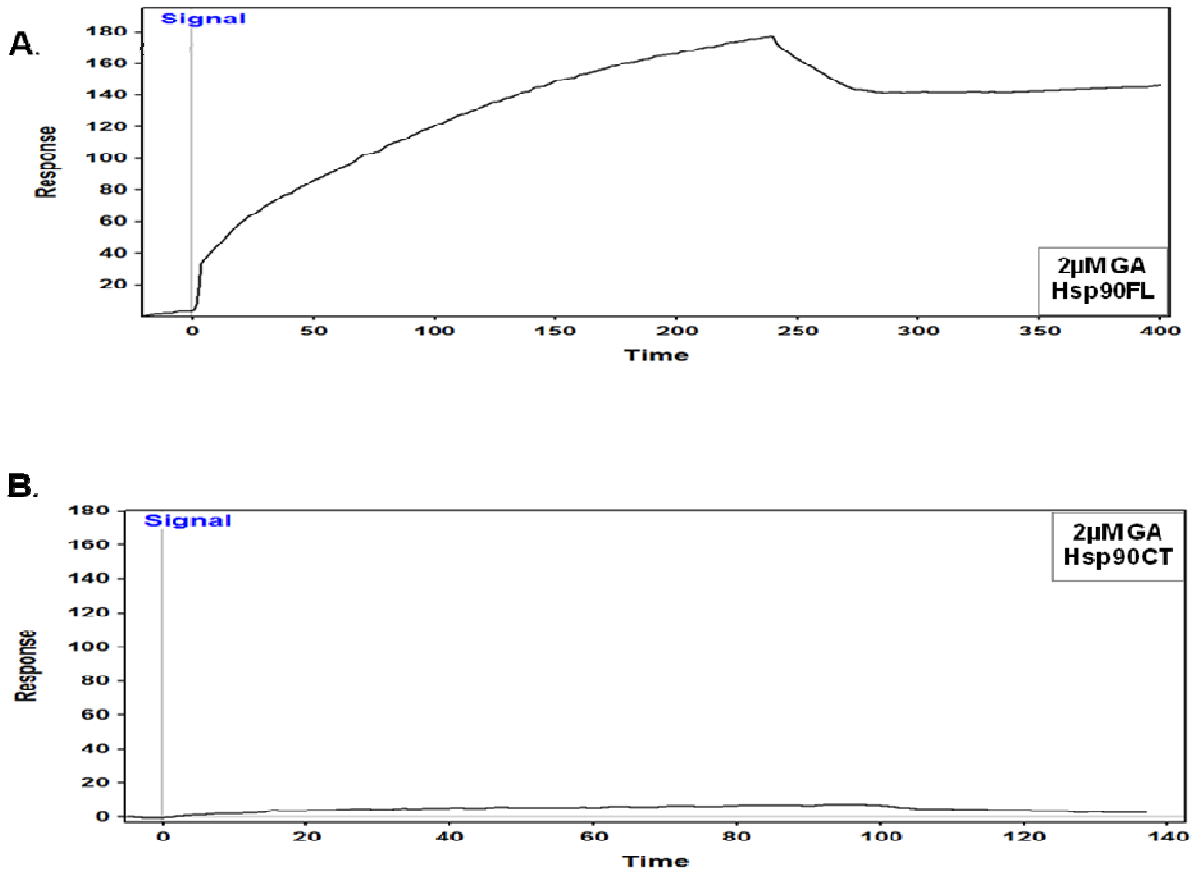

Figure 9: Binding of Geldanamycin to Hsp90 Constructs:
(A) To facilitate access of Hsp90's N-terminal nucleotide binding site, 0.01% Igepal was dissolved in standard running buffer and successively injected over a surface of 33nmols/mm^2 Hsp90FL in a series of three injections. 2µM GA was then dissolved in standard SPR running buffer and injected over this pretreated surface at a flow rate of 25uL/min(n=3). (B) 2µM GA was dissolved in standard SPR running buffer and injected over an SPR chip coupled with 100nmols/mm^2 (2500RU) Hsp90CT at a flow rate of 25uL/min(n=3).

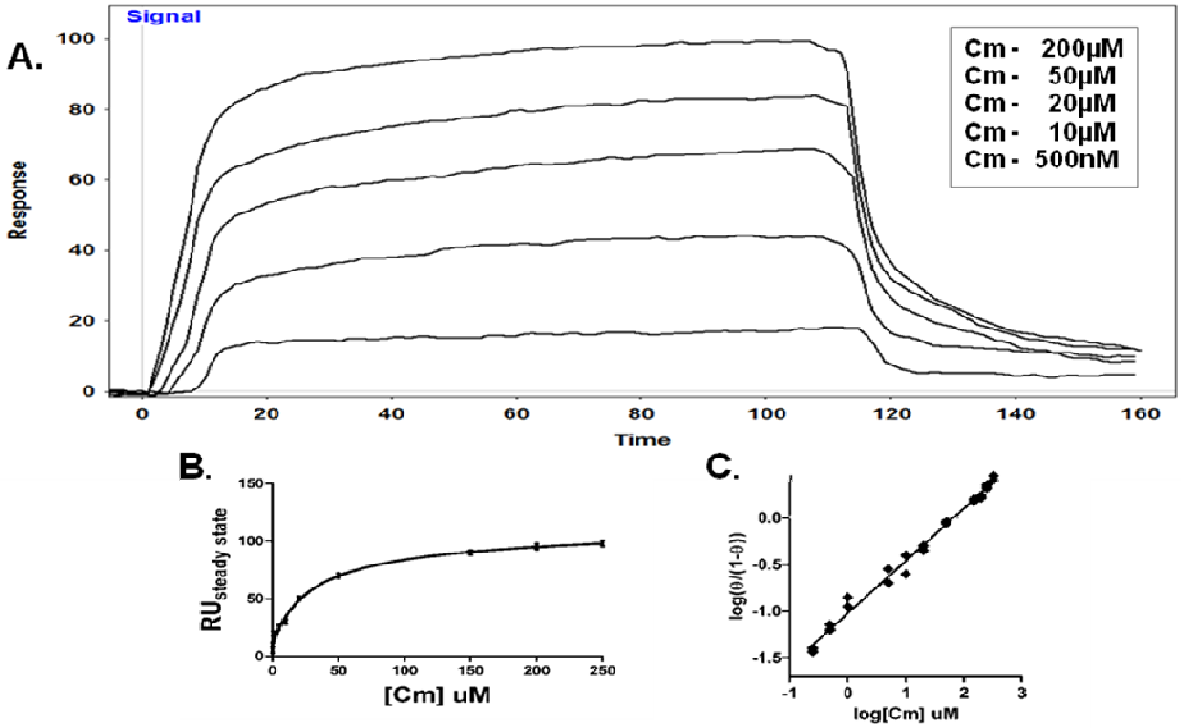

Figure 10: Effect of GA on the Binding of Coumermycin A1 to Hsp90FL:
(A). Coumermycin A1 was dissolved in Geldanamycin running buffer (10mM PIPES, 300mM NaCL, 2uM GA, 2% DMSO, pH 7.4). Coumermycin A1 was assayed as described in Figure 1. SPR analysis software calculated a high affinity K_{D1} = 3.3 ± 5uM and a lower affinity K_{D2} = 20uM ± 15uM. (B). A hyperbolic replot of the steady state Cm sensorgram in the presence of GA. 10.75uM ± 2uM is the concentration of half maximal occupancy of Cm for Hsp90CT as calculated by nonlinear regression of the data points, R^2 =0.99. (C). A Hill plot of steady state Cm SPR signals; n = 1.0, R^2 =0.99.

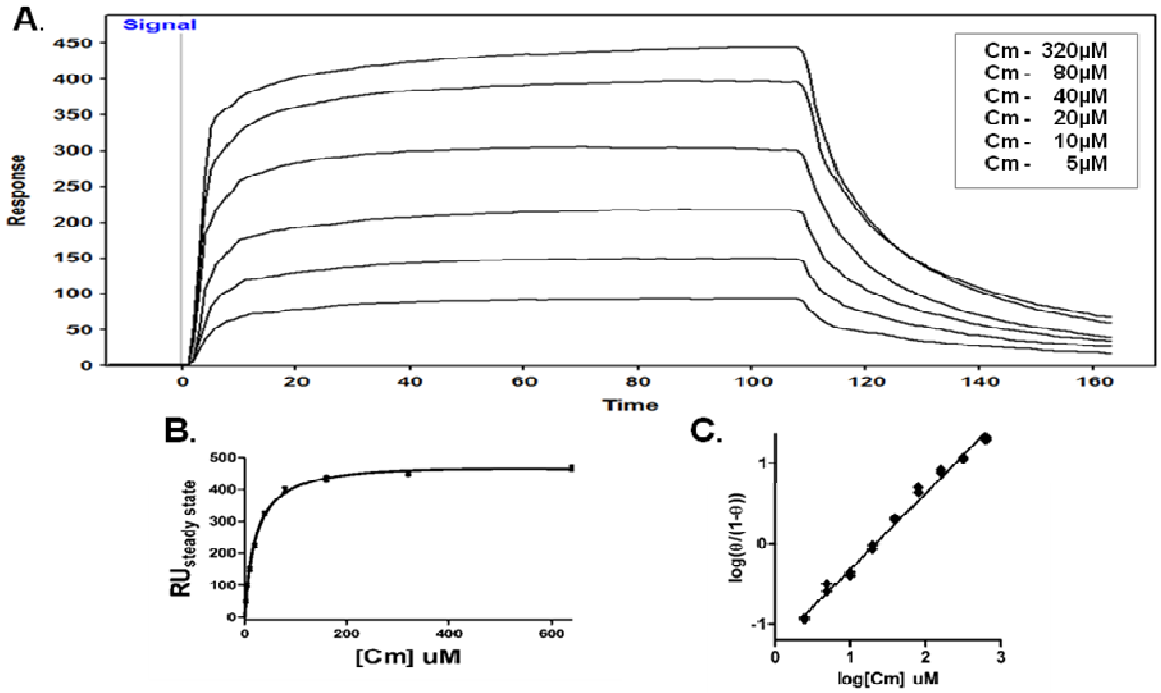

Figure 11: GA Does Not Alter the Affinity of Cm A1 for Hsp90CT:

(A). Coumermycin A1 was dissolved in Geldanamycin running buffer and assayed as described in Figure 2, with the exception that the assays were conducted over a surface bearing 100nmols/mm^2 (2500RU) Hsp90CT. Affinity analysis by SPR software calculated the K_D of Cm for Hsp90CT to be 40uM ± 10uM. (B). A hyperbolic replot of the steady state Cm sensorgram. Nonlinear regression estimated the K_D of Cm for Hsp90CT in the presence of GA to be 45uM ± 10uM, R^2 =0.99. (C). A Hill plot of steady state Cm SPR signals; n = 1, R^2 =0.99.

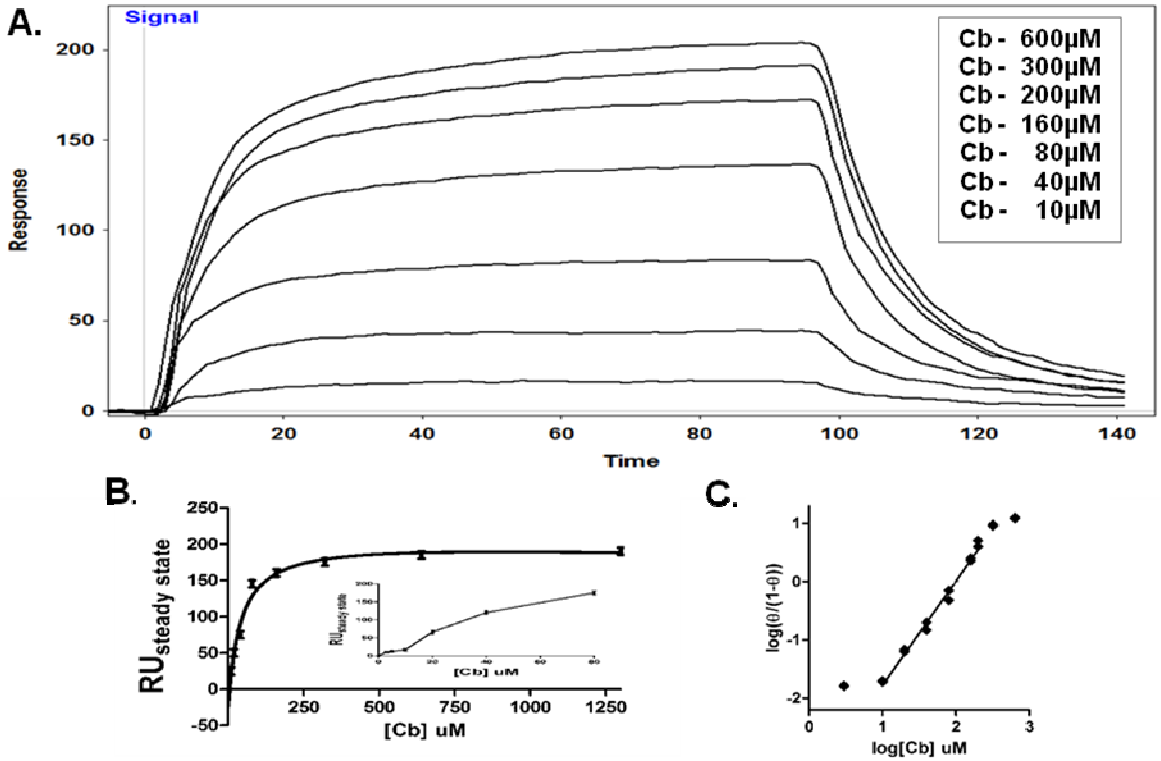

Figure 12: Effect of Geldanamycin on the Binding of Cb to Hsp90FL:
(A). Chlorobiocin was dissolved in GA running buffer and assayed as described in Figure 2. Affinity analysis by SPR analysis software calculated a high affinity K_{D1} = 45 ± 5uM and a low affinity K_{D2} = 170uM ± 20uM. (B). A hyperbolic replot of the steady state Cb sensorgram. Nonlinear regression estimated the concentration of half maximal occupancy of Cb for Hsp90FL_GA to be 120uM ± 20uM, R^2 =0.99. (C). A Hill plot of the steady state Cb response signals; *n* = 1.5, R^2 =0.99.

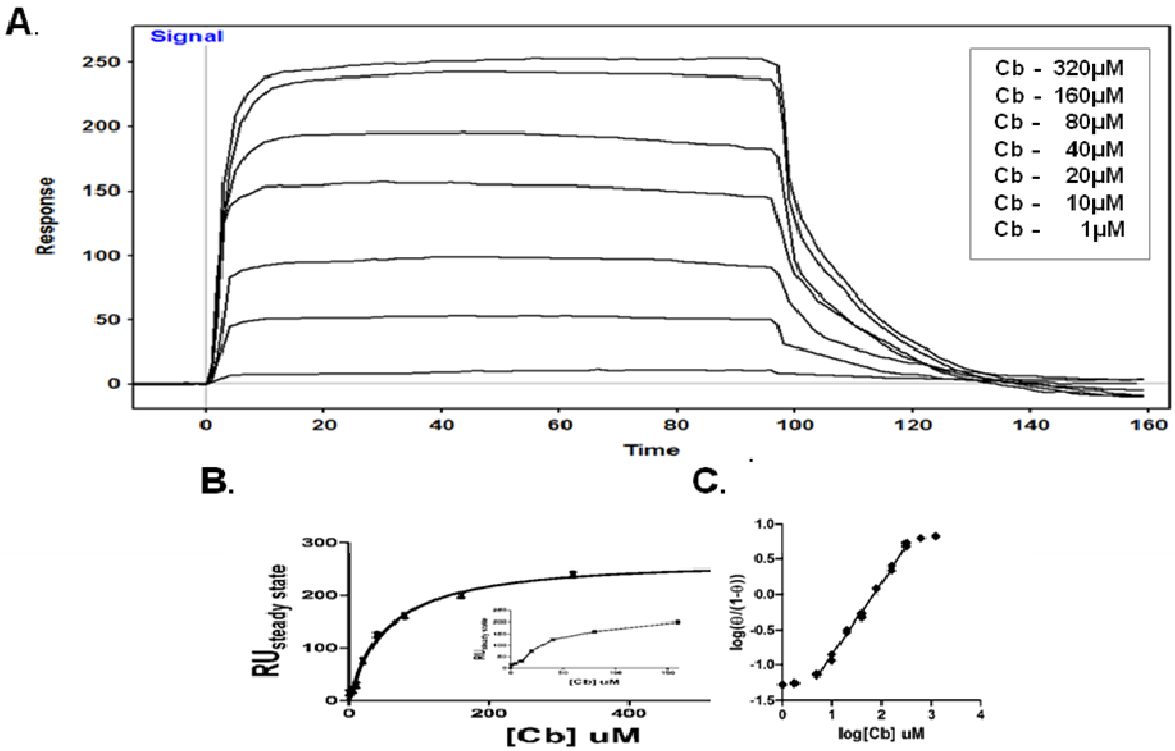

Figure 13: GA Does not Alter the Affinity of Chlorobiocin for Hsp90CT:
(A). Chlorobiocin was dissolved in GA running buffer and assayed over a surface bearing 100nmols/mm^2 (2500RU) Hsp90CT as described in Figure 4. Affinity analysis calculated a high affinity K_{D1} = 36 ± 5uM and a low affinity K_{D2} = 109uM ± 10uM. (B). A hyperbolic replot of the steady state Cb SPR response curves. 70uM ± 15uM is the concentration of half maximal occupancy of Cb for Hsp90CT in the presence of GA as calculated by nonlinear regression of the data points, R^2 =0.98. (C). A Hill plot of steady state SPR signals; *n* = 1.70, R^2 =0.99.

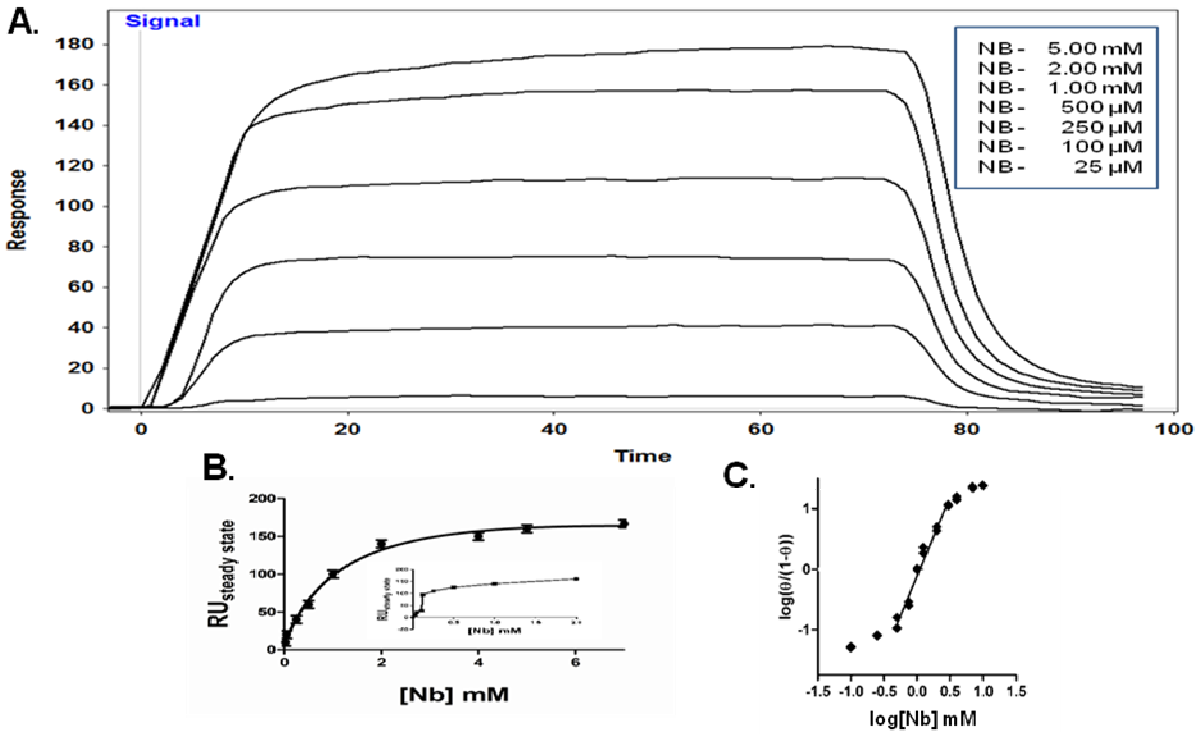

Figure 14: Effect of Geldanamycin on the Binding of Nb to Hsp90FL:
(A). Novobiocin was dissolved in GA running buffer and assayed as described in Figure 5. Affinity analysis calculated a high affinity K_{D1} = 800uM ± 80uM and a low affinity K_{D2} = 2.0mM ± 200uM. (B). A hyperbolic replot of the steady state Nb response curves. Nonlinear regression of the data points calculated the concentration of half maximal occupancy of Nb for Hsp90FL in complex with GA to be 1.3mM ± 200uM, R^2 =0.99. (C). A Hill plot of the steady state response signals; n = 1.3, R^2 =0.99.

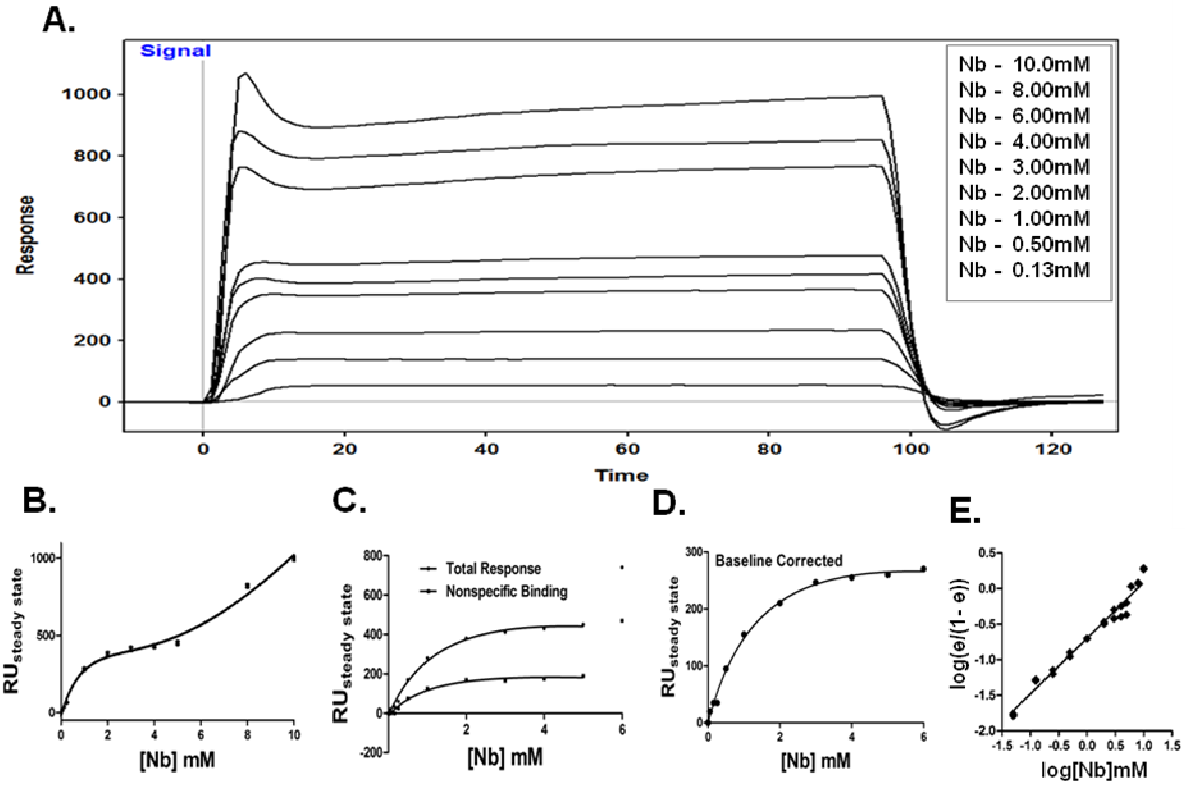

Figure 15: GA Does not Alter the Affinity of Nb for Hsp90CT

(A) Novobiocin was dissolved in GA running buffer and assayed over a surface bearing 100nmols/mm^2 Hsp90CT, as described in Figure 6. (B) A hyperbolic replot of steady state Nb response curves. (C) Nb binding isotherm globally fit for total and nonspecific binding, as described in Figure 6. (D). A baseline corrected hyperbolic replot of the Nb steady state response curves. Nonlinear regression of the baseline corrected data points estimated the $K_{0.5}$ of Nb for Hsp90CT with additive GA to be 1.86mM ± 0.58mM, R^2 =0.99. (E). A Hill plot of Nb SPR signals, n = 1.0, R^2 =0.98.

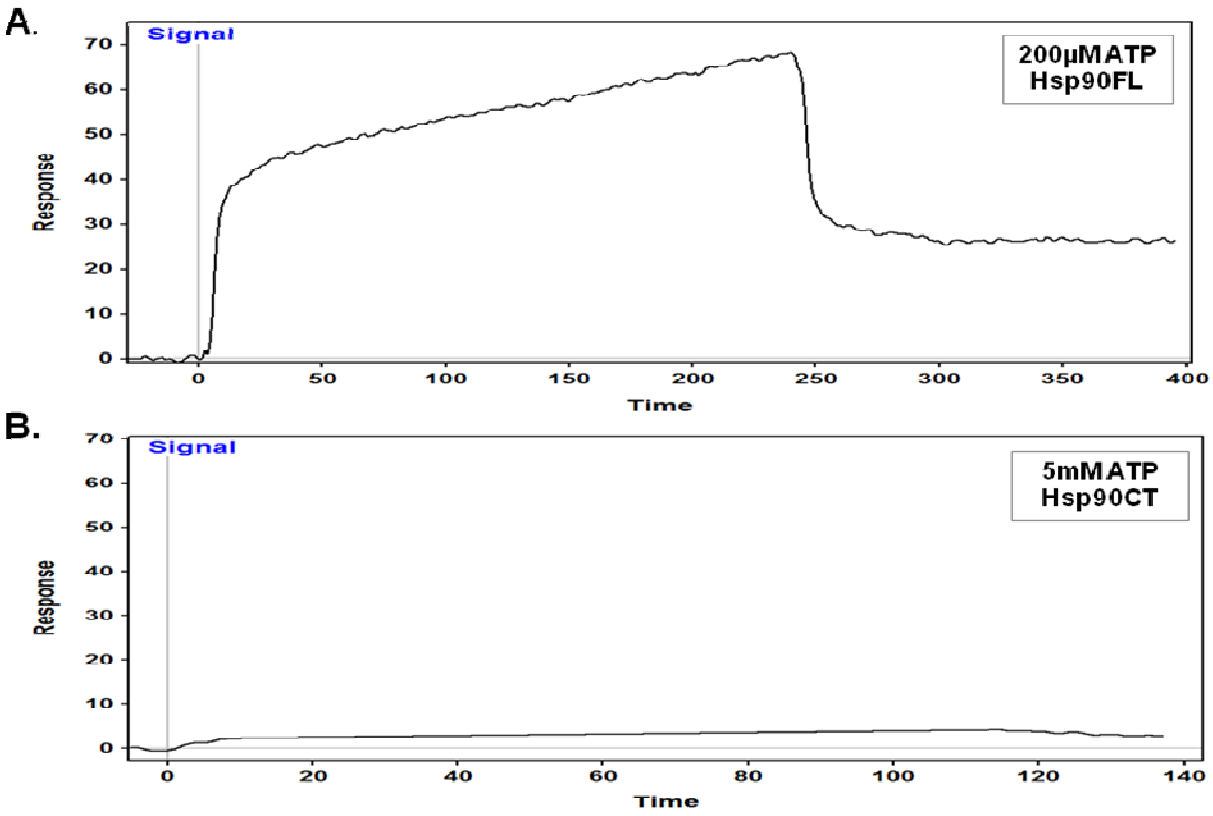

Figure 16: Binding of ATP to Hsp90 Constructs:

(A) 33nmols/mm^2 Hsp90FL was pretreated with 0.01% Igepal as described in Figure 7. ATP was dissolved in nucleotide running buffer (10mM PIPES, 300mM NaCL, 5mM $MgCL_2$, 2% DMSO, pH 7.4) and injected over the igepal pretreated surface at a flow rate of 25uL/min(n=3). (B) 5mM ATP was dissolved in nucleotide running buffer and injected over a surface bearing 100nmols/mm^2 (2500RU) Hsp90CT at a flow rate of 25uL/min(n=3).

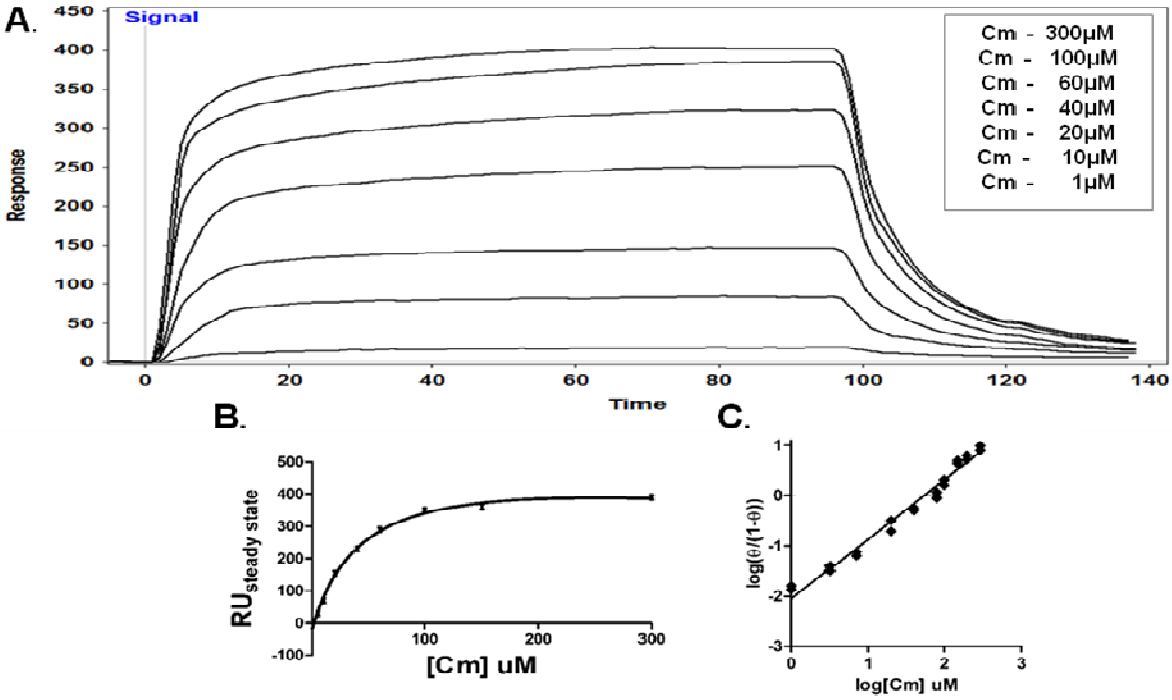

Figure 17: ATP Does not Alter the Affinity of Cm A1 for Hsp90FL

(A). Coumermycin A1 was dissolved in ATP assay buffer (10mM PIPES, 300mM NaCL, 5mM $MgCL_2$, 5mM ATP, 2% DMSO, pH 7.4) and assayed as described in Figure 1. Affinity analysis calculated the K_D of Cm A1 for the Hsp90FL_ATP permutation to be equal to 49uM ± 7uM. (B). A hyperbolic replot of the steady state Cm sensorgram. Nonlinear regression estimated the K_D of Cm for the Hsp90FL ATP conjugate to be 55uM ± 20uM, R^2 =0.99. (C). A Hill plot of steady state SPR signals; n = 1, R^2 =0.99.

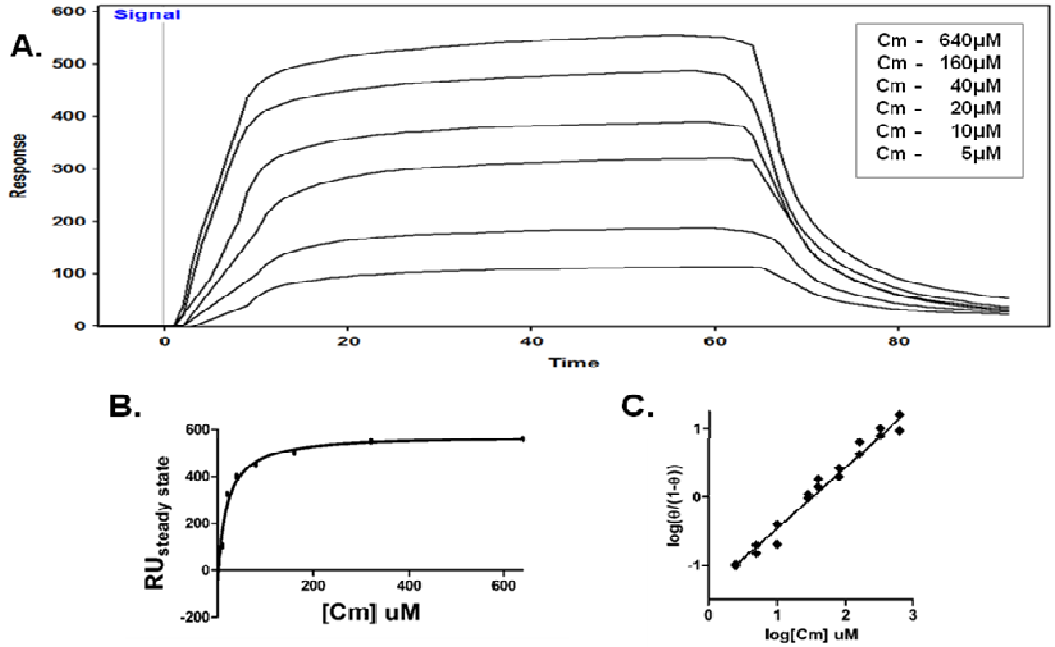

Figure 18: ATP Does Not Alter the Affinity of Coumermycin A1 for Hsp90CT
(A). Coumermycin A1 was dissolved in ATP running buffer and assayed over a surface bearing 100nmols/mm^2 (2500RU) Hsp90CT as described in Figure 2. Affinity analysis calculated the K_D of Cm A1 for Hsp90CT under conditions of saturating ATP be equal to 18.6uM ± 10uM. (B). A hyperbolic replot of the steady state Cm sensorgram. Nonlinear regression estimated the K_D of Cm A1 for Hsp90CT in the presence of ATP additive to be 20uM ± 10uM, R^2 =0.99. (C). A Hill plot of steady state Cm A1 SPR signals; n = 1, R^2 =0.99.

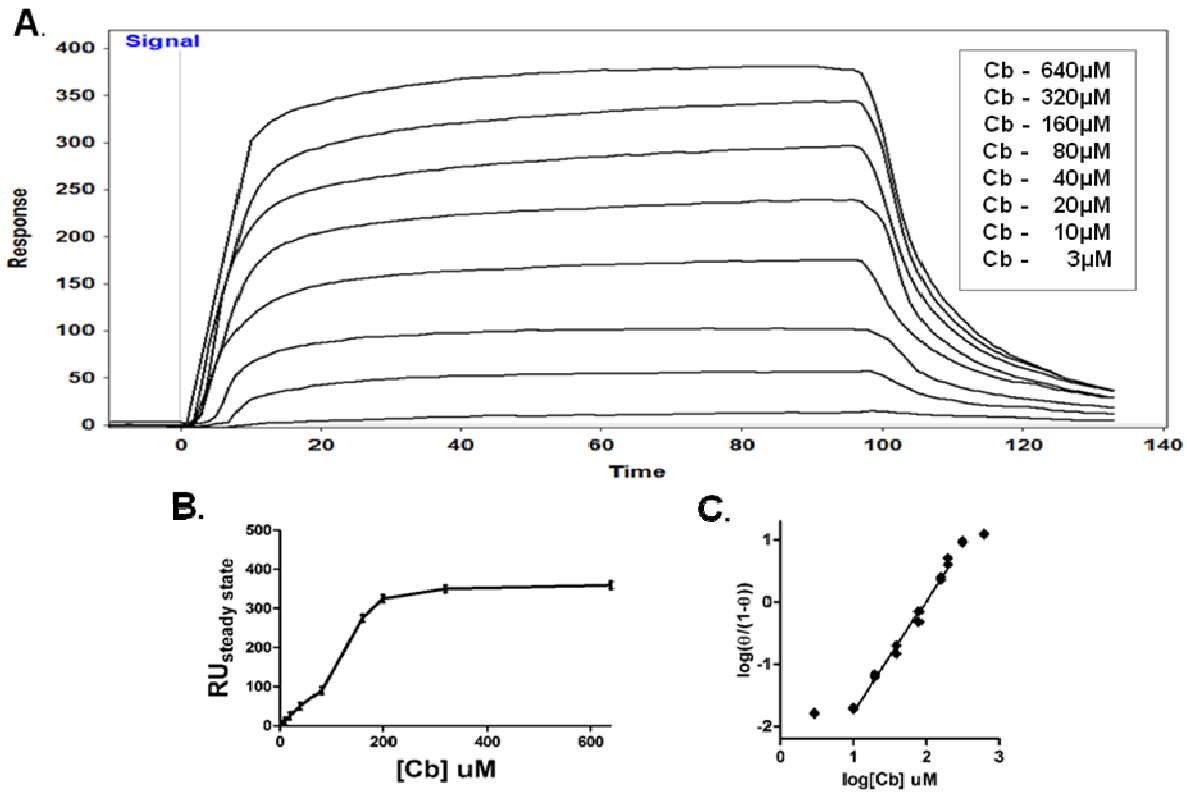

Figure 19: ATP Does Not Alter the Affinity of Chlorobiocin for Hsp90FL:
(A). Chlorobiocin was dissolved in ATP running buffer and assayed as described in Figure3. Affinity analysis established a high affinity K_{D1} = 40 ± 10uM and a low affinity K_{D2} = 170uM ± 20uM. (B). A hyperbolic replot of the steady state Cb SPR response curves. 110uM ± 20uM is the concentration of half maximal occupancy of Cb for the Hsp90FL_ATP permutation, as calculated by nonlinear regression of the data points, R^2 =0.975. (C). A Hill plot of steady state SPR signals; *n* = 2.0, R^2 =0.99.

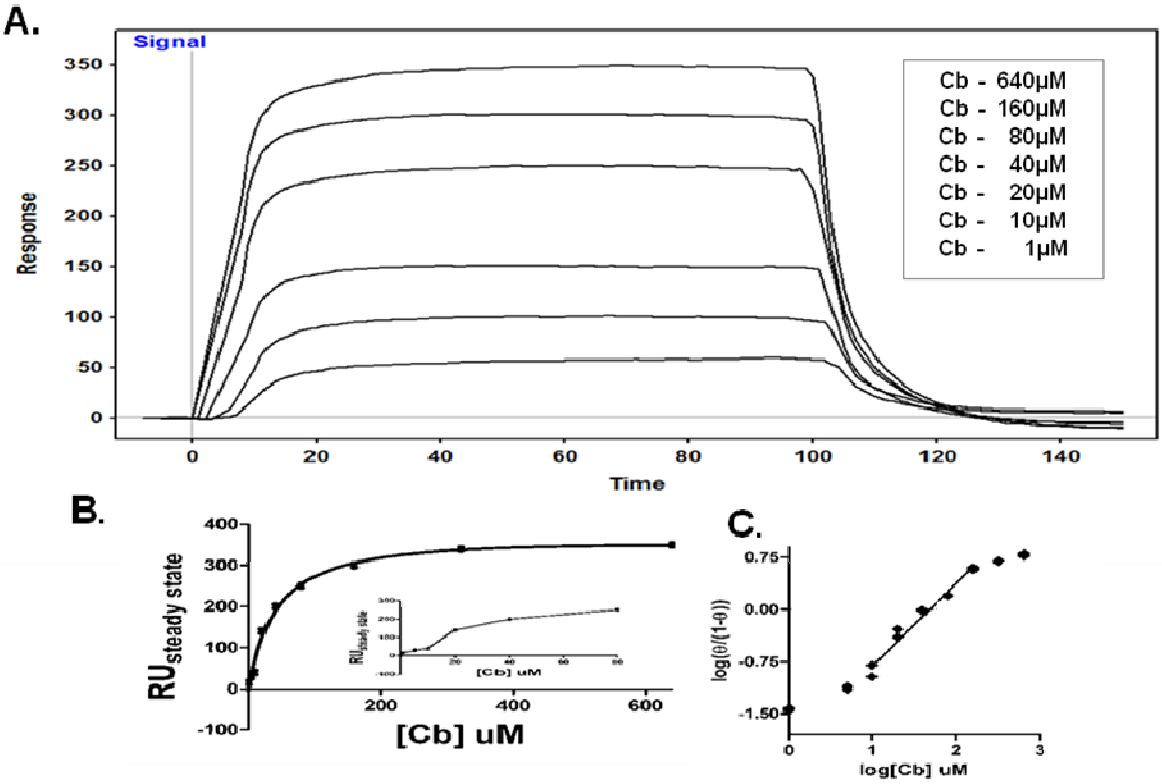

Figure 20: ATP Does Not Alter the Affinity of Chlorobiocin for Hsp90CT:
(A). Chlorobiocin was dissolved in ATP running buffer and assayed over a surface bearing 100nmols/mm^2 (2500RU) Hsp90CT as described in Figure 4. Affinity analysis established a high affinity K_{D1} = 30 ± 5uM and a low affinity K_{D2} = 110uM ± 10uM. 68uM ± 15uM is the concentration of half maximal occupancy of Cb for Hsp90CT under conditions of saturating ATP, as calculated by nonlinear regression of the data points, R^2 =0.98. (C). A Hill plot of steady state Cb SPR signals; *n* = 1.7, R^2 =0.99.

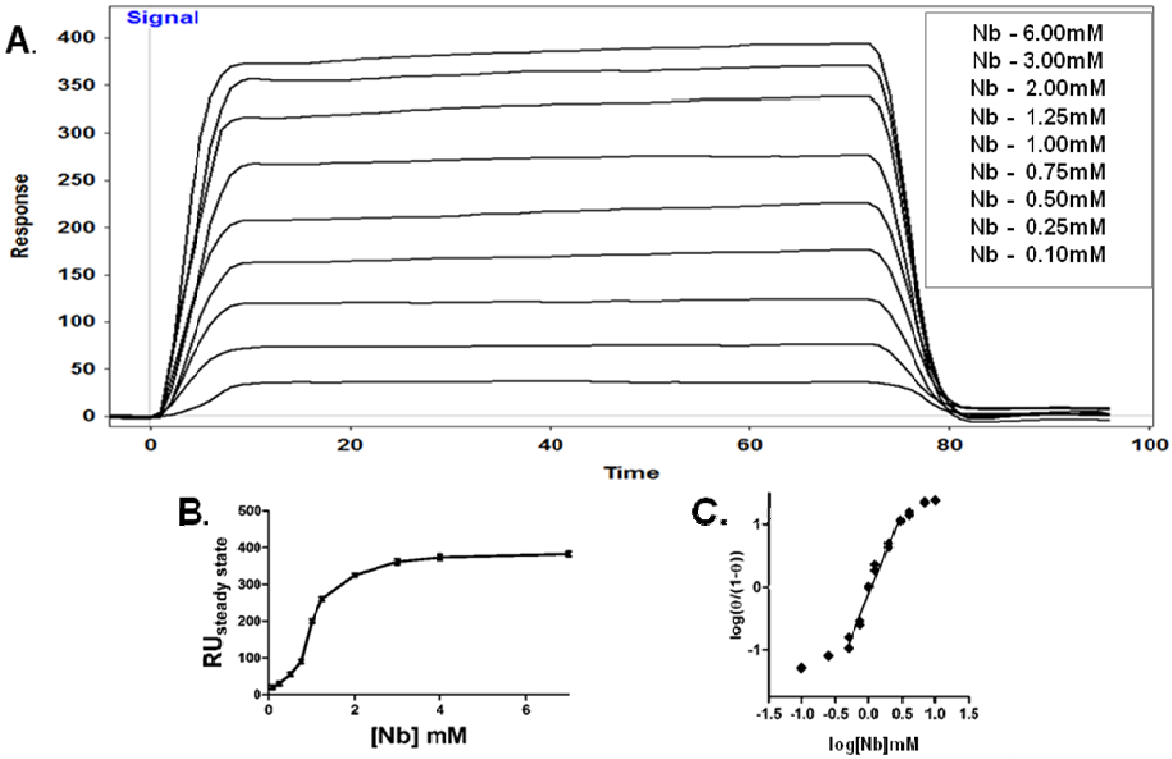

Figure 21: ATP Does Not Alter the Affinity of Novobiocin for Hsp90FL

(A). Novobiocin was dissolved in ATP running buffer and assayed as described in Figure 5. Affinity analysis established a high affinity K_{D1} = 980uM ± 80uM and a low affinity K_{D2} = 2.1mM ± 200uM. (B). A hyperbolic replot of the steady state Nb SPR response curves. 1.5mM ± 0.50mM is the concentration of half maximal occupancy of Nb for the Hsp90FL_ATP conjugate, as calculated by nonlinear regression of the data points, R^2 =0.975. (C). A Hill plot of steady state SPR signals; *n* = 2.0, R^2 =0.99.

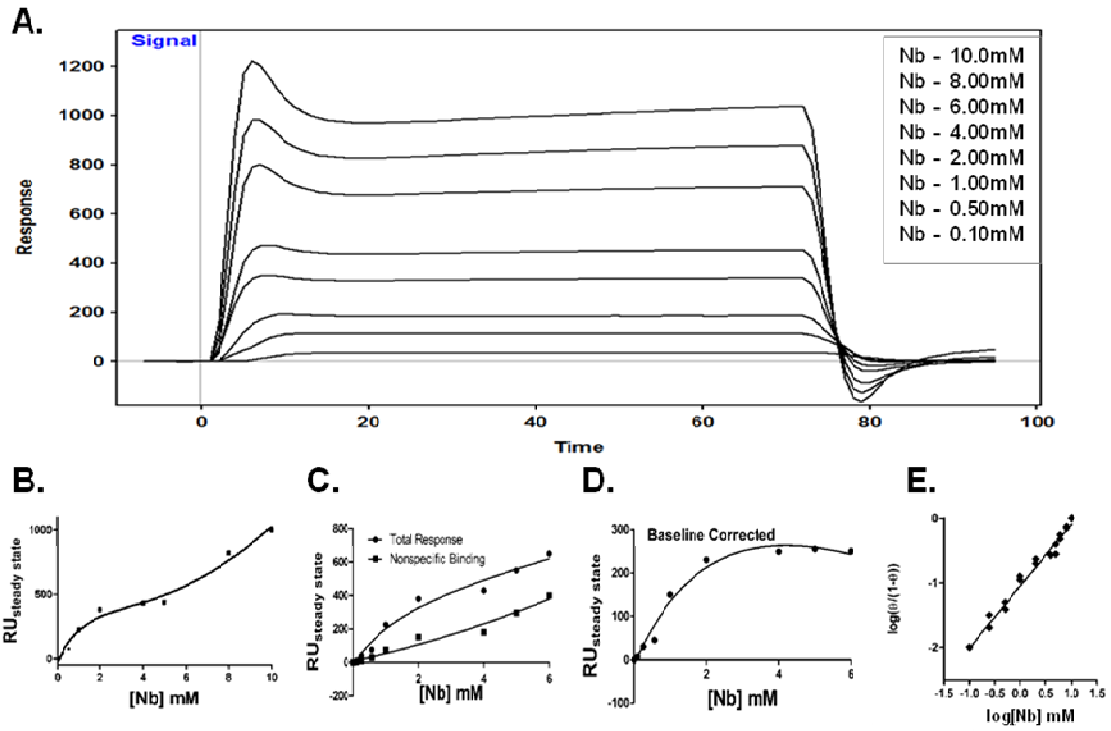

Figure 22: ATP Does Not Alter the Affinity of Novobiocin for Hsp90CT:
(A). Novobiocin was dissolved in ATP running buffer and assayed over a surface bearing 100nmols/mm^2 Hsp90CT, as described in Figure 6. (B) A hyperbolic replot of steady state Nb response curves. (C) Nb binding isotherm globally fit for total and nonspecific binding, as described in Figure 6. (D). A baseline corrected hyperbolic replot of the Nb steady state response curves. Nonlinear regression of the baseline corrected data points estimated the $K_{0.5}$ of Nb for Hsp90CT with additive ATP to be 1.6mM ± 0.7mM, R^2 =0.97. (E). A Hill plot of NbSPR signals, n = 1.0, R^2 =0.98.

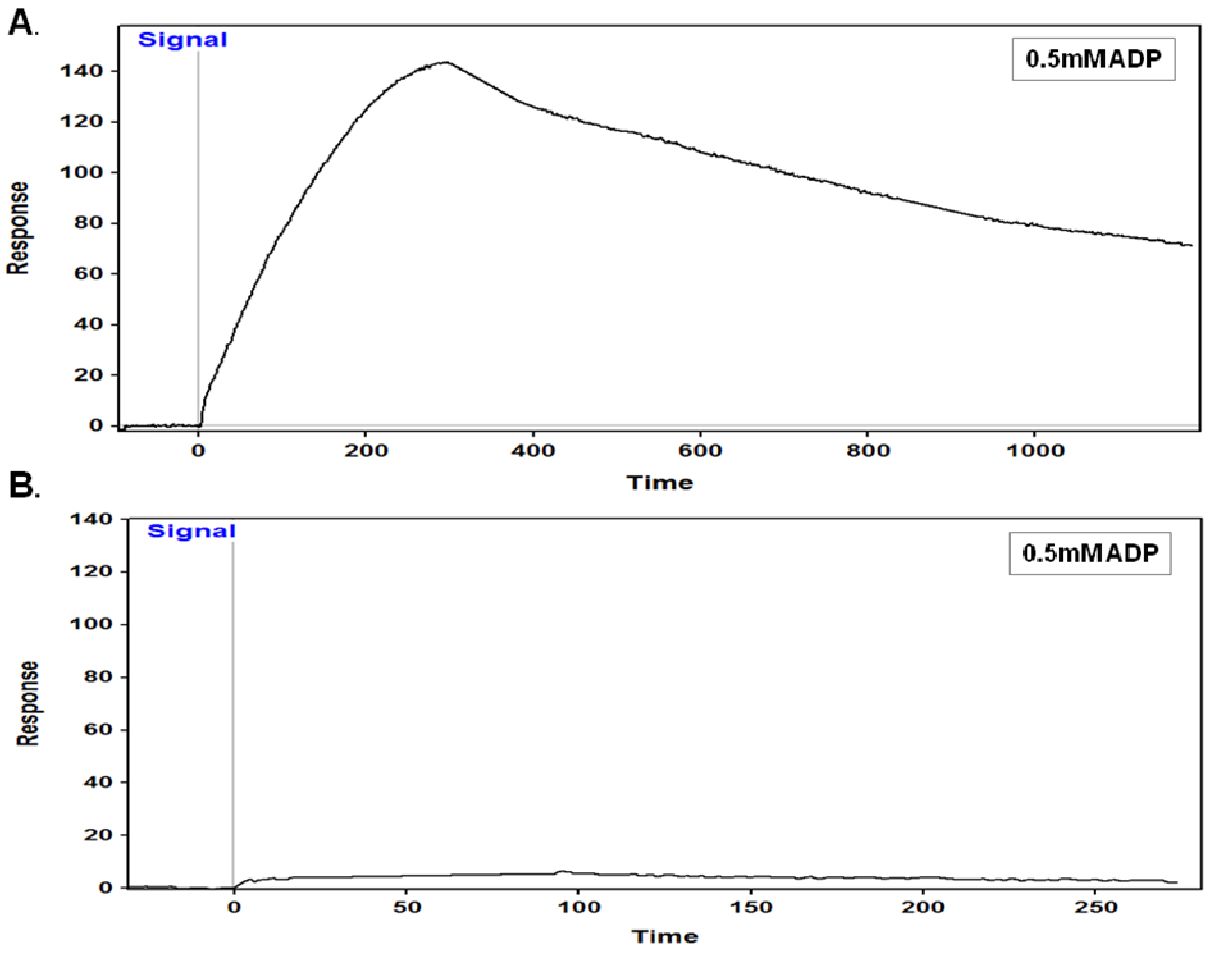

Figure 23: Binding of ADP to Hsp90 Constructs

(A) 33nmols/mm^2 Hsp90FL was pretreated with 0.01% Igepal as described in Figure 7. 0.5mM ADP was dissolved in nucleotide running buffer (10mM PIPES, 300mM NaCL, 5mM $MgCL_2$, 2% DMSO, pH 7.4) and injected over the igepal pretreated surface at a flow rate of 25uL/min (n=3). (B) 0.5mM ADP was dissolved in nucleotide running buffer and injected over a surface bearing 100nmols/mm^2 (2500RU) Hsp90CT at a flow rate of 25uL/min (n=3).

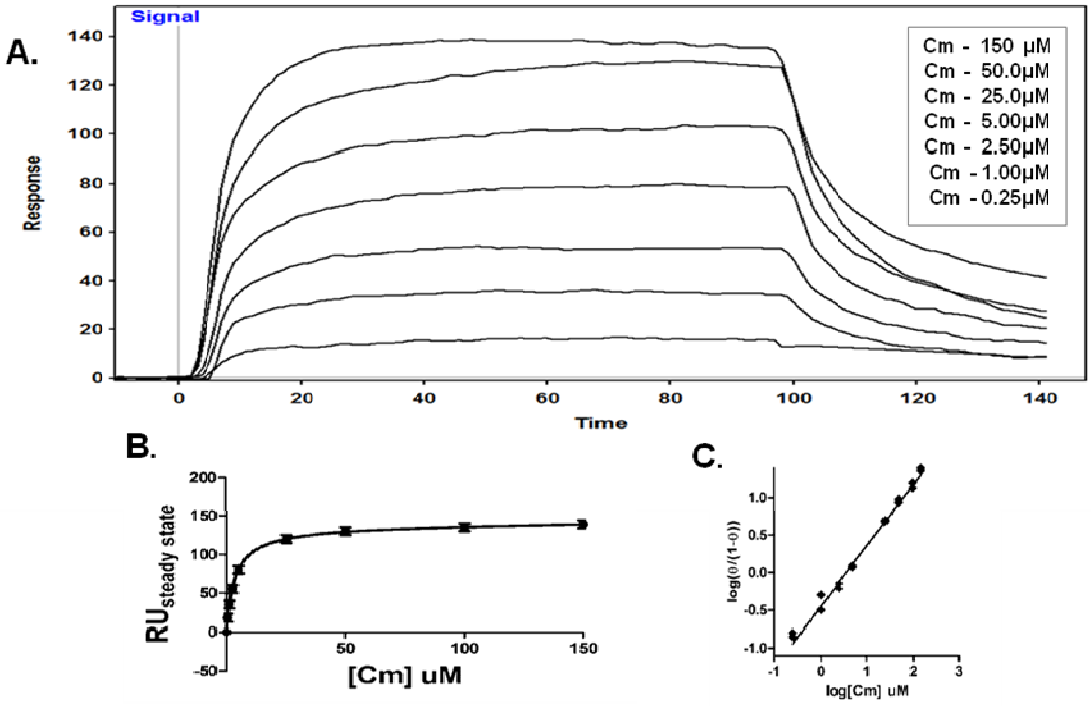

Figure 24: ADP Allosterically Enhances the Affinity of Cm Al for Hsp90FL:
(A). Coumermycin A1 was dissolved in ADP running buffer (10mM PIPES, 300mM NaCL, 5mM $MgCL_2$, 0.5mM ADP, 2% DMSO, pH 7.4), and assayed as described in Figure 1. Affinity analysis established a high affinity K_{D1} = 1.5uM ± 0.5uM and a low affinity K_{D2} = 7.5uM ± 2uM. (B). A hyperbolic replot of the steady state Cm A1 sensorgram. 3.6uM ± 1.5uM is the concentration of half maximal occupancy of Cm A1 for Hsp90FL_ADP, as calculated by nonlinear regression of the data points, R^2 =0.98.(C). A Hill plot of steady state SPR signals; n = 1, R^2 =0.98.

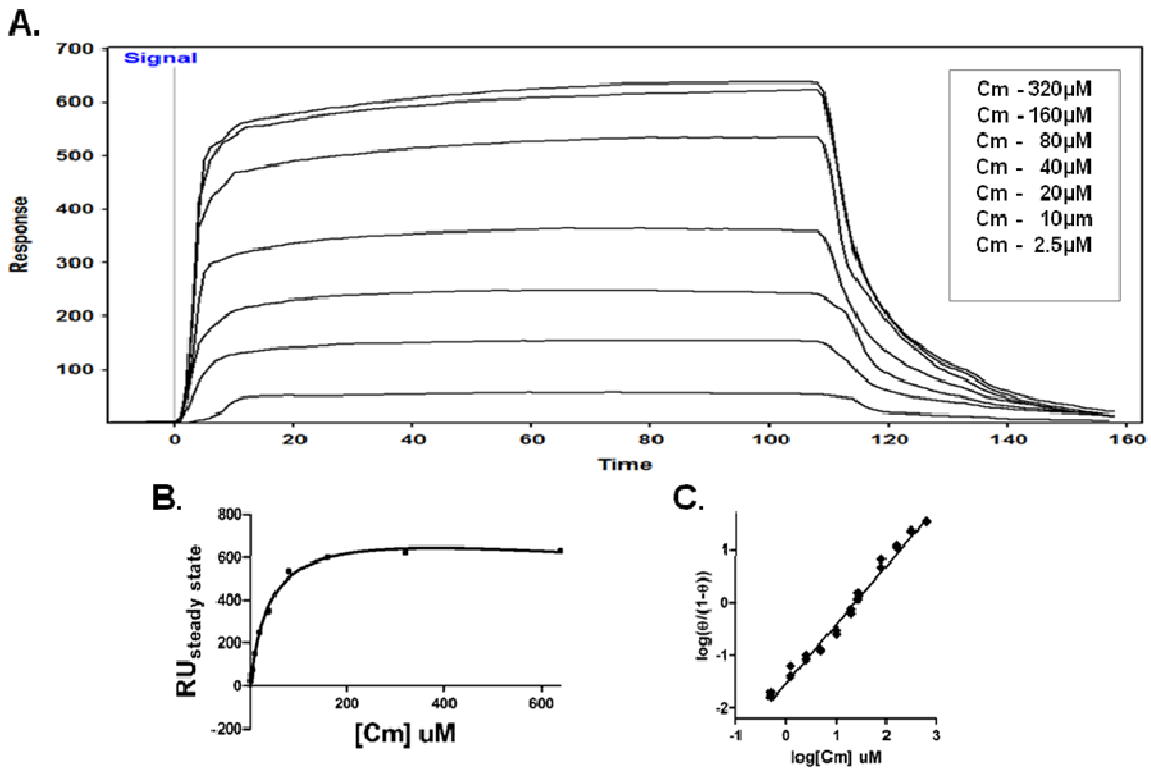

Figure 25: ADP Does Not Alter the Affinity of Coumermycin A1 for Hsp90CT: (A). Cm A1 was dissolved in ADP running buffer and assayed over a surface bearing 100nmols/mm^2 (2500RU) Hsp90CT as described in Figure 2. Affinity analysis estimated the K_D of Cm A1 for Hsp90CT in the presence of ADP to be 38uM ± 10uM. (B). A hyperbolic replot of the steady state Cm sensorgram. Nonlinear regression of the data points calculated the K_D of Cm for Hsp90CT in the presence of ADP to be 39uM ± 10uM, R^2 =0.99. (C). A Hill plot of steady state Cm SPR signals; n = 1, R^2 =0.99.

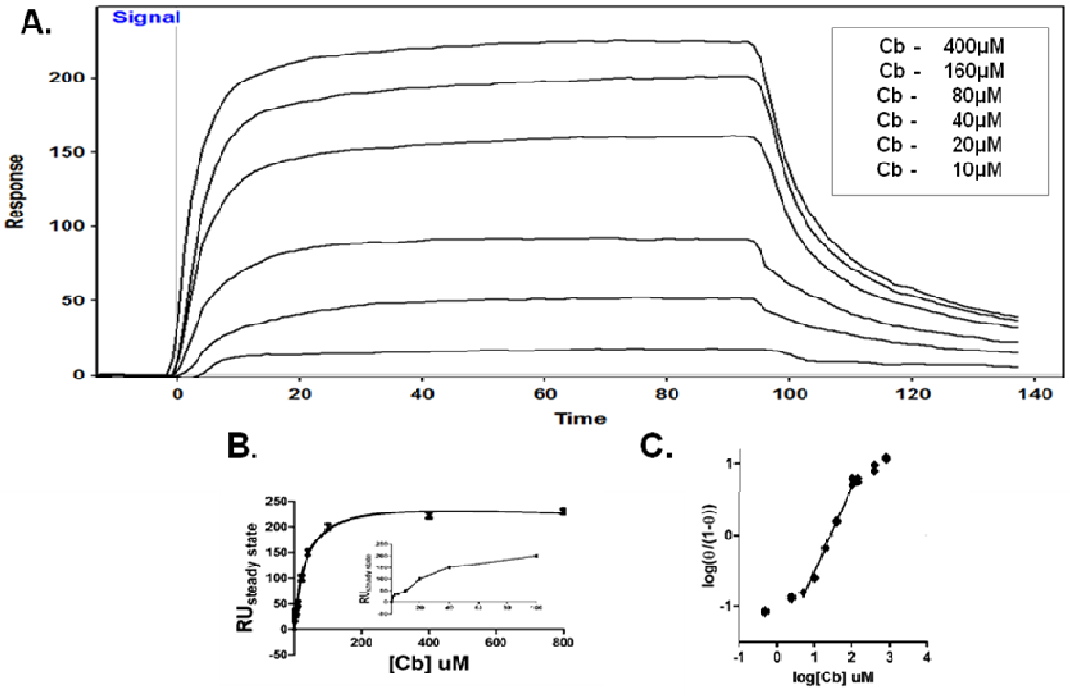

Figure 26: ADP Allosterically Enhances the Affinity of Cb for Hsp90FL:
(A). Cb was dissolved in ADP running buffer and assayed as described in Figure 3. Affinity analysis calculated a high affinity K_{D1} = 15uM ± 5uM and a low affinity K_{D2} = 30uM ± 20uM. (B). A hyperbolic replot of the steady state Cb SPR response curves. 30uM ± 20uM is the concentration of half maximal occupancy of Cb for Hsp90FL_ADP, as calculated by nonlinear regression of the data points, R^2 =0.98. (C). A Hill plot of steady state SPR signals; n = 2.6, R^2 =0.99.

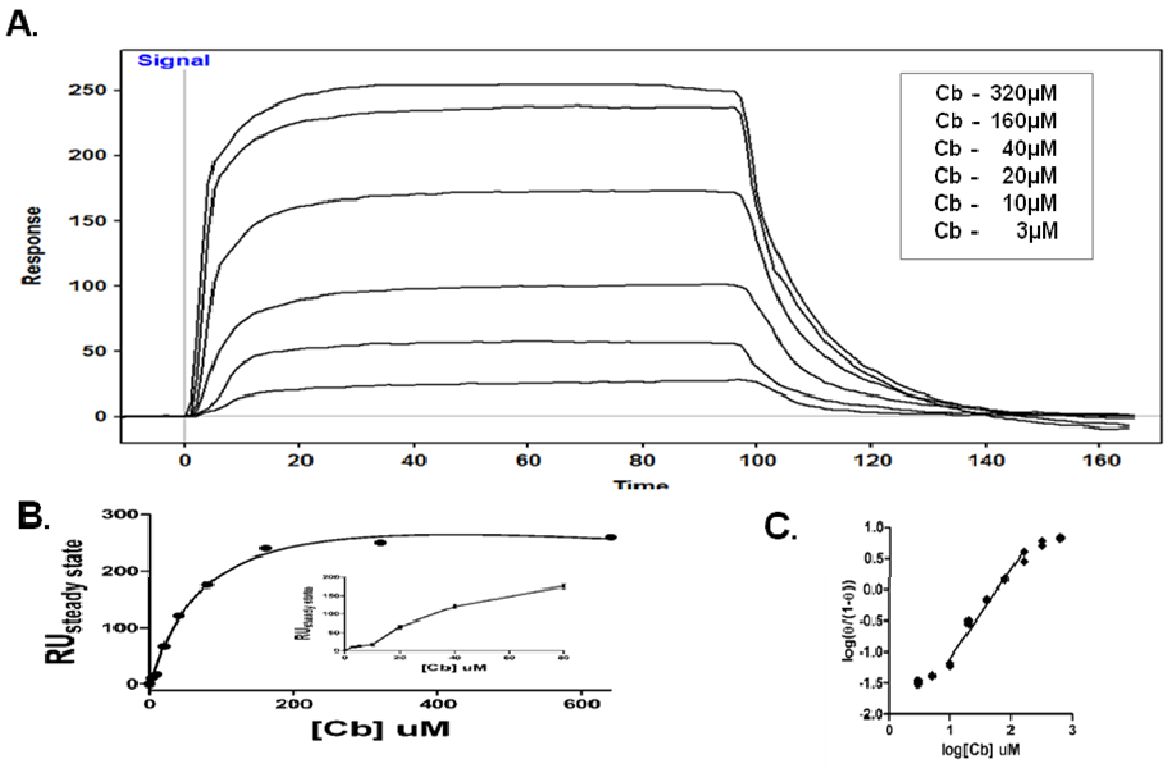

Figure 27: ADP Does Not Alter the Affinity of Chlorobiocin for Hsp90CT:
(A). Cb was dissolved in ADP running buffer and assayed over a surface bearing 100nmols/mm^2(2500RU) Hsp90CT as described in Figure 4. Affinity analysis calculated a high affinity K_{D1} = 35uM ± 5uM and a low affinity K_{D2} = 88uM ± 10uM. (B). A hyperbolic replot of the steady state Cb SPR response curves. 65uM ± 15uM is the concentration of half maximal occupancy of Cb for Hsp90CT under saturating conditions of ADP as calculated by nonlinear regression, R^2 =0.98. (C). A Hill plot of steady state SPR signals; *n* = 1.8, R^2 =0.99.

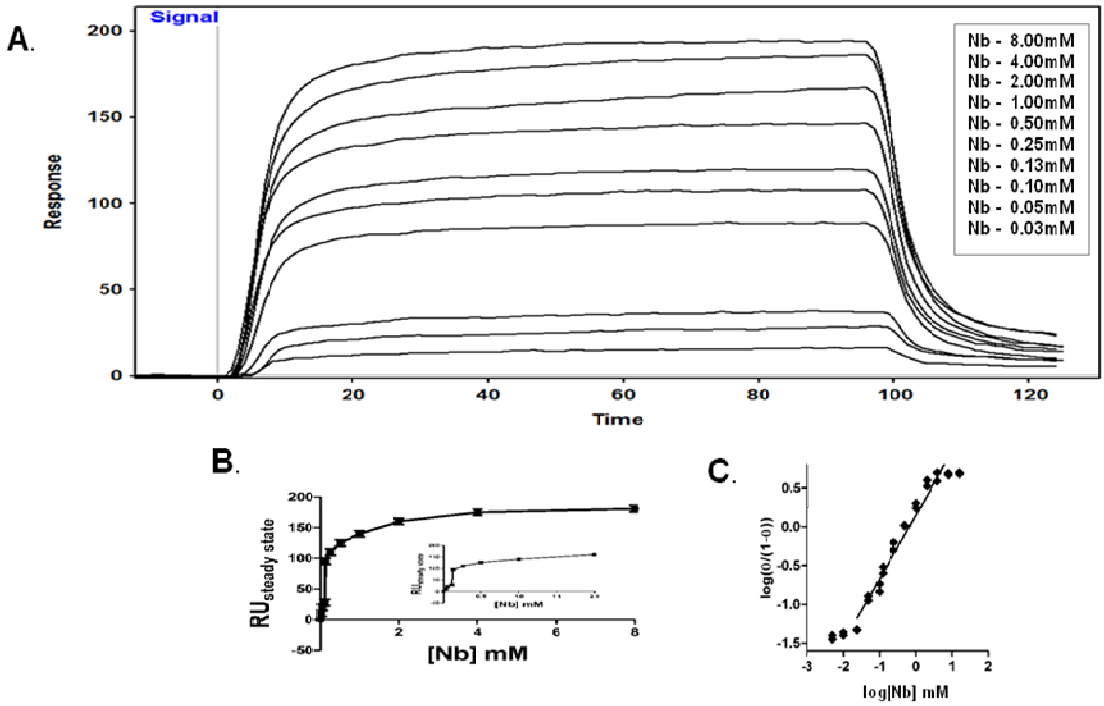

Figure 28: ADP Allosterically Enhances the Affinity of Nb for Hsp90FL: (A). Nb was dissolved in ADP running buffer and assayed as described in Figure 5. Affinity analysis calculated a high affinity K_{D1} = 130uM ± 30uM and a low affinity K_{D2} = 600uM ± 200uM. (B). A hyperbolic replot of the steady state Nb sensorgram. 250uM ± 50uM is the concentration of half maximal occupancy of Nb for Hsp90FL_ADP, as calculated by nonlinear regression of the data points, R^2 =0.975. (C). A Hill plot of steady state Nb SPR response curves; n = 3.0, R^2 =0.99

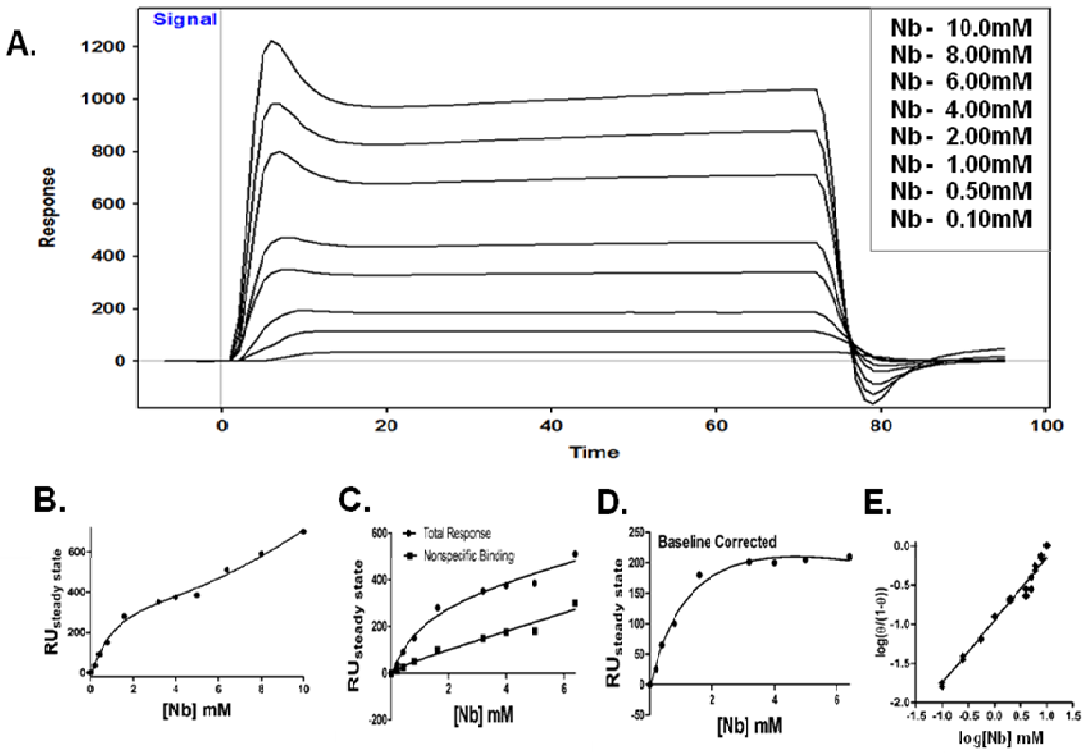

Figure 29: ADP Does Not Alter the Affinity of Novobiocin for Hsp90CT:

(A). Novobiocin was dissolved in ADP running buffer and assayed over a surface containing 100nmols/mm^2 Hsp90CT, as described in Figure 6. (B) A hyperbolic replot of the steady state Nb response curves. (C) Nb binding isotherm globally fit for total and nonspecific binding, as described in Figure 6. (D). A baseline corrected hyperbolic replot of the Nb steady state SPR signals. Nonlinear regression of the baseline corrected data points estimated the $K_{0.5}$ of Nb for Hsp90CT with additive ADP to be 1.7mM ± 0.69mM, R^2 =0.97. (E). A Hill plot of Nb SPR signals, n = 1.0, R^2 =0.98

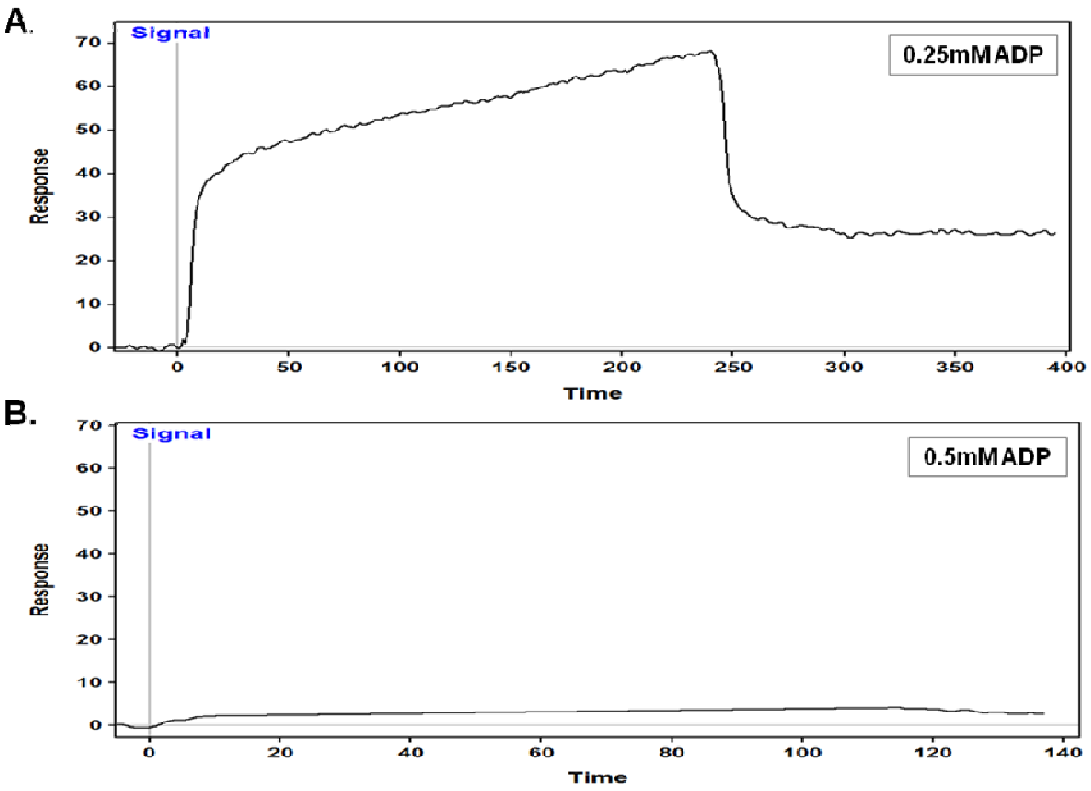

Figure 30: Binding of ADP/ phosphate to Hsp90 Constructs

(A) 33nmols/mm^2 Hsp90FL was pretreated with 0.01% Igepal as described in Figure 7. 0.25mM ADP was dissolved in nucleotide-phosphate running buffer (10mM PIPES, 300mM NaCL, 5mM $MgCL_2$, 100mM phosphate 2% DMSO, pH 7.4) and injected over the igepal pretreated surface at a flow rate of 25uL/min (n=3). (B) 0.5mM ADP was dissolved in nucleotide- phosphate running buffer and injected over a surface bearing 100nmols/mm^2 (2500RU) Hsp90CT at a flow rate of 25uL/min (n=3).

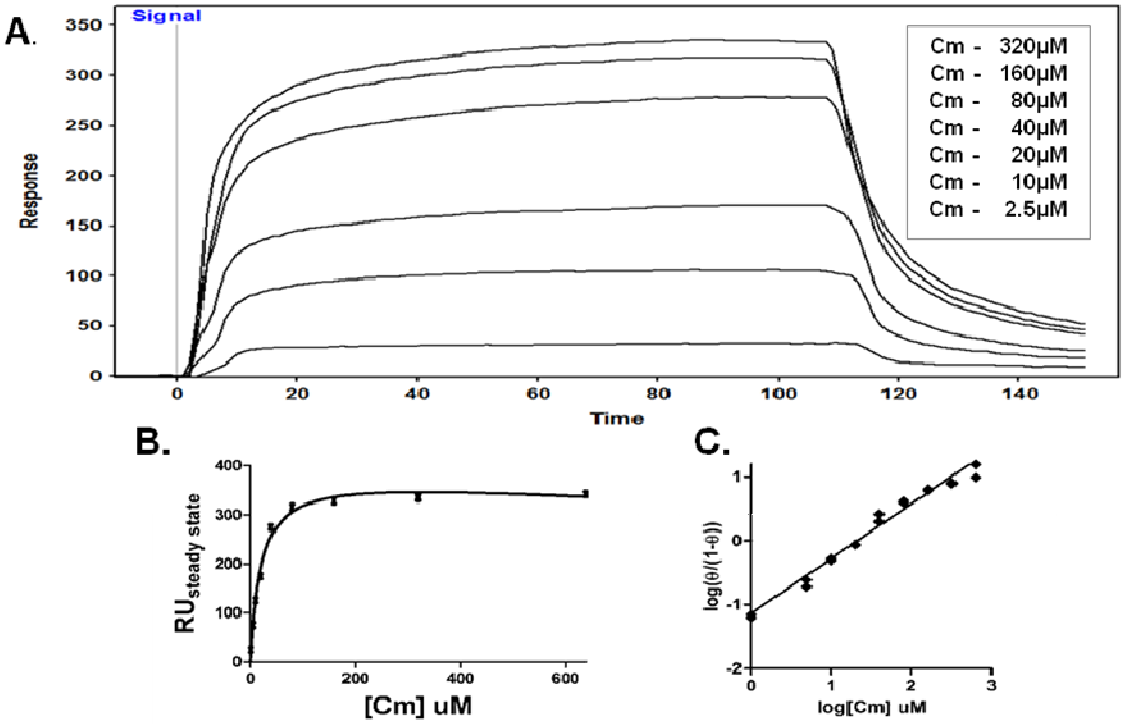

Figure 31: ADP/ phosphate Does Not Alter the Affinity of Cm A1 for Hsp90FL

(A). Coumermycin A1 was dissolved in ADP/phosphate running buffer (10mM PIPES, 300mM NaCL, 5mM $MgCL_2$, 0.5mM ADP, 100mM phosphate, 2% DMSO, pH 7.4) and assayed as described in Figure 1. Affinity analysis estimated the K_D of Cm A1 for the Hsp90FL ADP/ phosphate permutation to be 25uM ± 10uM. (B). A hyperbolic replot of the steady state Cm sensorgram. Nonlinear regression of the data points calculated the K_D of Cm A1 for Hsp90FL_ADP/ phosphate to be 20uM ± 15uM, R^2 =0.99. (C). A Hill plot of steady state Cm SPR signals; n = 1, R^2 =0.99

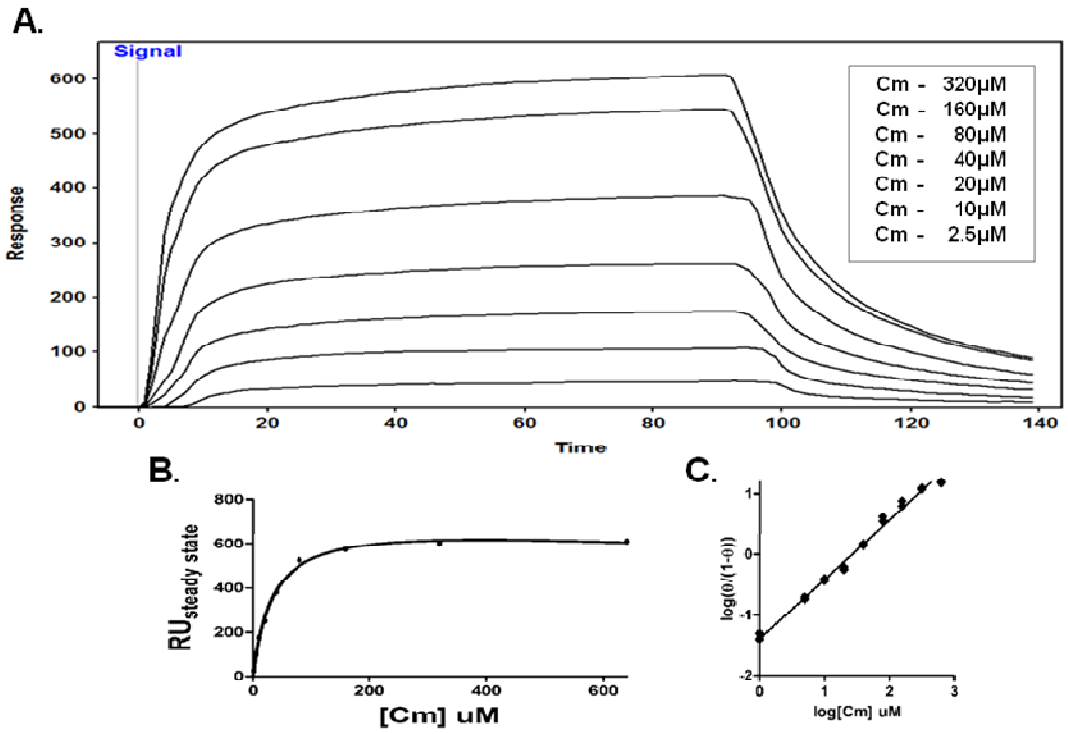

Figure 32: ADP/ phosphate Does Not Alter the Affinity of Cm A1 for Hsp90CT

(A). Coumermycin A1 was dissolved in ADP/ phosphate running buffer and assayed over a surface bearing 100nmol/mm^2 (2500RU) Hsp90CT, as described in Figure 2. Affinity analysis estimated the K_D of Cm A1 for the Hsp90CT in the presence of ADP/ phosphate to be 25uM ± 10uM. (B). A hyperbolic replot of the steady state Cm sensorgram. Nonlinear regression of the data points calculated the K_D of Cm A1 for Hsp90FL_ADP/ phosphate to be 20uM ± 15uM, R^2 =0.99. (C). A Hill plot of steady state Cm SPR signals; n = 1, R^2=0.99

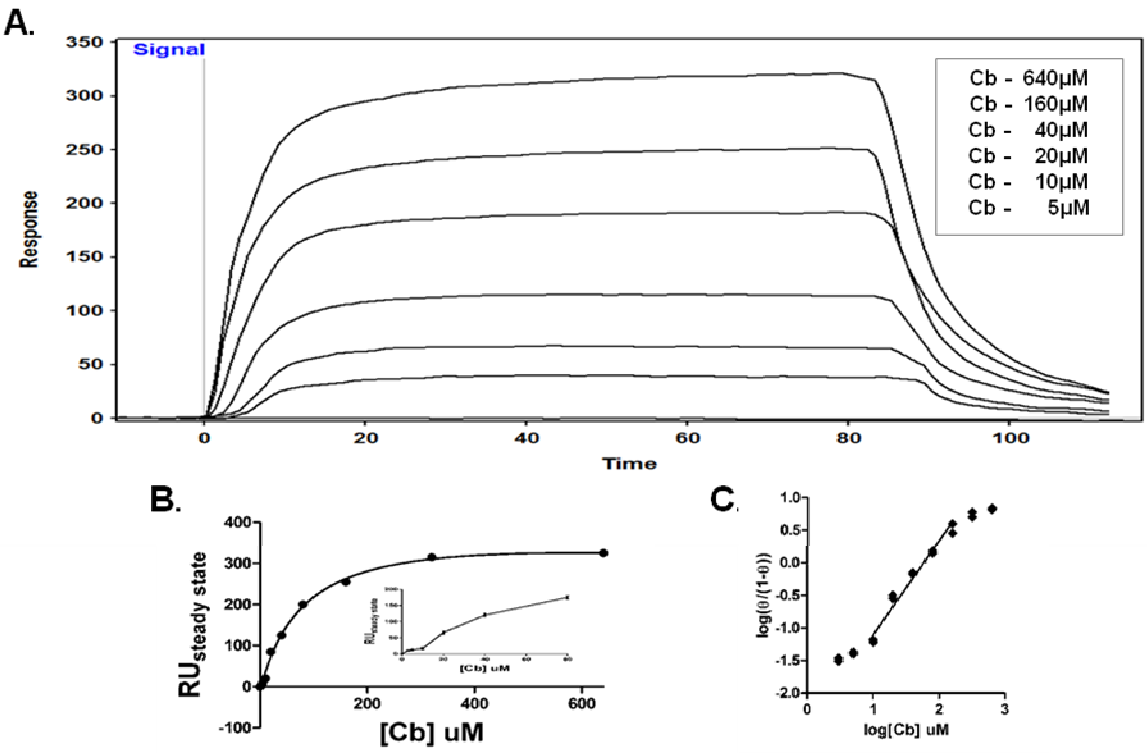

Figure 33: ADP/ phosphate Does Not Alter the Affinity of Cb for Hsp90FL: (A). Cb was dissolved in ADP/ phosphate running buffer and assayed as described in Figure 3. Affinity analysis calculated a high affinity K_{D1} = 35 ± 8uM and a lower affinity K_{D2} = 145uM ± 20uM. (B). A hyperbolic replot of the steady state Cb sensorgram. 86uM ± 18uM is the concentration of half maximal occupancy of Cb for Hsp90FL_ADP/ phosphate, as calculated by nonlinear regression of the data points, R^2 =0.98. (C). A Hill plot of steady state SPR signals; n = 1.6, R^2 = 0.99

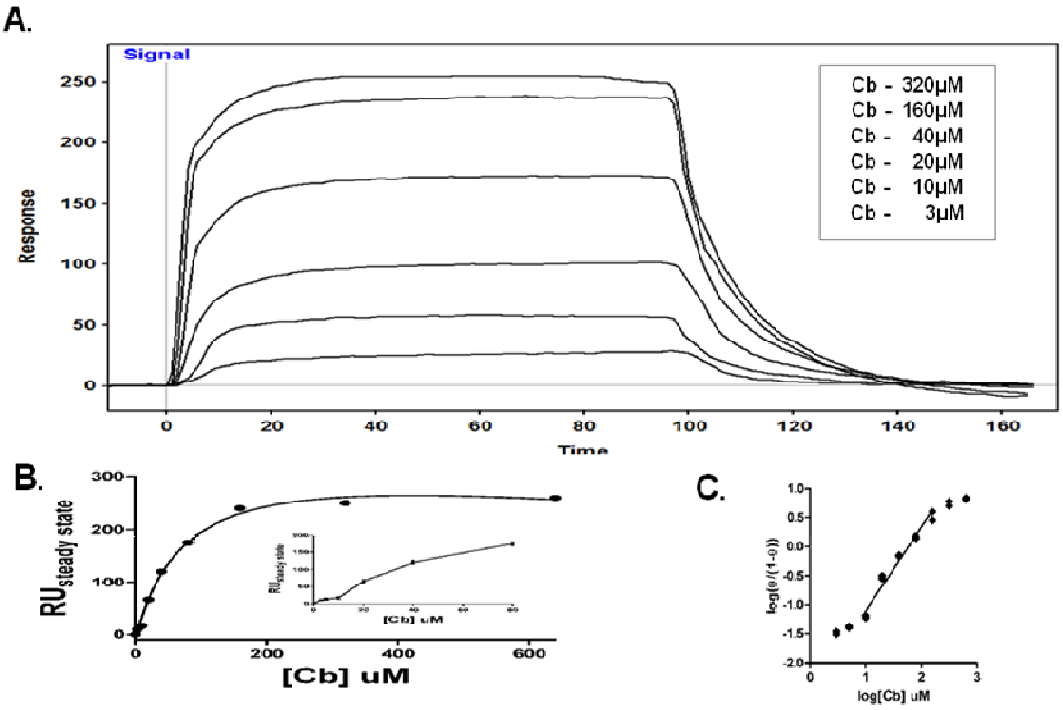

Figure 34: ADP/ phosphate Does Not Alter the Affinity of Cb for Hsp90CT:
(A). Cb was dissolved in ADP/ phosphate running buffer and assayed over a chipbearing 100nmols/mm^2 (2500RU) Hsp90CT, as described in Figure 4. Affinity analysis estimated a high affinity K_{D1} = 35 ± 5uM and a lower affinity K_{D2} = 110uM ± 10uM. (B). A hyperbolic replot of the steady state Cb sensorgram. 70uM ± 15uM is the concentration of half maximal occupancy of Cb for Hsp90CT in the presence of ADP/ phosphate, as calculated by nonlinear regression of the data points, R^2 =0.98. (C). A Hill plot of steady state Cb SPRresponse curves; *n* = 1.8, R^2 = 0.99

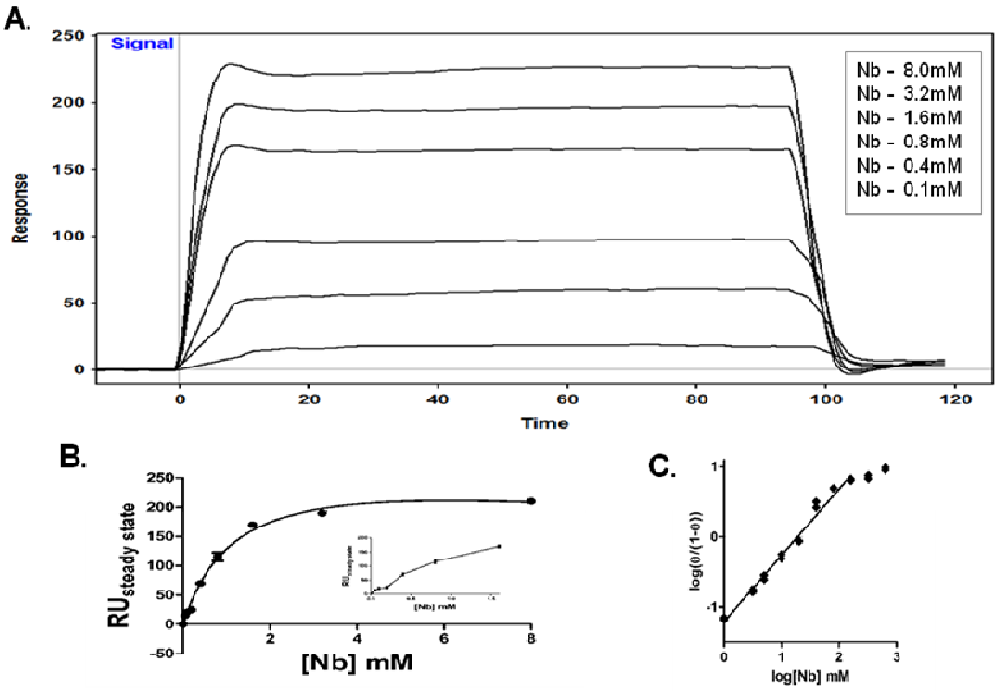

Figure 35: ADP/ phosphate Does Not Alter the Affinity of Nb for Hsp90FL: (A). Nb was dissolved in ADP/ phosphate running buffer and assayed as described in Figure 5. Affinity analysis calculated a high affinity K_{D1} = 900uM ± 100uM and a lower affinity K_{D2} = 2.2mM ± 250uM. (B). A hyperbolic replot of the steady state Nb sensorgram. 1.24mM ± 0.30mM is the concentration of half maximal occupancy of Nb for Hsp90FL_ADP/ phosphate, as determined by nonlinear regression of the data points, R^2 =0.97. (C). A Hill plot of steady state Nb response curves; n = 1.6, R^2 = 0.99

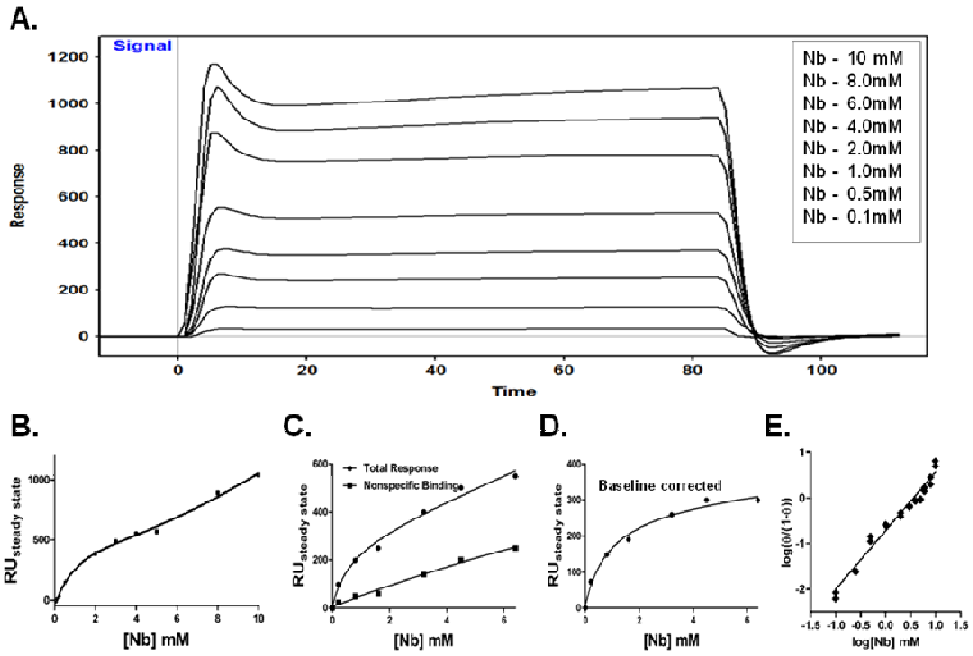

Figure 36: ADP/ phosphate Does Not Alter the Affinity of Nb for Hsp90CT: (A). Novobiocin was dissolved in ADP/ phosphate running buffer and assayed over a surface bearing 100nmols/mm^2 Hsp90CT, as described in Figure 6. (B) A hyperbolic replot of steady state Nb response curves. (C) Nb binding isotherm globally fit for total and nonspecific binding, as described in Figure 6. (D). A baseline corrected hyperbolic replot of the Nb steady state response curves. Nonlinear regression of the baseline corrected data points estimated the $K_{0.5}$ of Nb for Hsp90CT with additive ADP/ phosphate to be 0.95mM ± 0.5mM, R^2 =0.97. (E). A Hill plot of Nb SPR signals, n = 1.0, R^2 =0.98.

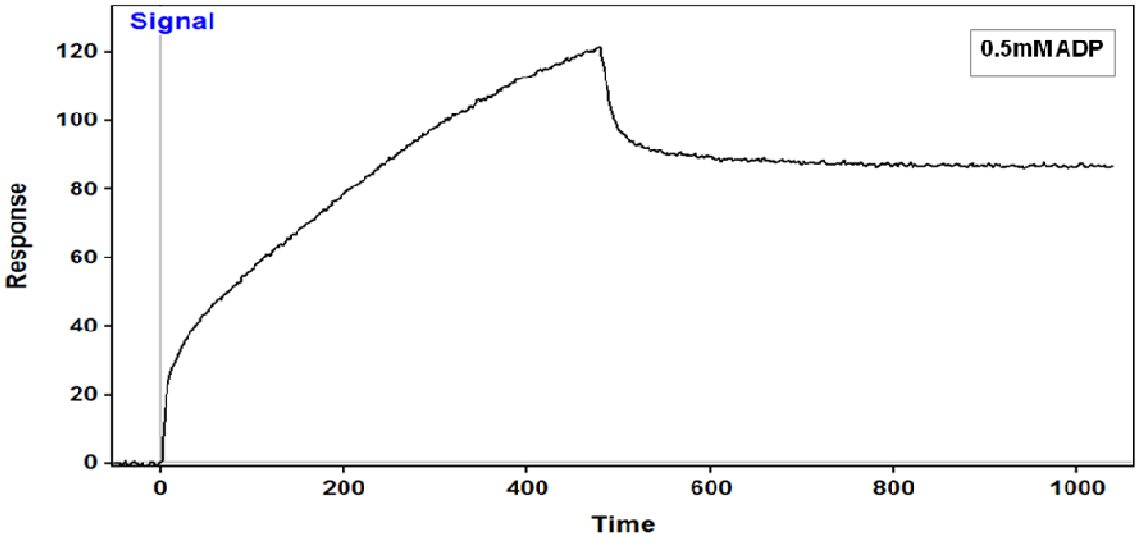

Figure 37: Binding of ADP/ molybdate to Hsp90FL:
33nmols/mm^2 Hsp90FL was pretreated with 0.01% Igepal as described in Figure 7. 0.5mM ADP was dissolved in nucleotide-molybdate running buffer (10mM PIPES, 300mM NaCL, 5mM $MgCL_2$, 20mM Na_2MoO_4, 2% DMSO, pH 7.4) and injected over the igepal pretreated surface at a flow rate of 25uL/min (n=3).

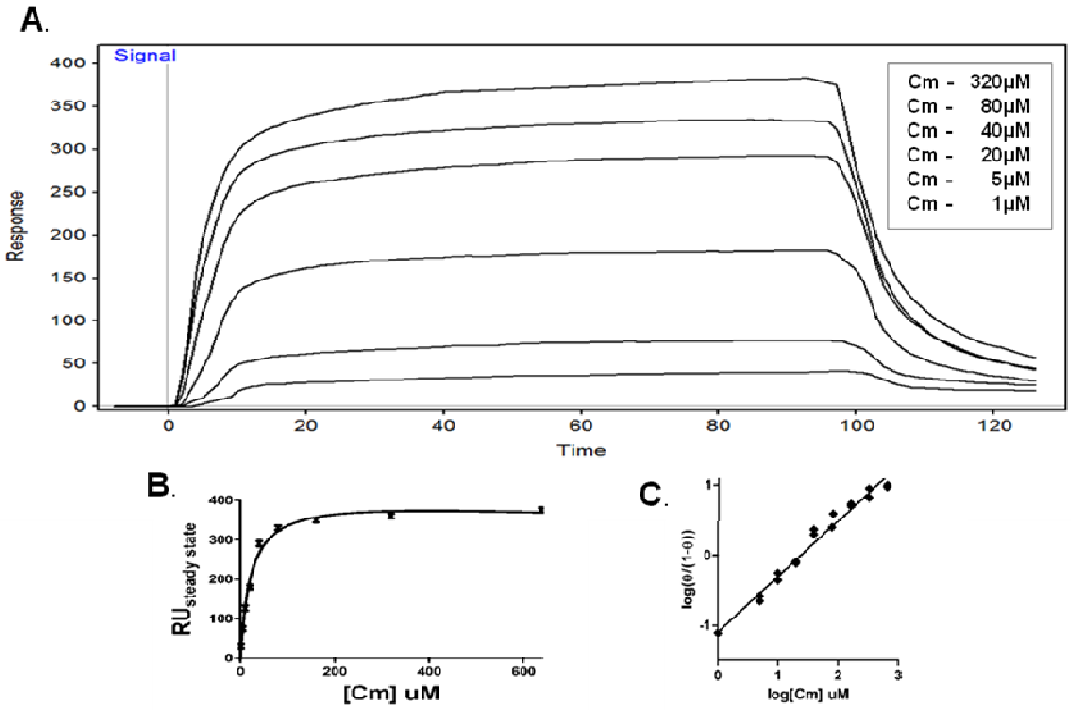

Figure 38: ADP/ molybdate Does not Alter the Affinity of Cm A1 for Hsp90FL: (A). Coumermycin A1 was dissolved in ADP/ molybdate running buffer (10mM PIPES, 300mM NaCL, 5mM $MgCL_2$, 0.5mM ADP, 20mM Na_2MoO_4, 2% DMSO, pH 7.4) and assayed as described in Figure 1. Affinity analysis estimated the K_D of Cm A1 for the Hsp90FL_ADP/ molybdate conjugate to be 33uM ± 15uM. (B). A hyperbolic replot of the steady state Cm sensorgram. Nonlinear regression of the data points calculated the K_D of Cm A1 for Hsp90FL_ADP/ molybdate to be 30uM ± 10uM, R^2 =0.99. (C). A Hill plot of steady state Cm SPR signals; n = 1, R^2 =0.99

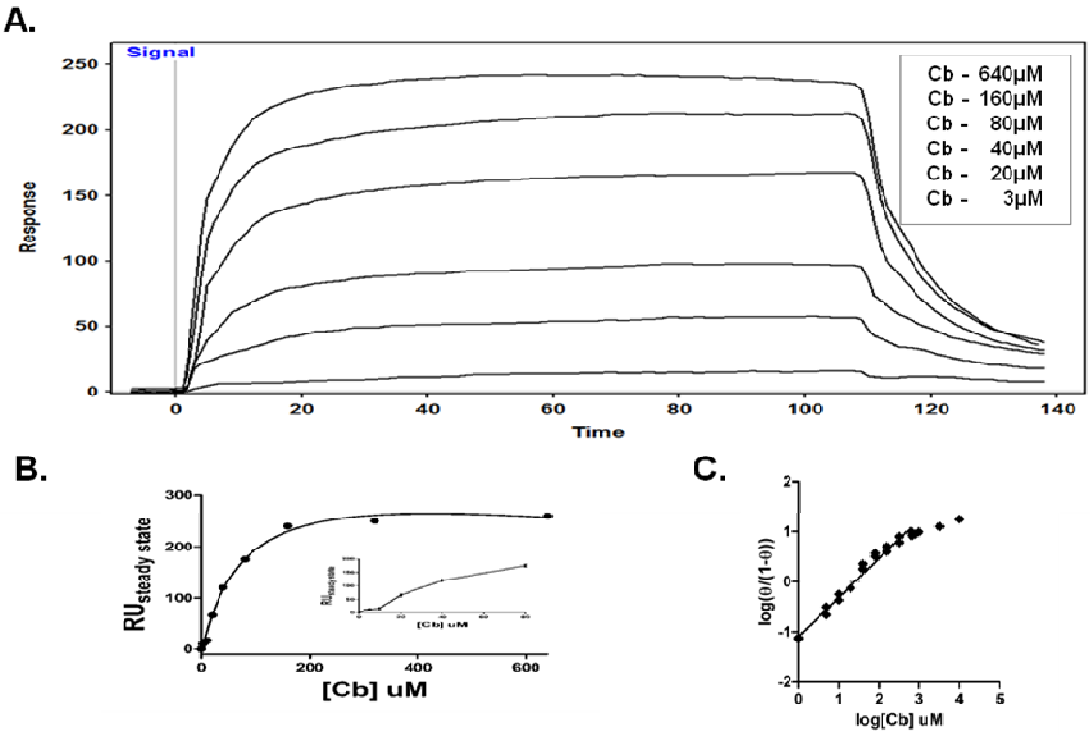

Figure 39: ADP/ molybdate Does not Alter the Affinity of Cb for Hsp90FL: (A). Cb was dissolved in ADP/ molybdate running buffer and assayed as described in Figure 3. Affinity analysis calculated a high affinity K_{D1} = 30 ± 8uM and a lower affinity K_{D2} = 125uM ± 20uM. (B). A hyperbolic replot of the steady state Cb sensorgram. 79uM ± 18uM is the concentration of half maximal occupancy of Cb for Hsp90FL_ADP/ molybdate, as calculated by nonlinear regression of the data points, R^2 =0.98. (C). A Hill plot of steady state SPR signals; n = 1.3, R^2 = 0.99.

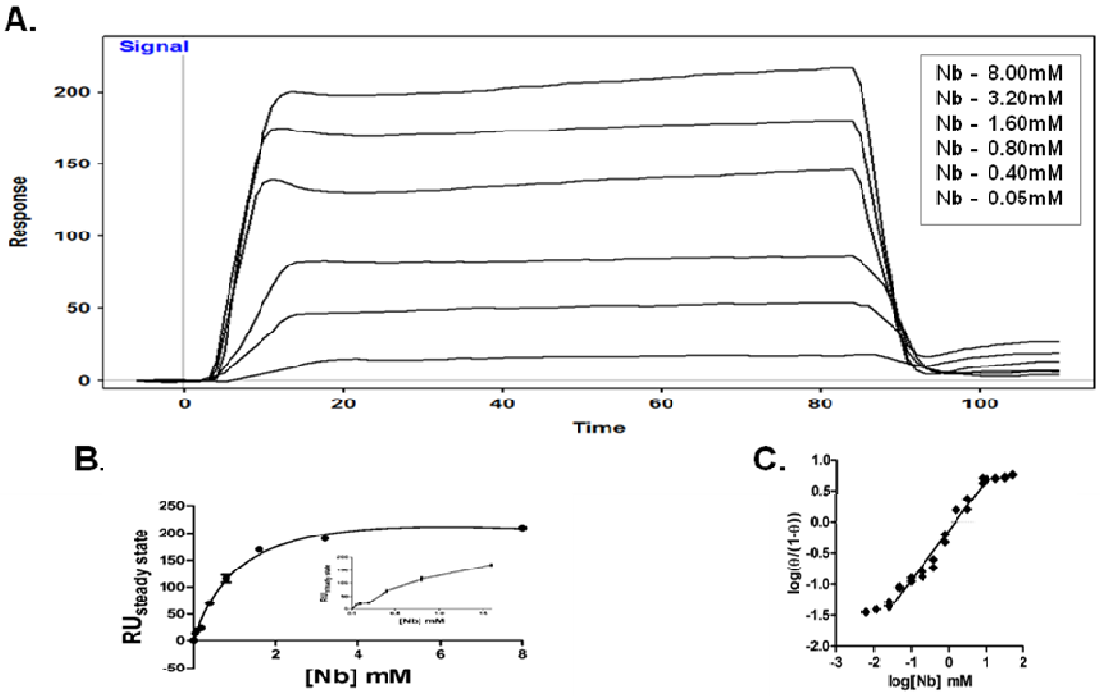

Figure 40: ADP/ molybdate Does not Alter the Affinity of Nb for Hsp90FL:
(A). Nb was dissolved in ADP/ molybdate running buffer and assayed as described in Figure 5. Affinity analysis calculated a high affinity K_{D1} = 750uM ± 100uM and a lower affinity K_{D2} = 2.3mM ± 200uM. (B). A hyperbolic replot of the steady state Cb sensorgram. 1.3mM ± 200uM is the concentration of half maximal occupancy of Nb for Hsp90FL_ADP/ molybdate, as calculated by nonlinear regression of the data points, R^2 =0.98. (C). A Hill plot of steady state SPR signals; n = 1.4, R^2 = 0.99

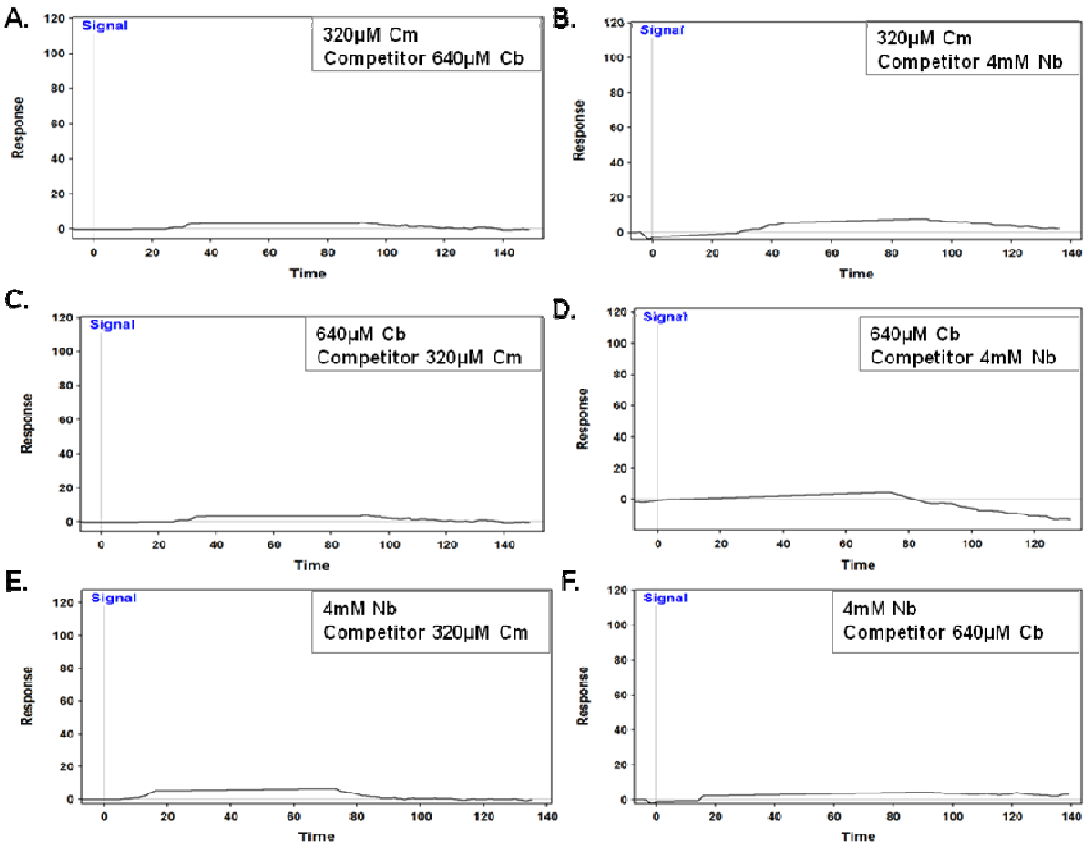

Figure 41: Competition Assays:
(A) 320uM Cm A1 was injected at a flow rate of 25uL/min over 33nmol/mm^2 Hsp90FL after the protein surface had been preequilibrated with standard running buffer containing 640uM of competitor, chlorobiocin, (n=3). (B) 320uM Cm A1 was assayed as described in (A) with 4mM of competitor, novobiocin (n=3). (C) 640uM Cb was assayed as described in (A) in conjunction with 320uM of antagonist, coumermycin A1 (n=3). (D) 640uM Cb was assayed as described in (A) in tandem with 4mM of antagonist, novobiocin (n=3). (E). 4mM Nb was assayed as described in (A) in combination with 320uM of competitor, coumermycin A1 (n=3). (F). 4mM Nb was assayed as described in (A) in tandem with 640uM of antagonist, chlorobiocin, (n=3). Assays done immediately prior to addition of each competitor and immediately following the removal of each competitor revealed typical response curves for all analytes examined.

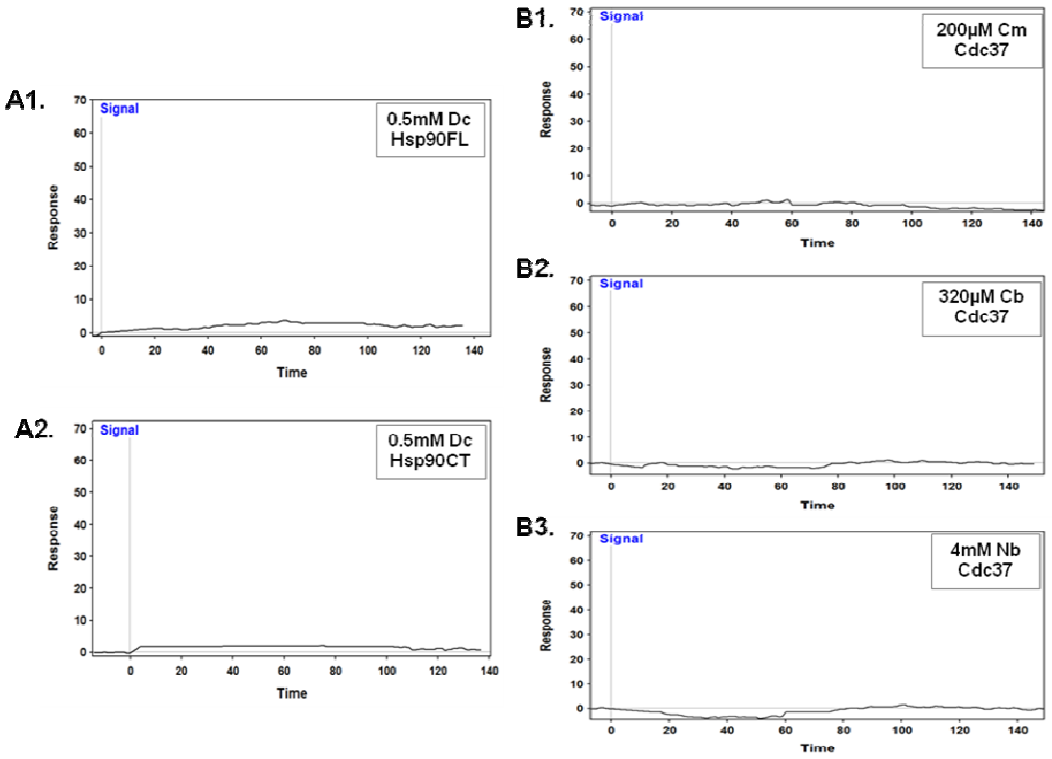

Figure 42: Negative Controls:

(A). 0.5mM Dicoumarol was dissolved in standard running buffer and injected at a flow rate of 25uL /min over *(A1)* 33nmols/mm^2 Hsp90FL and *(A2)* 100nmols/mm^2 Hsp90CT in independent assays (n=3). (B). *(B1)* 200uM Coumermycin A1 was dissolved in standard running buffer and injected at a flow rate of 25uL/min over a surface bearing 40nmols/mm2 Cdc37 (n=3). *(B2-B3)* 320uM chlorobiocin and 4mM novobiocin were assayed as described in B1 (n=3).

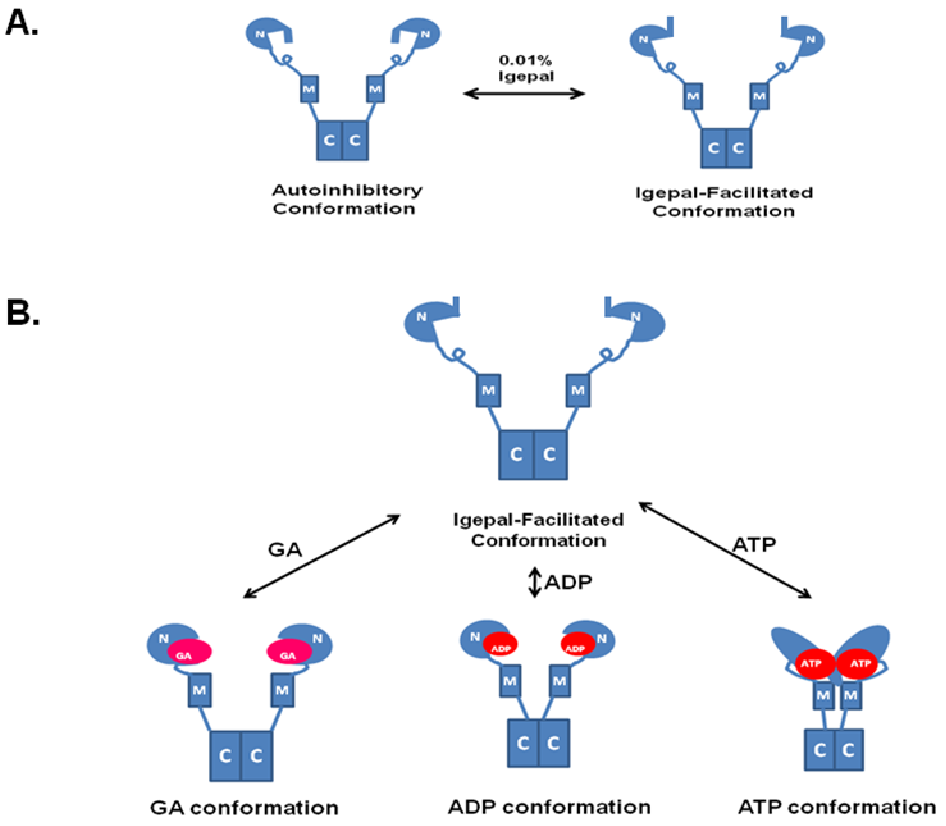

Figure 43: Model:
(A). An autoinhibitory conformation of Hsp90 which induced by steric hindrance of nucleotide capping lid causing an occlusion of the NTD nucleotide binding pocket. Injection of Igepal induces an Igepal-facilitated conformation of Hsp90, in which the nucleotide capping lid no longer occludes the NTD nucleotide binding pocket. (B). The Igepal facilitated conformation of Hsp90 readily binds GA, ADP, and/or ATP, whereas the autoinhibitory conformation of Hsp90 is unable to bind N-terminal ligands. Binding of N-terminal ligand to the Igepal-facilitated conformation of Hsp90 leads to a reduction in the hydrodynamic radius of Hsp90.

Hsp90FL Summary of Values:

	Cm	Cb	Nb	Replicates
Hsp90	**50 ± 10 μM**	**45 ± 5 μM** **155 ± 10 μM**	**3.3 ± 0.9 mM**	**n = 3**
Hsp90: GA	**3.3 ± 5 μM** **20 ± 15 μM**	**45 ± 5 μM** **170 ± 20μM**	**800 ± 80 μM** **2 ± 0.2 mM**	**n = 3**
Hsp90: ATP	**49 ± 7 μM**	**40 ± 10 μM** **170 ± 20 μM**	**980 ± 80 μM** **2.1 ±0.2 mM**	**n = 3**
Hsp90: ADP	**1.5 ± 0.5 μM** **7.5 ± 2.0 μM**	**15 ± 5 μM** **30 ± 20 μM**	**130 ± 30 μM** **600 ± 200 mM**	**n = 3**
Hsp90: ADP/PoO_4	**25 ± 10 μM**	**35 ± 8 μM** **145 ± 20μM**	**900 ± 100 μM** **2.2 ±0.3mM**	**n = 3**
Hsp90: ADP/MoO_4	**33 ± 15 μM**	**30 ± 8μM** **125 ± 20 μM**	**750 ± 100 μM** **2.3 ± 0.2 mM**	**n = 3**

Table 1:
Summary of affinity constants obtained for Hsp90FL interactions. All constants are reported as K_D's with the exception for the apo Hsp90: Nb interaction. Nb's binding constant for apo Hsp90 FL is reported as the concentration of half maximal occupancy ($K_{0.5}$).

Hsp90CT Summary of Values:

	Cm	Cb	Nb	Replicates
Hsp90CT	**40 ± 10 μM**	**35 ± 5 μM** **110 ± 10 μM**	**1.9 ± 0.6 mM**	**n = 3**
Hsp90CT: GA	**40 ± 10 μM**	**36 ± 5 μM** **109 ± 10 μM**	**1.9 ± 0.6 mM**	**n = 3**
Hsp90CT: ATP	**20 ± 10 μM**	**30 ± 5 μM** **110 ± 10 μM**	**1.6 ± 0.7 mM**	**n = 3**
Hsp90CT: ADP	**38 ± 10 μM**	**35 ± 5 μM** **88 ± 10 μM**	**1.7 ± 0.69 mM**	**n = 3**
Hsp90CT: ADP/PoO_4	**25 ± 10 μM**	**35 ± 5 μM** **110 ± 10 μM**	**0.95 ± 0.5 mM**	**n = 3**

Table 2:
Summary of affinity constants obtained for Hsp90CT interactions. All constants are reported as K_D's with the exception for the Hsp90CT: Nb interactions. Nb's binding constants for all Hsp90CT interactions are reported as concentrations of half maximal occupancy ($K_{0.5}$).

REFERENCES

Abbas-Terki, T., P. A. Briand, O. Donze & D. Picard, (2002) The Hsp90 co-chaperones Cdc37 and Sti1 interact physically and genetically. *Biol Chem* **383**: 1335-1342.

Acerenza, L. & E. Mizraji, (1997) Cooperativity: a unified view. *Biochim Biophys Acta* **1339**: 155-166.

Ali, M. M., S. M. Roe, C. K. Vaughan, P. Meyer, B. Panaretou, P. W. Piper, C. Prodromou & L. H. Pearl, (2006) Crystal structure of an Hsp90-nucleotide-p23/Sba1 closed chaperone complex. *Nature* **440**: 1013-1017.

Allan, R. K., D. Mok, B. K. Ward & T. Ratajczak, (2006) Modulation of chaperone function and cochaperone interaction by novobiocin in the C-terminal domain of Hsp90: evidence that coumarin antibiotics disrupt Hsp90 dimerization. *J Biol Chem* **281**: 7161-7171.

Alnemri, E. S. & G. Litwack, (1993) The steroid binding domain influences intracellular solubility of the baculovirus overexpressed glucocorticoid and mineralocorticoid receptors. *Biochemistry* **32**: 5387-5393.

Basso, A. D., D. B. Solit, G. Chiosis, B. Giri, P. Tsichlis & N. Rosen, (2002) Akt forms an intracellular complex with heat shock protein 90 (Hsp90) and Cdc37 and is destabilized by inhibitors of Hsp90 function. *J Biol Chem* **277**: 39858-39866.

Bron, P., E. Giudice, J. P. Rolland, R. M. Buey, P. Barbier, J. F. Diaz, V. Peyrot, D. Thomas & C. Garnier, (2008) Apo-Hsp90 coexists in two open conformational states in solution. *Biol Cell* **100**: 413-425.

Buchner, J., (1999) Hsp90 & Co. - a holding for folding. *Trends Biochem Sci* **24**: 136-141.

Burlison, J. A., C. Avila, G. Vielhauer, D. J. Lubbers, J. Holzbeierlein & B. S. Blagg, (2008) Development of novobiocin analogues that manifest anti-proliferative activity against several cancer cell lines. *J Org Chem* **73**: 2130-2137.

Burlison, J. A. & B. S. Blagg, (2006) Synthesis and evaluation of coumermycin A1 analogues that inhibit the Hsp90 protein folding machinery. *Org Lett* **8**: 4855-4858.

Callebaut, I., M. G. Catelli, D. Portetelle, X. Meng, F. Cadepond, A. Burny, E. E. Baulieu & J. P. Mornon, (1994) Redox mechanism for the chaperone activity of heat shock proteins HSPs 60, 70 and 90 as suggested by hydrophobic cluster analysis: hypothesis. *C R Acad Sci III* **317**: 721-729.

Caplan, A. J., S. Jackson & D. Smith, (2003) Hsp90 reaches new heights. Conference on the Hsp90 chaperone machine. *EMBO Rep* **4**: 126-130.

Chadli, A., I. Bouhouche, W. Sullivan, B. Stensgard, N. McMahon, M. G. Catelli & D. O. Toft, (2000) Dimerization and N-terminal domain proximity underlie the function of the molecular chaperone heat shock protein 90. *Proc Natl Acad Sci U S A* **97**: 12524-12529.

Chen, S., W. P. Sullivan, D. O. Toft & D. F. Smith, (1998) Differential interactions of p23 and the TPR-containing proteins Hop, Cyp40, FKBP52 and FKBP51 with Hsp90 mutants. *Cell Stress Chaperones* **3**: 118-129.

Chiosis, G., B. Lucas, H. Huezo, D. Solit, A. Basso & N. Rosen, (2003) Development of purine-scaffold small molecule inhibitors of Hsp90. *Curr Cancer Drug Targets* **3**: 371-376.

Cotten, M., D. Bresnahan, S. Thompson, L. Sealy & R. Chalkley, (1986) Novobiocin precipitates histones at concentrations normally used to inhibit eukaryotic type II topoisomerase. *Nucleic Acids Res* **14**: 3671-3686.

Du, J., D. H. Daniels, C. Asbury, S. Venkataraman, J. Liu, D. R. Spitz, L. W. Oberley & J. J. Cullen, (2006) Mitochondrial production of reactive oxygen species mediate dicumarol-induced cytotoxicity in cancer cells. *J Biol Chem* **281**: 37416-37426.

Flatmark, T., A. J. Stokka & S. V. Berge, (2001) Use of surface plasmon resonance for real-time measurements of the global conformational transition in human phenylalanine hydroxylase in response to substrate binding and catalytic activation. *Anal Biochem* **294**: 95-101.

Fontana, J., D. Fulton, Y. Chen, T. A. Fairchild, T. J. McCabe, N. Fujita, T. Tsuruo & W. C. Sessa, (2002) Domain mapping studies reveal that the M domain of hsp90 serves as a molecular scaffold to regulate Akt-dependent phosphorylation of endothelial nitric oxide synthase and NO release. *Circ Res* **90**: 866-873.

Galam, L., M. K. Hadden, Z. Ma, Q. Z. Ye, B. G. Yun, B. S. Blagg & R. L. Matts, (2007) High-throughput assay for the identification of Hsp90 inhibitors based on Hsp90-dependent refolding of firefly luciferase. *Bioorg Med Chem* **15**: 1939-1946.

Garnier, C., D. Lafitte, P. O. Tsvetkov, P. Barbier, J. Leclerc-Devin, J. M. Millot, C. Briand, A. A. Makarov, M. G. Catelli & V. Peyrot, (2002) Binding of ATP to heat shock protein 90: evidence for an ATP-binding site in the C-terminal domain. *J Biol Chem* **277**: 12208-12214.

Gestwicki, J. E., H. V. Hsieh & J. B. Pitner, (2001) Using receptor conformational change to detect low molecular weight analytes by surface plasmon resonance. *Anal Chem* **73**: 5732-5737.

Graf, C., M. Stankiewicz, G. Kramer & M. P. Mayer, (2009) Spatially and kinetically resolved changes in the conformational dynamics of the Hsp90 chaperone machine. *EMBO J* **28**: 602-613.

Harris, S. F., A. K. Shiau & D. A. Agard, (2004) The crystal structure of the carboxy-terminal dimerization domain of htpG, the Escherichia coli Hsp90, reveals a potential substrate binding site. *Structure* **12**: 1087-1097.

Hartson, S. D., V. Thulasiraman, W. Huang, L. Whitesell & R. L. Matts, (1999) Molybdate inhibits hsp90, induces structural changes in its C-terminal domain, and alters its interactions with substrates. *Biochemistry* **38**: 3837-3849.

Hernandez, A., G. Lopez-Lluch, J. A. Bernal, P. Navas & J. A. Pintor-Toro, (2008) Dicoumarol down-regulates human PTTG1/Securin mRNA expression through inhibition of Hsp90. *Mol Cancer Ther* **7**: 474-482.

Hessling, M., K. Richter & J. Buchner, (2009) Dissection of the ATP-induced conformational cycle of the molecular chaperone Hsp90. *Nat Struct Mol Biol* **16**: 287-293.

Itoh, H., M. Ogura, A. Komatsuda, H. Wakui, A. B. Miura & Y. Tashima, (1999) A novel chaperone-activity-reducing mechanism of the 90-kDa molecular chaperone HSP90. *Biochem J* **343 Pt 3**: 697-703.

Johnson, B. D., R. J. Schumacher, E. D. Ross & D. O. Toft, (1998) Hop modulates Hsp70/Hsp90 interactions in protein folding. *J Biol Chem* **273**: 3679-3686.

Kosano, H., B. Stensgard, M. C. Charlesworth, N. McMahon & D. Toft, (1998) The assembly of progesterone receptor-hsp90 complexes using purified proteins. *J*

Biol Chem **273**: 32973-32979.
Krukenberg, K. A., U. M. Bottcher, D. R. Southworth & D. A. Agard, (2009) Grp94, the endoplasmic reticulum Hsp90, has a similar solution conformation to cytosolic Hsp90 in the absence of nucleotide. *Protein Sci*.
Krukenberg, K. A., F. Forster, L. M. Rice, A. Sali & D. A. Agard, (2008) Multiple conformations of E. coli Hsp90 in solution: insights into the conformational dynamics of Hsp90. *Structure* **16**: 755-765.
Langer, T., H. Schlatter & H. Fasold, (2002) Evidence that the novobiocin-sensitive ATP-binding site of the heat shock protein 90 (hsp90) is necessary for its autophosphorylation. *Cell Biol Int* **26**: 653-657.
Louvion, J. F., R. Warth & D. Picard, (1996) Two eukaryote-specific regions of Hsp82 are dispensable for its viability and signal transduction functions in yeast. *Proc Natl Acad Sci U S A* **93**: 13937-13942.
Marcu, M. G., A. Chadli, I. Bouhouche, M. Catelli & L. M. Neckers, (2000a) The heat shock protein 90 antagonist novobiocin interacts with a previously unrecognized ATP-binding domain in the carboxyl terminus of the chaperone. *J Biol Chem* **275**: 37181-37186.
Marcu, M. G., T. W. Schulte & L. Neckers, (2000b) Novobiocin and related coumarins and depletion of heat shock protein 90-dependent signaling proteins. *J Natl Cancer Inst* **92**: 242-248.
Marszall, M. P., R. Moaddel, K. Jozwiak, M. Bernier & I. W. Wainer, (2008a) Initial synthesis and characterization of an immobilized heat shock protein 90 column for online determination of binding affinities. *Anal Biochem* **373**: 313-321.
Marszall, M. P., R. Moaddel, S. Kole, M. Gandhari, M. Bernier & I. W. Wainer, (2008b) Ligand and protein fishing with heat shock protein 90 coated magnetic beads. *Anal Chem* **80**: 7571-7575.
Maruya, M., M. Sameshima, T. Nemoto & I. Yahara, (1999) Monomer arrangement in HSP90 dimer as determined by decoration with N and C-terminal region specific antibodies. *J Mol Biol* **285**: 903-907.
Mayer, M. P., C. Prodromou & J. Frydman, (2009) The Hsp90 mosaic: a picture emerges. *Nat Struct Mol Biol* **16**: 2-6.
McLaughlin, S. H., H. W. Smith & S. E. Jackson, (2002) Stimulation of the weak ATPase activity of human hsp90 by a client protein. *J Mol Biol* **315**: 787-798.
McLaughlin, S. H., L. A. Ventouras, B. Lobbezoo & S. E. Jackson, (2004) Independent ATPase activity of Hsp90 subunits creates a flexible assembly platform. *J Mol Biol* **344**: 813-826.
Meyer, P., C. Prodromou, B. Hu, C. Vaughan, S. M. Roe, B. Panaretou, P. W. Piper & L. H. Pearl, (2003) Structural and functional analysis of the middle segment of hsp90: implications for ATP hydrolysis and client protein and cochaperone interactions. *Mol Cell* **11**: 647-658.
Mickler, M., M. Hessling, C. Ratzke, J. Buchner & T. Hugel, (2009) The large conformational changes of Hsp90 are only weakly coupled to ATP hydrolysis. *Nat Struct Mol Biol* **16**: 281-286.
Minami, Y., Y. Kimura, H. Kawasaki, K. Suzuki & I. Yahara, (1994) The carboxy-terminal region of mammalian HSP90 is required for its dimerization and function in vivo. *Mol Cell Biol* **14**: 1459-1464.

Myszka, D. G., (1999) Improving biosensor analysis. *J Mol Recognit* **12**: 279-284.
Nemoto, T., N. Sato, H. Iwanari, H. Yamashita & T. Takagi, (1997) Domain structures and immunogenic regions of the 90-kDa heat-shock protein (HSP90). Probing with a library of anti-HSP90 monoclonal antibodies and limited proteolysis. *J Biol Chem* **272**: 26179-26187.
Panaretou, B., G. Siligardi, P. Meyer, A. Maloney, J. K. Sullivan, S. Singh, S. H. Millson, P. A. Clarke, S. Naaby-Hansen, R. Stein, R. Cramer, M. Mollapour, P. Workman, P. W. Piper, L. H. Pearl & C. Prodromou, (2002) Activation of the ATPase activity of hsp90 by the stress-regulated cochaperone aha1. *Mol Cell* **10**: 1307-1318.
Pearl, L. H. & C. Prodromou, (2000) Structure and in vivo function of Hsp90. *Curr Opin Struct Biol* **10**: 46-51.
Pearl, L. H. & C. Prodromou, (2001) Structure, function, and mechanism of the Hsp90 molecular chaperone. *Adv Protein Chem* **59**: 157-186.
Pearl, L. H. & C. Prodromou, (2006) Structure and mechanism of the Hsp90 molecular chaperone machinery. *Annu Rev Biochem* **75**: 271-294.
Phillips, J. J., Z. P. Yao, W. Zhang, S. McLaughlin, E. D. Laue, C. V. Robinson & S. E. Jackson, (2007) Conformational dynamics of the molecular chaperone Hsp90 in complexes with a co-chaperone and anticancer drugs. *J Mol Biol* **372**: 1189-1203.
Picard, D., (2002) Heat-shock protein 90, a chaperone for folding and regulation. *Cell Mol Life Sci* **59**: 1640-1648.
Pratt, W. B. & D. O. Toft, (2003) Regulation of signaling protein function and trafficking by the hsp90/hsp70-based chaperone machinery. *Exp Biol Med (Maywood)* **228**: 111-133.
Prodromou, C., B. Panaretou, S. Chohan, G. Siligardi, R. O'Brien, J. E. Ladbury, S. M. Roe, P. W. Piper & L. H. Pearl, (2000) The ATPase cycle of Hsp90 drives a molecular 'clamp' via transient dimerization of the N-terminal domains. *EMBO J* **19**: 4383-4392.
Prodromou, C. & L. H. Pearl, (2003) Structure and functional relationships of Hsp90. *Curr Cancer Drug Targets* **3**: 301-323.
Prodromou, C., S. M. Roe, R. O'Brien, J. E. Ladbury, P. W. Piper & L. H. Pearl, (1997a) Identification and structural characterization of the ATP/ADP-binding site in the Hsp90 molecular chaperone. *Cell* **90**: 65-75.
Prodromou, C., S. M. Roe, P. W. Piper & L. H. Pearl, (1997b) A molecular clamp in the crystal structure of the N-terminal domain of the yeast Hsp90 chaperone. *Nat Struct Biol* **4**: 477-482.
Prodromou, C., G. Siligardi, R. O'Brien, D. N. Woolfson, L. Regan, B. Panaretou, J. E. Ladbury, P. W. Piper & L. H. Pearl, (1999) Regulation of Hsp90 ATPase activity by tetratricopeptide repeat (TPR)-domain co-chaperones. *EMBO J* **18**: 754-762.
Richter, K., S. Moser, F. Hagn, R. Friedrich, O. Hainzl, M. Heller, S. Schlee, H. Kessler, J. Reinstein & J. Buchner, (2006) Intrinsic inhibition of the Hsp90 ATPase activity. *J Biol Chem* **281**: 11301-11311.
Rutherford, S. L. & S. Lindquist, (1998) Hsp90 as a capacitor for morphological evolution. *Nature* **396**: 336-342.
Sato, S., N. Fujita & T. Tsuruo, (2000) Modulation of Akt kinase activity by binding to Hsp90. *Proc Natl Acad Sci U S A* **97**: 10832-10837.

Sgobba, M., G. Degliesposti, A. M. Ferrari & G. Rastelli, (2008) Structural models and binding site prediction of the C-terminal domain of human Hsp90: a new target for anticancer drugs. *Chem Biol Drug Des* **71**: 420-433.

Shiau, A. K., S. F. Harris, D. R. Southworth & D. A. Agard, (2006) Structural Analysis of E. coli hsp90 reveals dramatic nucleotide-dependent conformational rearrangements. *Cell* **127**: 329-340.

Siligardi, G., B. Panaretou, P. Meyer, S. Singh, D. N. Woolfson, P. W. Piper, L. H. Pearl & C. Prodromou, (2002) Regulation of Hsp90 ATPase activity by the co-chaperone Cdc37p/p50cdc37. *J Biol Chem* **277**: 20151-20159.

Soti, C., A. Racz & P. Csermely, (2002) A Nucleotide-dependent molecular switch controls ATP binding at the C-terminal domain of Hsp90. N-terminal nucleotide binding unmasks a C-terminal binding pocket. *J Biol Chem* **277**: 7066-7075.

Southworth, D. R. & D. A. Agard, (2008) Species-dependent ensembles of conserved conformational states define the Hsp90 chaperone ATPase cycle. *Mol Cell* **32**: 631-640.

Stebbins, C. E., A. A. Russo, C. Schneider, N. Rosen, F. U. Hartl & N. P. Pavletich, (1997) Crystal structure of an Hsp90-geldanamycin complex: targeting of a protein chaperone by an antitumor agent. *Cell* **89**: 239-250.

Sullivan, W., B. Stensgard, G. Caucutt, B. Bartha, N. McMahon, E. S. Alnemri, G. Litwack & D. Toft, (1997) Nucleotides and two functional states of hsp90. *J Biol Chem* **272**: 8007-8012.

Sullivan, W. P., B. A. Owen & D. O. Toft, (2002) The influence of ATP and p23 on the conformation of hsp90. *J Biol Chem* **277**: 45942-45948.

Taiyab, A., A. S. Sreedhar & M. Rao Ch, (2009) Hsp90 inhibitors, GA and 17AAG, lead to ER stress-induced apoptosis in rat histiocytoma. *Biochem Pharmacol* **78**: 142-152.

Terasawa, K., M. Minami & Y. Minami, (2005) Constantly updated knowledge of Hsp90. *J Biochem* **137**: 443-447.

Wandinger, S. K., K. Richter & J. Buchner, (2008) The Hsp90 chaperone machinery. *J Biol Chem* **283**: 18473-18477.

Wegele, H., L. Muller & J. Buchner, (2004) Hsp70 and Hsp90--a relay team for protein folding. *Rev Physiol Biochem Pharmacol* **151**: 1-44.

Whitesell, L. & S. L. Lindquist, (2005) HSP90 and the chaperoning of cancer. *Nat Rev Cancer* **5**: 761-772.

Winzor, D. J., (2003) Surface plasmon resonance as a probe of protein isomerization. *Anal Biochem* **318**: 1-12.

Young, J. C., I. Moarefi & F. U. Hartl, (2001) Hsp90: a specialized but essential protein-folding tool. *J Cell Biol* **154**: 267-273.

Young, J. C., W. M. Obermann & F. U. Hartl, (1998) Specific binding of tetratricopeptide repeat proteins to the C-terminal 12-kDa domain of hsp90. *J Biol Chem* **273**: 18007-18010.

Yun, B. G., W. Huang, N. Leach, S. D. Hartson & R. L. Matts, (2004) Novobiocin induces a distinct conformation of Hsp90 and alters Hsp90-cochaperone-client interactions. *Biochemistry* **43**: 8217-8229.

Zhang, W., M. Hirshberg, S. H. McLaughlin, G. A. Lazar, J. G. Grossmann, P. R. Nielsen, F. Sobott, C. V. Robinson, S. E. Jackson & E. D. Laue, (2004)

Biochemical and structural studies of the interaction of Cdc37 with Hsp90. *J Mol Biol* **340**: 891-907.

.

VITA

Kristen Lynn Szabla

Candidate for the Degree of

Master of Science

Thesis: HSP90 C-TERMINAL DOMAIN BINDING SITE FOR NOVOBIOCIN AND RELATED COUMARINS

Major Field: Biochemistry and Molecular Biology

Biographical:

Education:

Bachelor of Science
Biochemistry and Molecular Biology 2006

Completed the requirements for
Master of Science
Biochemistry & Molecular Biology at
Oklahoma State University,
Stillwater, Oklahoma
May, 2010.

Professional Memberships:
American Academy for the Advancement of Science

Name: Kristen Lynn Szabla Date of Degree: May, 2010

Institution: Oklahoma State University Location: Stillwater, Oklahoma

Title of Study: HSP90 C-TERMINAL DOMAIN BINDING SITE FOR NOVOBIOCIN & RELATED COUMARINS

Pages in Study: 118 Candidate for the Degree of Master of Science

Major Field: Biochemistry and Molecular Biology

Scope and Method of Study: Biophysical

Findings and Conclusions:

Heat shock protein 90 (Hsp90) is a highly conserved, eukaryotic, molecular chaperone which stabilizes an assortment of oncogenic proteins. Currently, novobiocin and related coumarins are being developed into higher affinity analogs for the treatment of various cancers based on their inhibition of Hsp90 chaperone function. However, direct binding to Hsp90 has yet to be demonstrated; the existence of an Hsp90 binding site for these compounds has, to date, been based on a number of indirect assays. In order to address this gap in our knowledge, we used the technique of surface plasmon resonance (SPR) to assay the affinities of novobiocin derivatives for full length Hsp90 (Hsp90FL) and a C-terminal Hsp90 truncation (Hsp90CT). We also examined the effect of bound N-terminal ligands, ATP, ADP, and geldanamycin (GA), on the affinities for our compounds of interest. Results demonstrate that novobiocin and related coumarins bind to apo Hsp90FL and apo Hsp90CT with comparable affinities. Additionally, novobiocin and related compounds did not bind to the N terminal nucleotide binding pocket on Hsp90FL. Moreover, coumarin derivatives bound to Hsp90: ADP complexes with enhanced affinity. Our results demonstrate that a binding site for novobiocin related compounds resides on the C-terminus of Hsp90. Our results also support the hypothesis that the N-terminal and C-terminal domains of Hsp90 interact to moderate Hsp90 chaperone activity. Our results provide new insights into the mode of action by which novobiocin related compounds interact with Hsp90 *in vitro* and may suggest novel approaches to the development of higher affinity novobiocin derivatives in the treatment of cancer and related diseases.

ADVISER'S APPROVAL: Dr. Robert Matts

ADVISER’S APPROVAL: Dr. Robert Matts